Acousto - Electric Effects in Cadmium Sulphide at Microwave Frequencies.

A Thesis submitted to the Faculty of Engineering of the University of Glasgow for the degree of Doctor of Philosophy.

by

Peter A. M. Stewart. B.Sc.

ProQuest LLC.
789 East Eisenhower Parkway
P.O. Box 1346
Ann Arbor, MI 48106 – 1346

Summary.

Acoustic amplifiers, operating at frequencies of 1GHz and above, have been constructed from hexagonal cadmium sulphide crystals. The main problem in making these devices was in obtaining efficient acousto-electric transducers for microwave frequencies. Evaporated thin films of CdS were used as transducers, and a close study was made of their properties, in order to obtain efficient generation of both shear and longitudinal acoustic waves, above 1 GHz.

The transducers were deposited on heated substrates by direct vacuum evaporation of CdS crystals. X-ray analysis showed that under most deposition conditions, the films were polycrystalline, composed of hexagonal phase crystallites of CdS, preferentially oriented with their c-axes perpendicular to the substrate. The degree of structural order increased with film thickness, and films under 0.5μ thick had a high degree of disorder. Acoustic waves were generated by applying an r.f. electric field perpendicular to the substrate, and parallel to the transducer thickness, so that normal films were thickness resonant longitudinal mode transducers. Evaporation at an oblique angle to the substrate, and at a deposition rate in excess of 0.1μ/min, caused the c-axes of the crystallites to tilt away from the normal, and grow towards the direction of evaporation. With the electric field normal to the substrate, and the c-axis at about 38.5° to the normal, there is no coupling to longitudinal waves in CdS, and only shear waves are generated.

A finite thickness was required to bend the c-axis to 38.5° to the normal, and it was thought initially, that this limited the frequency for which this type of fundamentally resonant shear transducer could be made. A technique was developed to extend the frequency range, by making the transducer a two-layer structure. The bottom layer, in which the c-axis was bending, was cadmium doped to render it highly conducting, and the top layer was of high resistivity CdS. The r.f. electric field was developed across the top layer, which acted as a resonant transducer and dominated the transducer frequency response, while the bottom layer acted as an acoustic transmission line, producing a ripple in the response.

When excited from a 50Ω line, the transducers had broad band responses, and the untuned insertion loss was typically 30 dB. With tuning, the insertion loss could be reduced to less than 10 dB. The impedance presented by the transducer is determined by a number of parameters, such as the electromechanical coupling constant, resistivity, active area and contact resistance, which are difficult to measure independently. The high level of insertion loss is due to the impedance mismatch between the transducer and the excitation system. By considering the properties of the acoustic waves launched in a transducer, the theoretical input impedance and frequency dependence of the insertion loss were evaluated. Good agreement was obtained between the theoretical and experimental transducer frequency responses, and in order to investigate further the various transducer parameters,

impedance measurements were made on a number of transducers.

CdS transducers are frequently non-stoichiometric in composition, and can have low resistivities, which increase the insertion loss. A new method of compensation was developed, in which deep trapping levels were introduced into the CdS lattice by thermal neutron bombardment. Resonance anti-resonance measurements on single crystal CdS, showed that the damage caused by neutron bombardment reduced the electro-mechanical coupling constant, although the damage could be partially removed by annealing.

Acoustic amplifiers were constructed by bonding slices of CdS between sapphire delay rods, which had evaporated CdS transducers on their free ends. Thermo-compression indium bonds, made completely in vacuum, were used, and measurements made between 1 and 2 GHz showed that transmission losses could be very low (< 3 dB), for both shear and longitudinal waves. Ohmic contacts were made to CdS by indium diffusion, and a relationship was observed between the degree of difficulty encountered in making ohmic contacts, and the dislocation density in CdS. The implication is that diffusion into dislocations is an important mechanism in contact formation.

The observed behaviour of acoustic amplifiers, above 1 GHz, was compared with the linear theory, and differences were attributed to either the generation of acoustic noise, or non-uniformities in the CdS. Gain of up to 450 dB/cm was observed in shear mode amplifiers, and up to 100 dB/cm in longitudinal mode amplifiers, but a much higher level of acoustic noise was generated in the longitudinal amplifiers.

The most significant measurements were made on CdS transducers, showing that longitudinal and shear accustic waves could be generated efficiently at microwave frequencies, using double layer transducers. Although it was clear from the measurements that net gain acoustic amplifiers could be constructed to operate at microwave frequencies, they would not be comparable devices to transistor amplifiers, because of their greater complexity, and the generation of acoustic noise.

Acknowledgements.

I wish to express my gratitude to Professor J. Lamb for the provision of excellent research facilities, and for his interest and encouragement throughout the course of the work. A great deal of valuable assistance was given by the two members of staff who supervised my work, Dr. R. B. Wilson and Dr. J. Richter. I also wish to thank Dr. W. Duncan and Mr. R. H. Hutchins for their constant interest and encouragement, and without whose collaboration the work described in this thesis would not have been possible. Assistance and advice were also given by Mr. G. A. Bennett, Mr. Seān S.Ō'Tuama, Mr. J. D. Adam and Mr. D. H. R. Price, and for help with the construction of apparatus, and preparation of specimens, I wish to acknowledge the assistance of Mrs. E. Scott, Mr. R. Darkin, Mr.T.Wright, Mr. G. Boyle and Mr. L. Hart.

The research was supported by contracts from the Ministry of Defence, C.V.D. (RU17/4), and the Science Research Council (B/SR/4216). In connection with the former contract, the guidance and interest of the sponsor, Dr. E. G. S. Paige of R.R.E., Malvern, is acknowledged.

For the use of the facilities of the Scottish Research Reactor Centre, N.E.L., East Kilbride, I must thank Dr. J. Scobie and Dr. J. Whitley, and for the use of X-ray equipment, Dr. P. Hancock of the department of Mechanical Engineering, University of Glasgow.

I wish to thank A.E.I. Central Research Laboratories, Rugby (1965-68), and the Faculty of Engineering (1968-69), for personal financial support.

Last, and not least, I wish to thank my wife, for much forbearance, and my parents, for providing me with the opportunities to continue my education.

CONTENTS

CHAPTER 1

INTRODUCTION

1.1 Historical Review

Piezoelectricity was discovered by the Curies in 1880, and was of largely academic interest until the First World War when Langevin discovered that quartz could be used to generate acoustic waves. From this time, quartz, and other insulating piezoelectric crystals, were used as electromechanical resonators and transducers[2]. In the 1950s, interactions between electrons and acoustic waves in piezoelectric materials began to be studied[3], and large, conductivity sensitive, attenuations were observed in such materials[4]. The electrons were thought to be absorbing energy from the acoustic waves, and theories were developed to explain this phenomenon[5,6]. Hutson,McFee and White[7,8,9] studied the interaction between electrons and acoustic waves, when the electrons were drifted at velocities up to and exceeding the velocity of sound. They observed the acoustic wave to be amplified when the elctrons drifted faster than the velocity of sound in the same direction as the wave, and to be attenuated when the electrons travelled at less than the velocity of sound.

Figure 1 is a diagram of a simple acoustic amplifier, showing the essential features. The original work on acoustic amplification was performed at frequencies between 10 and 60 MHz[8,9], but measurements have been published on amplification at higher frequencies[6,10].

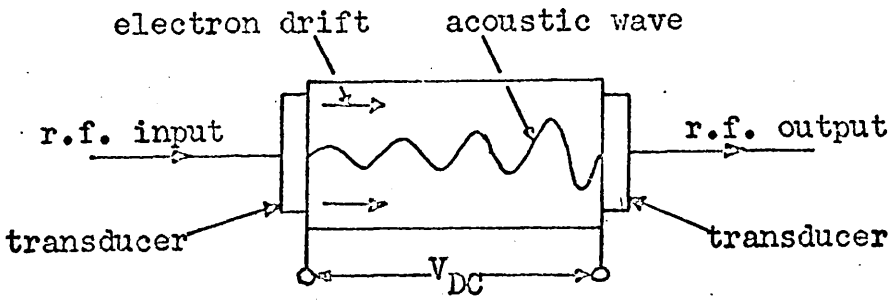

Figure 1. Schematic diagram of acoustic amplifier.

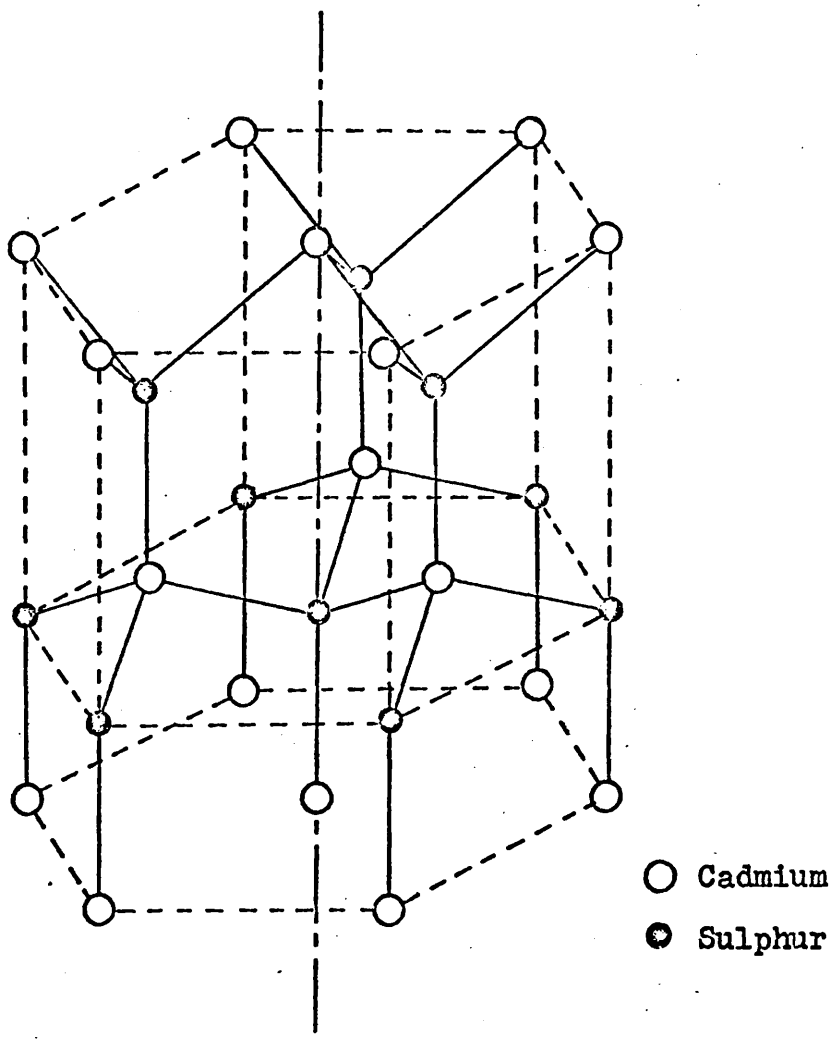

Figure 2. Wurtzite crystal structure of CdS.

1.2 Aims of the Investigation.

The object of the work described in this thesis, was the construction and study of acoustic amplifiers at frequencies of 1 GHz and above. Emphasis was laid on the development of techniques which might be used in practical devices. The principal technical difficulty was the manufacture of efficient acousto-electric transducers for this frequency range, and suitable thin film evaporated CdS transducers were developed[11]. Thin films can readily be deposited for the appropriate resonant thicknesses of 2μ and less. The study of transducer properties was directed towards finding how the crystal structure, and the electrical and mechanical properties, of the evaporated films, affected the insertion loss. In particular, a new method of efficiently generating shear waves above 1 GHz had to be found, because shear amplifiers produce less acoustic noise[9], and have longer delays, than longitudinal mode amplifiers.

It was thought that operation of acoustic amplifiers above 1 GHz would be advantageous, since very high gains per unit length are predicted theoretically[8], and an integral amplifier and delay device might have uses as a store, or lossless delay line. CdS was used in the experiments, because it was a readily available piezoelectric semiconductor with reasonably strong piezoelectric properties[5].

1.3 The Piezoelectric Effect.

Crystals can be divided into 7 systems and 32 classes, depending on the symmetry they possess, and of these 32 classes, 20 possess the property of piezoelectricity[2]. The criterion which determines whether or not a crystal is piezoelectric is the existence of a centre of

symmetry. If a crystal lacks this property, the application of stress can separate the centres of the positive and negative charges, and a dipole is produced. The converse effect also exists in that an electric field produces a stress within the crystal. Cadmium sulphide has a Wurtzite structure (point group symmetry 6mm), and consists of two interpenetrating hexagonal lattices, one of cadmium atoms, and the other of sulphur atoms, as shown in figure 2.

The basal plane of sulphur atoms does not lie midway between two basal planes of cadmium atoms, and so this crystal has an obvious lack of symmetry, and the opposite directions of the hexagonal axis are not equivalent. Thus the sign of an induced piezoelectric field is reversed by changing the sign of an applied stress. Each atom sits at the centre of a tetrahedron of atoms of the other type under equilibrium conditions, but the charge centres seperate when stress is applied.

A complete description of the piezoelectric properties of a crystal involves a treatment in terms of electrical, mechanical and piezoelectric effects, since these are all interdependent[2]. A crystal with no symmetry at all (triclinic) possesses 21 elastic constants, 18 piezoelectric constants and 6 dielectric constants. As the symmetry is increased, the number of possible constants decreases, until the most symmetrical type of crystal has only 3 elastic constants, no piezoelectric constant, and 1 dielectric constant.

The coupling between mechanical and electrical stored energy in a particular crystal can be described in terms of an electromechanical coupling constant K, where

$$K^2 = e^2/\varepsilon c, \quad \text{if K is small,}$$

and e, ε and c are the piezoelectric, dielectric and elastic constants, respectively, for the crystal[2]. Before a unique meaning can be ascribed to each of these constants, the approriate experimental boundary conditions must be known. K^2 arises in calculations involving coupling between mechanical and electrical energy in piezoelectric materials[5]. The K^2 for II-VI compounds increases, as the relative weights of the atoms increases.

1.4 Plane Wave Propagation in CdS.

The piezoelectric equations of state, derived from thermodynamic considerations by Mason[2] are

$$T_{ij} = c_{ijkl} \cdot S_{kl} - e_{lij} \cdot E_l \quad \ldots\ldots\ldots\ldots\ldots \quad 1$$

$$D_k = e_{klm} \cdot S_{lm} + \varepsilon_{ik} \cdot E_i \quad \ldots\ldots\ldots\ldots\ldots \quad 2$$

where repeated suffices mean summation. T is the stress, S the strain, E the electric field, D the electric displacement, and e, ε and c the piezoelectric, dielectric and elastic stiffness constant tensors respectively.

For hexagonal CdS these tensors are as follows

$$\begin{vmatrix} c_{11} & c_{12} & c_{13} & 0 & 0 & 0 \\ c_{12} & c_{11} & c_{13} & 0 & 0 & 0 \\ c_{13} & c_{13} & c_{33} & 0 & 0 & 0 \\ 0 & 0 & 0 & c_{44} & 0 & 0 \\ 0 & 0 & 0 & 0 & c_{44} & 0 \\ 0 & 0 & 0 & 0 & 0 & \frac{(c_{11}-c_{12})}{2} \end{vmatrix}$$

elastic constants

$c_{ijkl} = c_{mn}$

$$\begin{vmatrix} 0 & 0 & 0 & 0 & e_{15} & 0 \\ 0 & 0 & 0 & e_{15} & 0 & 0 \\ e_{31} & e_{31} & e_{33} & 0 & 0 & 0 \end{vmatrix}$$

piezoelectric constants

$$e_{klm} = e_{kn}$$

$$\begin{vmatrix} \varepsilon_{11} & 0 & 0 \\ 0 & \varepsilon_{11} & 0 \\ 0 & 0 & \varepsilon_{33} \end{vmatrix}$$

dielectric constants ε_{ik}

In equation 2, $e_{klm} \cdot S_{lm}$ is the piezoelectric polarisation P_k produced by the strain, and P_k has the following components[13].

$$P_1 = 2.e_{1,13} \cdot S_{13} \quad \ldots\ldots\ldots\ldots\ldots\ldots \quad 3.$$

$$P_2 = 2.e_{2,23} \cdot S_{23} \quad \ldots\ldots\ldots\ldots\ldots\ldots \quad 4$$

$$P_3 = e_{3,11} \cdot S_{11} + e_{3,22} \cdot S_{22} + e_{3,33} \cdot S_{33} \ldots\ldots\ldots \quad 5$$

The 1 and 2 axes are orthogonal directions in the basal plane perpendicular to the hexagonal, or 3, axis. The shear strain S_{13} (or S_{23}) is the resulting deformation when a plane shear wave propagates in the 3 direction, with particle displacement in the basal plane. It is also the strain produced when a plane shear wave propagates in the basal plane, with particle displacement in the 3 direction. In the former case the piezoelectric field is perpendicular to the direction of propagation, and in the latter, the piezoelectric field is in the direction of propagation. Equation 5 shows that a plane longitudinal wave (S_{11} or S_{22}) propagating in the basal plane produces a piezoelectric polarisation in the 3 direction, whereas,

for a plane longitudinal wave propagating in the 3 direction, the piezoelectric polarisation is in the 3 direction. Equations 1 and 2 show that the acoustic wave equations will contain electric field terms, and conversely, that Maxwell's equations will contain terms involving stress. In a piezoelectric medium there is a coupling between the acoustic modes (two transverse and one longitudinal) and the two transverse electromagnetic modes. An electromagnetic wave propagating in a piezoelectric medium will be accompanied by an acoustic wave, travelling at the phase velocity of the electromagnetic wave($v_{e.m.}$). Conversely, an acoustic wave will be accompanied by a transverse electromagnetic wave, produced by the displacement current arising from the piezoelectric polarisation, and travelling with the acoustic wave phase velocity (v_s). This problem has been analysed in detail by Kyame[3,14], and as expected, the effects of this electromechanical coupling are small, because the velocity of light is five orders of magnitude larger than the velocity of sound.

The piezoelectric polarisation also gives rise to electrostatic fields, which produce the significant effects of piezoelectricity on acoustic wave propagation. Hutson and White have shown that the acoustic wave dispersion, caused by coupling to the electromagnetic waves, is smaller, by a factor approximately $(v_s/v_{e.m.})^2$, than the acoustic dispersion caused by coupling to the electrostatic fields[5]. Hence it is justifiable to ignore the electromagnetic waves travelling at the velocity of sound. For the plane wave assumption to be valid, the

acoustic wavelength must be much less than the dimensions of the sample being considered, and so transverse components of piezoelectric polarisation give rise to charges only at the boundaries of the sample. Components of the polarisation which are in the direction of propagation produce charges which are separated by half an acoustic wavelength. These "longitudinal" electrostatic fields are therefore much stronger than any transverse electrostatic fields arising from charges at the sample boundaries. Consequently, only waves which have a "longitudinal" piezoelectric polarisation are accompanied by a significant electric field, and need be considered as piezoelectrically active in the presence of charged carriers.

Considering propagation along the crystalline axes, only the longitudinal wave propagating in the 3 direction (along the c-axis) with polarisation along the c-axis, and the shear wave propagating in the basal plane, with polarisation along the c-axis, are piezoelectrically active. In general, one longitudinal and two shear waves can propagate in any crystallographic direction in CdS[15]. The pure shear wave is non-piezoelectric, and in the 3 direction the shear modes are degenerate in velocity.

1.5 Acousto-Electric Interactions in Semiconductors.

(a) Carrier Bunching and Acousto-Electric Current.

If an acoustic wave is transmitted through a material which is piezoelectrically active for the particular mode of propagation, then an electric field will travel with the acoustic wave. Should charge carriers be present in the material, then in general, the

piezoelectric field will cause currents to flow, and energy will be dissipated[8]. When the piezoelectric field is in the direction of wave propagation, it will cause the carriers to bunch, and they will move to and fro in response to the field. A space charge wave will thus accompany the piezoelectrically active acoustic wave. The bunching will take place in the regions of potential minima, and since the carriers move in response to the wave, the wave loses energy to the carriers. This can be treated as a quantum effect, in which the wave, by colliding with the carriers, loses quanta of momentum to the carriers, which, in turn, lose momentum by collisions with other carriers and the lattice.

Thus far, the discussion has been on the behaviour of carriers moving about equilibrium positions in response to a moving acoustic wave, and causing the wave to be attenuated. Now, considering electrons as the carriers, if a D.C. electric field is applied to the material, so that the carriers drift in the direction of the acoustic wave, the position of the carrier bunches with respect to the net piezoelectric field is changed, and so the energy transfer is altered. When the carriers drift at the velocity of sound, they are bunched at positions of minimum potential energy, and there is no energy transfer. The situation for a longitudinal piezoelectric field is given in figure 3, which shows the piezoelectric field, the carrier density modulation it produces, and the space charge field due to the bunched carriers, which opposes the applied piezoelectric field. The carrier density varies about a mean value, and the piezoelectric field is $-\partial V/\partial x$, where V is the potential of the wave. In figure 3, the electric field and the

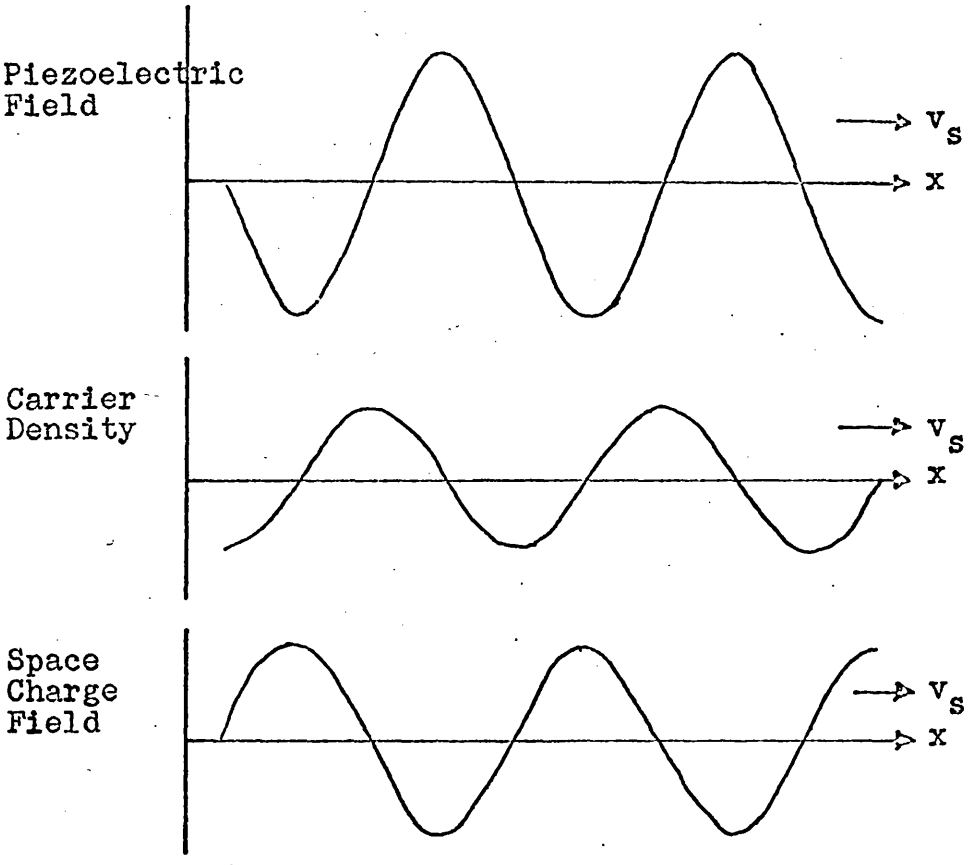

Figure 3. The piezoelectric field, carrier density and space charge field in a piezoelectric semiconductor, with the carriers drifting at the velocity of sound.

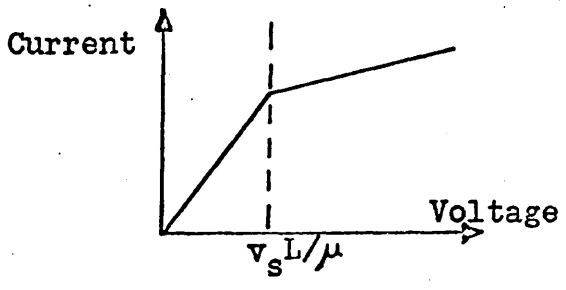

Figure 4. V-I characteristic of a piezoelectric semiconductor.

space charge waves are 90^{o} out of phase, so that no energy dissipation is taking place. If the phase is not 90^{o}, energy and momentum transfer take place. When the drift velocity of the carriers v_d, is greater than the acoustic velocity, then the carriers lose momentum to the acoustic wave, and it is amplified.

The forward momentum of the carriers is depleted by the amplification process[16]. This effect represents an electron flow counter to the direction of drift, and is known as the acousto-electric current. Consequently, the V - I characteristic of a piezoelectric semiconductor has a saturation region[17], which develops when the carriers are drifted faster than the velocity of sound (Figure 4). This is true even when there is no input acoustic wave, and the momentum given up by the electrons drifting faster than the velocity of sound amplifies the random motion of the lattice, and results in a high level of acoustic noise.

Shear waves travel at a lower velocity than longitudinal waves in CdS. If an attempt is made to drift electrons faster than the longitudinal sound velocity, they exceed the shear velocity at a much lower drift field, and start to lose momentum to shear acoustic noise. It is clearly impractical to design longitudinal mode amplifiers, and strong amplification may only be expected from shear mode amplifiers[9].

Weinreich[16] defined the acousto-electric field E_{ac}, produced by momentum change of the carriers as $E_{ac} = \alpha . S_d / qnv_s$ 6

where α is the acoustic wave attenuation per unit length, S_d is the acoustic power density, q the charge on an electron, n the carrier density, and v_s the velocity of sound. The acousto-electric field is

a D.C. quantity, and is determined purely from wave dynamics, without reference to the detailed mechanism of the process linking electrons and acoustic waves. Since momentum is conserved, the result is obtained by equating the rates of change of momentum, which are fordes, in the acoustic and electrical regimes.

The rate of change of momentum of the electrons in the acousto-electric field/unit volume = $E_{ac}.q.n$.....7

Wave Momentum/unit volume = (Wave Energy)/v_s

= (Power Density)/v_s^2

$\therefore$ Rate of change of Wave Momentum/unit volume = $\alpha.S_d/v_s$ 8

(b) Relaxation Effects.

The acoustic gain available in a piezoelectric semiconductor is a function of the conductivity modulation. Any influence which tends to debunch the carriers therefore tends to reduce the gain. Two important mechanisms are involved, and these are dielectric relaxation and diffusion.

The dielectric relaxation frequency $\omega_c = \sigma/\varepsilon$, where σ is the conductivity and ε is the dielectric constant, defines the rate at which charged carriers in a solid can move, under the influence of a local electric field, in an attempt to cancel that field. Consider an acoustic wave, with angular frequency ω, to propagate in a piezoelectric material, in the absence of a drift field. If $\omega \ll \omega_c$, the carriers can move fast enough to cancel the piezoelectric field, and sit exactly in potential wells so that they do not interact with the acoustic wave.

If $\omega \gg \omega_c$, the carrier distribution is not disturbed by the wave. In the absence of drift field and diffusion effects, the interaction between the acoustic waves and bunched carriers is maximised when $\omega = \omega_c$[8]. In CdS, at frequencies of 1GHz and above, a suitable resistivity is 500Ω cm or less. When a drift field is present the condition for maximum interaction is $(1 - {}^{v_d}/_{v_s}).\omega = \omega_c$.

The random motion of the carriers tends to cause the bunches to decay by out-diffusion. As the frequency increases, and the acoustic wavelength λ, falls, the concentration gradient between carrier bunches increases, and diffusion out of the bunches becomes significant. If the number of carriers crossing unit area per unit time is N_o, and the concentration gradient is grad (N), where N is the particle density,

$$N_o = D_n . \text{grad } (N) \quad \ldots\ldots\ldots\ldots\ldots\ldots \quad 9$$

where D_n is the diffusion constant, defined as

$$D_n = \mu kT/q \quad \ldots\ldots\ldots\ldots\ldots\ldots\ldots \quad 10$$

where μ is the carrier mobility, k is Boltzmann's constant, T is the absolute temperature, and q is the charge on an electron[18].

A local non-equilibrium concentration of carriers will decay with a time constant $\tau_D \sim {}^{\lambda^2}/_{D_n}$, where λ is the distance over which a concentration gradient exists, and can be identified with the acoustic wavelength in this case.

Diffusion effects are important when τ_D is less than the period of the ultrasonic wave, i.e. when $\frac{\lambda^2}{D_n} < \frac{1}{\omega}$, or ${}^{\omega^2\lambda^2}/_{D_n} < \omega$. $\omega\lambda$ is of the order of the acoustic wave velocity v_s, and $({}^{v_s^2}/_{D_n})$ has

been defined as the diffusion frequency, ω_D. Diffusion is important therefore when $\omega > \omega_D$.

A further understanding of relaxation effects can be obtained by evaluating

$$\frac{\omega_C \omega_D}{\omega^2} = \frac{\sigma}{\varepsilon} \times \frac{v_s^2}{D_n} \times \frac{1}{\omega^2} = \left(\frac{\lambda}{2\pi L_D} \right)^2 \quad \ldots\ldots\ldots 11$$

where $L_D = (\varepsilon kT/q^2 n)^{\frac{1}{2}}$ is the Debye screening length[8]. Screening is the reduction of the piezoelectric field accompanying an acoustic wave, by the oppositely directed field due to the carrier bunches. When $\lambda \sim L_D$, diffusion effects become important, and carrier bunching on a scale much smaller than L_D (i.e. $\lambda << L_D$) will tend to be smeared out by the thermal motion of the carriers. When $\lambda << L_D$ the piezoelectric field is not screened by the carrier bunches, and momentum transfer between the carriers and acoustic wave starts to decrease when $L_D > \lambda$, i.e. when $\omega > (\omega_C \omega_D)^{\frac{1}{2}}$.

1.6 Microwave Transducers.

If the acoustic amplifier is to be a practical device at microwave frequencies, efficient acousto-electric transducers must be used. At 1 GHz, the thickness of a resonant half wavelength transducer will lie between 0.5 and 2.0μ, depending on the material, and the acoustic mode to be generated. Thin plates of single crystal piezoelectric material cannot therefore be used if broad band fundamental mode transducers are required, although there is the possibility of bonding a slice of the transducer material on to the required substrate, and optically polishing the slice down to the

required thickness. Surface excitation of piezoelectric materials is not an efficient method of acoustic wave generation[19]. Diffusion layer transducers[20], made by diffusing compensating materials into semiconductors (e.g. copper into CdS) are limited in frequency to about 300 MHz for shear waves, because the compensating materials continue to diffuse at room temperature, and it is difficult to make abrupt boundaries with short diffusion depths. Depletion layer transducers[21], using the Schottky barriers formed between metals and semiconductors as the resonant elements, are a further possibility. The high resistivity layer acts as a transducer, and the upper frequency limit should be in X band. Conversion efficiencies have, however, proved to be low.

The use of evaporated CdS transducers appears to be the most promising method of obtaining efficient, broad band, acoustic wave generation at microwave frequencies[11,22]. When the project was begun, published measurements showed that evaporated CdS transducers could be operated efficiently above 1 GHz for longitudinal waves, but not above 600 MHz for shear waves[11]. At microwave frequencies, a good conversion efficiency is essential, for experimental, as well as practical, devices, as the acoustic loss in most materials becomes quite high, and experiments have to be performed under conditions of high total loss.

1.7 Theory of Acoustic Amplification

(a) The White Linear Theory

D.L. White[8] produced a small signal analysis to describe

the interaction discussed qualitatively in section 1.5. The analysis is performed for extrinsic semiconductors, with electrons as carriers, and an allowance is made for the fact that some of the free carriers may be trapped. A one dimensional treatment is given, and it is not necessary to invoke boundary conditions to solve the problem. Only one acoustic mode is considered and, as explained in section 1.4, there is only one piezoelectric field associated with the wave, and this field is longitudinally polarised.

The piezoelectric equations of state may be written in the form

$$T = c.S - e.E \quad \ldots\ldots\ldots\ldots\ldots\ldots\ldots 12$$

$$D = e.S + \varepsilon.E \quad \ldots\ldots\ldots\ldots\ldots\ldots\ldots 13$$

where T is the stress, S is the strain, E is the piezoelectric field in the x direction of propagation, and D is the electric displacement. c, e, and ε are the appropriate elastic, piezoelectric and dielectric constants.

If u is the particle displacement

$$S = \frac{\partial u}{\partial x} \quad \ldots\ldots\ldots\ldots\ldots\ldots\ldots 14$$

Newton's Law is

$$\frac{\partial T}{\partial x} = \rho . \frac{\partial^2 u}{\partial t^2} \quad \ldots\ldots\ldots\ldots\ldots\ldots\ldots 15$$

where ρ is the density of the material.

Equation 13 shows that the piezoelectric effect can be represented an an additional stiffening effect on the lattice, and may therefore be represented by a modified elastic constant c'.

The wave equation is

$$\rho.\frac{\partial^2 u}{\partial t^2} = \frac{\partial T}{\partial x} = c.\frac{\partial^2 u}{\partial x^2} - e.\frac{\partial E}{\partial x} \quad \ldots\ldots\ldots 16$$

Gauss's equation, div D = Q, where Q is the space charge, reduces to

$$\frac{\partial D}{\partial x} = Q \quad \ldots\ldots\ldots 17$$

and the equation of charge continuity is

$$\frac{\partial J}{\partial x} = -\frac{\partial Q}{\partial t} \quad \ldots\ldots\ldots 18$$

The density of electrons n, in the conduction band, may be written as

$$n = n_o + f_t . n_s \quad \ldots\ldots\ldots 19$$

where n_o is the mean electron density, and n_s is the excess electron density necessary to produce the space charge Q, so that

$$Q = - q.n_s \quad \ldots\ldots\ldots 20$$

where q is the charge on an electron. f_t is the fraction of the space charge which is mobile, where $0 < f_t < 1$. The fraction $(1 - f_t)$ of the space charge is assumed to be trapped in sites with a relaxation time much shorter than the period of the acoustic wave. When the mean free path of the electrons is much shorter than the acoustic wavelength, the current density J, is given by

$$J = q\,(n_o + f_t.n_s)\,\mu.E + q\,D_n.\frac{\partial n_s}{\partial x} \quad \ldots\ldots\ldots 21$$

where the first term on the R.H.S. represents conduction by D.C. and piezoelectric fields, and the second term represents diffusion.

$$\therefore \quad \frac{\partial J}{\partial x} = q\frac{\partial n_s}{\partial t} = q.\mu\frac{\partial}{\partial x}(n.E) + q.D_n\frac{\partial^2 n_s}{\partial x^2} \quad \ldots\ldots\ldots 22$$

Eliminating J, n and n_s from the above equations leads to

$$\frac{-\partial^2 D}{\partial x \partial t} = \mu . \frac{\partial}{\partial x} \left((q.n_o - f_t \frac{\partial D}{\partial x}) E \right) - D_n . \frac{\partial^3 D}{\partial x^3} \quad \ldots\ldots\ldots \quad 23$$

The electric field may be written as

$$E = E_o + E_1 . e^{j(kx-\omega t)} \quad \ldots\ldots\ldots\ldots\ldots\ldots\ldots \quad 24$$

where E_o is a D.C. field, and E_1 the piezoelectric field accompanying an acoustic wave in the medium.

The propagation constant is $k = \frac{\omega}{v_s} + j\alpha$, where α is the attenuation constant in Nepers/cm, and v_s is the phase velocity of the acoustic wave. The other variables associated with the wave are taken to have the same space and time dependence as E_1. Equation 13 is used to eliminate D in equation 23, resulting in an expression for E_1, in terms of u (if D.C. and harmonic terms are omitted). Substitution in the wave equation 16 yields

$$\rho . \omega^2 = c' . k^2 \quad \ldots\ldots\ldots\ldots\ldots\ldots\ldots\ldots\ldots\ldots \quad 25$$

where $c' = c \left(1 + \frac{e^2}{\varepsilon c} \left(1 + j \frac{\sigma}{\varepsilon \omega} \left(1 + f_t \mu \frac{k}{\omega} E_o + j D_n f_t \left(\frac{k}{\omega}\right)^2\right)^{-1}\right)^{-1}\right)$ .. 26

The solution of k is simplified since $|\alpha| \ll \frac{\omega}{v_s}$, $K^2 = \frac{e^2}{\varepsilon c}$, $\omega_c = \frac{\sigma}{\varepsilon}$, $\omega_D = v_s^2 / f_t . D_n$, and $\gamma = 1 - f_t E_o \mu / v_s$. ω_c and ω_D are the dielectric relaxation and diffusion frequencies discussed above.

Using these identities, expressions can be developed relating the main variables,

$$\text{i.e. } J = -\frac{\sigma e}{\varepsilon} \times \frac{S}{\gamma + j \left(\frac{\omega_c}{\omega} + \frac{\omega}{\omega_D} \right)} \quad \ldots\ldots\ldots \quad 27$$

$$n_s = \frac{\omega_c . e}{q . v_s} \times \frac{S}{\Upsilon + j\left(\frac{\omega_c}{\omega} + \frac{\omega}{\omega_D}\right)} \quad \ldots\ldots\ldots \quad 28$$

$$E_l = \frac{-e}{\varepsilon} \times \frac{\left(\Upsilon + j\frac{\omega}{\omega_D}\right)}{\Upsilon + j\left(\frac{\omega_c}{\omega} + \frac{\omega}{\omega_D}\right)} S \quad \ldots\ldots\ldots\ldots \quad 29$$

$$c' = c.\left(1 + K^2 \frac{\left(\Upsilon + j\frac{\omega}{\omega_D}\right)}{\left(\Upsilon + j\left(\frac{\omega_c}{\omega} + \frac{\omega}{\omega_D}\right)\right)}\right) \quad \ldots\ldots\ldots\ldots \quad 30$$

$K^2 \ll 1$, and therefore

$$\alpha = \frac{K^2}{2} \times \frac{\omega_c}{v_s \Upsilon}\left(1 + \frac{\omega_c^2}{\Upsilon^2 \omega^2}\left(1 + \frac{\omega^2}{\omega_c \omega_D}\right)^2\right)^{-1} \quad \ldots\ldots\ldots \quad 31$$

$$v_s = v_o \left(1 + \frac{K^2}{2} \times \frac{\left(1 + \frac{\omega_c}{\omega_D \Upsilon^2} + \frac{\omega^2}{\omega_D^2 \Upsilon^2}\right)}{\left(1 + \frac{\omega_c^2}{\Upsilon^2 \omega^2}\left(1 + \frac{\omega^2}{\omega_c \omega_D}\right)^2\right)}\right) \ldots\ldots \quad 32$$

where $v_o = \left(c/\rho\right)^{\frac{1}{2}}$

The main results of this theory can be expressed graphically (figure 5), where the electron drift velocity $v_d = - f_t \mu E$.

Calculation of these curves for shear waves, at 1 GHz, and at room temperature, for CdS with a resistivity of 10^3 Ωcm and $f_t . \mu$ = 200 cm^2/v sec, predicts maximum gain and loss of 1400 dB/cm, and a change in v_s at $\Upsilon = 0$ of less than 1%, so that dispersion can be ignored.

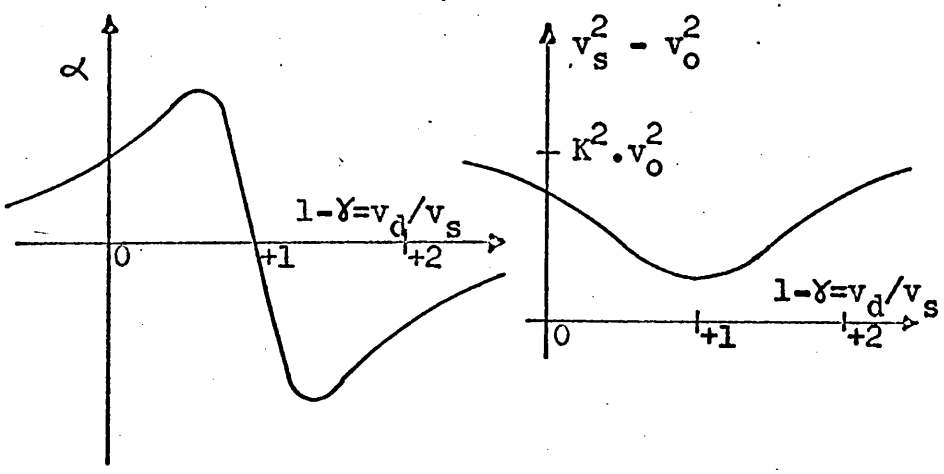

Figure 5. Attenuation α, and sound velocity v_s, as functions of drift field.

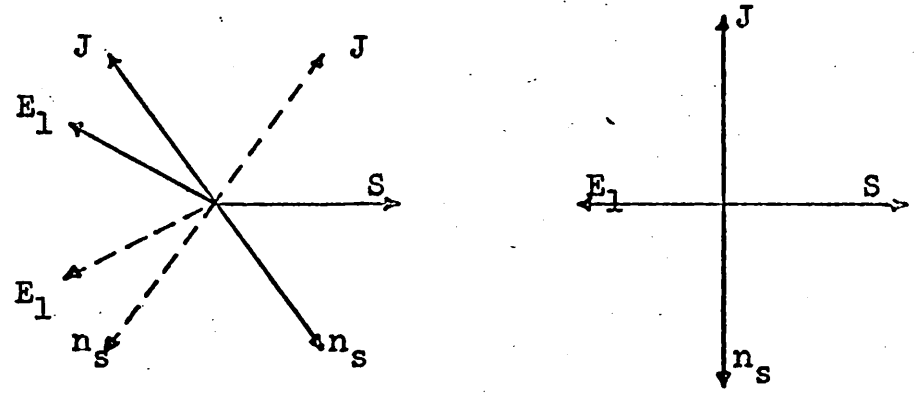

a) —— $\gamma > 0$

--- $\gamma < 0$

b) $\gamma = 0$

Figure 6. Phase relationships between strain S, current I, carrier density n_s, and piezoelectric field E_1.

The phase relationships of n_s, J, E_1 and S can be represented diagrammatically[13] (figure 6).

The power exchanged between the carrier bunches and the acoustic wave is given by J. E_1, and the phase angle between J and E_1 indicates whether the acoustic wave is gaining or losing energy.

The gain per unit length α, is given in equation 31, and the gain per wavelength is $\alpha \left(\frac{v_s 2\pi}{\omega}\right)$. The greatest gain per wavelength occurs when $\omega = \omega_c$, and $\omega^2 \ll \omega_c \omega_D$ and is $K^2/4$. When $\omega^2 = \omega_c \omega_D$, the gain per unit length is a maximum. Although the gain per wavelength is independent of frequency, there are more wavelengths in the path at higher frequencies, and consequently higher gain per unit length.

By differentiating equation 31 with respect to γ, the turning values of the attenuation curve (figure 5) can be found, and they occur when

$$-\gamma = \frac{\omega_c}{\omega} + \frac{\omega}{\omega_D} \qquad \text{33}$$

(b) Trapping Effects.

The above theory has been derived by assuming that the relaxation time of the carriers in traps is much less than the period of the acoustic wave. If this is not the case, then the bunched carriers in traps are out of phase with those in the conduction band. Thus the trapping factor f_t becomes complex, and Ishiguro, Uchida, Sasaki, and Susuki[23,24], have applied this condition to the White theory. The imaginary part of f_t leads to a phase shift between J and the net piezoelectric field E_1, which reduces the magnitude of

the interaction. The size of the out of phase component is proportional to the drift field, so that the reduction in the electron phonon interaction is more marked in the gaining region, than in the attenuating region. The attenuation against drift field curve then becomes asymetric.

If only one kind of trap is assumed to exist and n_1 and n_2 are the concentrations of the free and trapped bunched electrons respectively, τ is the trap relaxation time, and the 0 subscript refers to the parameters when $\tau \ll \frac{1}{\omega}$.

$$n_s = n_1 + n_2 \qquad n_{so} = n_{10} + n_{20}$$

$$n_1 = f_t \cdot n_s \qquad n_{10} = f_{to} \cdot n_{so}$$

$$n_2 = (1 - f_t)n_s \qquad n_{20} = (1 - f_{to})n_{so}$$

$$\frac{\partial n_s}{\partial t} = - \left(\frac{n_2 - n_{20}}{\tau} \right) \quad \ldots\ldots\ldots\ldots\ldots\ldots\ldots\ldots 34$$

Using $\frac{\partial}{\partial t} = j\omega$

$$f_t = \frac{f_{to} - j\omega\tau}{1 - j\omega\tau} = \frac{b \cdot f_{to}}{1 + ja} \quad \ldots\ldots\ldots\ldots\ldots\ldots\ldots\ldots 35$$

f_{to} is real, and is defined by Hutson and White[5] as the ratio of the change of mobile space charge to the change of total space charge, when the latter causes a small change of the electron Fermi level.

If $\omega\tau \ll f_{to}$, then $f_t \approx f_{to}$.

The second statement in equation 35 is written for convenience, so that $\gamma = 1 + {bf_{to}\mu E_o}/{v_s}$, and a is the ratio of $\mathrm{Re}(f_t)/\mathrm{Im}(f_t)$.

Equation 31 is modified, and it can be shown that

$$\frac{\alpha_{max}(\text{gain})}{\alpha_{min}(\text{loss})} = \frac{\sqrt{1 + a^2} - a}{\sqrt{1 + a^2} + a} \quad \ldots\ldots\ldots\ldots\ldots\ldots 36$$

White[25] proposed a different explanation for the observed asymmetry of the attenuation versus drift field curves in practical amplifiers. He suggested that variations in resistivity in the path of the acoustic wave would tend to reduce the gain more than the loss. In practice, both effects are likely to be present.

(c) Limits of the Linear Theory.

For the small signal analysis to be valid, the bunched electrons must be only a small fraction of the total free carrier concentration in the conduction band[8].

i.e. $f_t . n_s \ll n$

Using $\sigma = nq\mu$ and equation 28, it can be shown that, this condition is equivalent to

$$S \ll \varepsilon v_s / f_t . \mu . e \quad \ldots\ldots\ldots\ldots\ldots\ldots\ldots\ldots\ldots\ldots\ldots\ldots 37$$

In practise this means that the strain must be less than 10^{-5}.

For linearity $|\alpha| \ll \omega/v_s$, which means that the gain per wavelength must be small. The linear approximation involves neglecting the term $q\mu n_s E_1$ in the current density expression, equation 21. When bunching is large, this term cannot be ignored. A pure harmonic wave is no longer a solution, and each variable is then determined by a Fourier series. Each frequency component may interact with the others, by virtue of the non-linearity, and appreciable harmonic generation will occur.

(d) Choice of Material for an Acoustic Amplifier.

Several compounds of the II - VI and III - V groups are piezoelectric, and their theoretical behaviour as acoustic amplifiers can be compared[26]. The significant properties are the electro-mechanical coupling constant, available gain, and power handling capacity. In table 1, data is presented for a number of piezoelectric materials. The coupling constants appropriate to shear mode operation are given, and are K_{15} for the hexagonal materials, and K_{14} for the cubic[2]. The maximum gain per unit length at 1 GHz is given, using the condition $\omega^2 = \omega_c \omega_D$ in equations 31 and 33, whence $\alpha_{max} = K^2\omega/8v_s$. The drift power consumed per unit gain, for the optimum conditions, is

$$\frac{P_{dc}}{G} = \frac{\varepsilon . v_s^3}{4.34(\mu K^2)} \times \frac{\omega}{\omega_D}$$

The quantity μK^2, which occurs in the denominator, is described as a merit factor, and a high merit factor indicates low power consumption per unit gain. The data in table 1 refers to amplifiers of the type sketched in figure 1, except for InSb, for which the values refer to the situation of crossed electric and magnetic fields, at 77°K[27]. The conductivity and mobility of the InSb are modified to give useful results. For room temperature operation, ZnO appears to be the best material, but CdS has comparable properties.

Compound	Structure	K	Max. Gain at 1GHz dB/mm	Merit Factor μK^2 $cm^2/Vsec$
ZnO	Hexagonal	0.3	220	18
CdS	Hexagonal	0.19	140	11
CdSe	Hexagonal	0.13	78	10
ZnS	Cubic	0.079	20	0.6
InSb*	Cubic	0.068	6.7	37

Table 1. Basic data for acoustic amplifiers.

* For crossed electric and magnetic fields at 77°K.

CHAPTER 2.

2. Transducers.

2.1 General Introduction.

In this chapter, the techniques used to produce efficient, longitudinal and shear mode, evaporated CdS transducers, for frequencies of 1GHz and above, are described, and the behaviour of the transducers is analysed. Evaporated CdS films used as transducers must possess a high degree of structural order, and be of good stoichiometic composition. These properties are determined by the evaporation conditions, and a review article by de Klerk[28], shows that evaporated CdS transducers are normally polycrystalline, consisting of hexagonal crystallites which are oriented with their c-axes perpendicular to the substrate, and their a-axes randomly directed parallel to the substrate. The films have a tendency to be sulphur deficient, thus lowering their resistivity and making them inefficient transducers. The resistivity can be increased by annealing or doping, although this may cause the c-axes of some crystallites to rotate away from the perpendicular.

Evaporated transducers are required to generate either a shear or a longitudinal acoustic mode, and are usually excited by an electric field directed normal to the substrate, and parallel to the transducer thickness. An intense electric field is therefore developed between the metal electrodes sandwiching a thin film transducer.

Since, in evaporated CdS films, the crystalline c-axis usually grows perpendicular to the substrate, the films are most readily used as longitudinal mode transducers, and the appropriate piezoelectric constant is e_{33}^2. If a transducer is deposited on a substrate without metal electrodes, pure shear waves may be generated by directing an electric field, in a cavity, parallel to the substrate[19,28]. e_{15} is the appropriate piezoelectric constant[2], but this is an inefficient method of generation, as weaker electric fields are developed in the transducer. Shear waves, efficiently generated, are more useful than longitudinal waves in acoustic amplifiers (section 1.5).

If the c-axis of the transducer can be tilted away from the substrate normal, the electric field, directed along the normal, generates both shear and longitudinal waves. Calculations have been performed to determine how the electromechanical coupling constants for each mode (for thickness resonant CdS transducers) vary as the c-axis is tilted away from the normal electric field[15,29]. The behaviour of the coupling constants is given in figure 7.

The important result of the calculations is that there are several orientations of the c-axis, with respect to the electric field, in which only one mode is generated. In particular, with the c-axis inclined at 38.5° to the normal, only a shear mode is generated.

There are two methods of depositing CdS transducers; a direct evaporation technique in which a beam of evaporated CdS impinges directly on a substrate[11], and an indirect technique, in which cadmium and sulphur are separately evaporated, and the

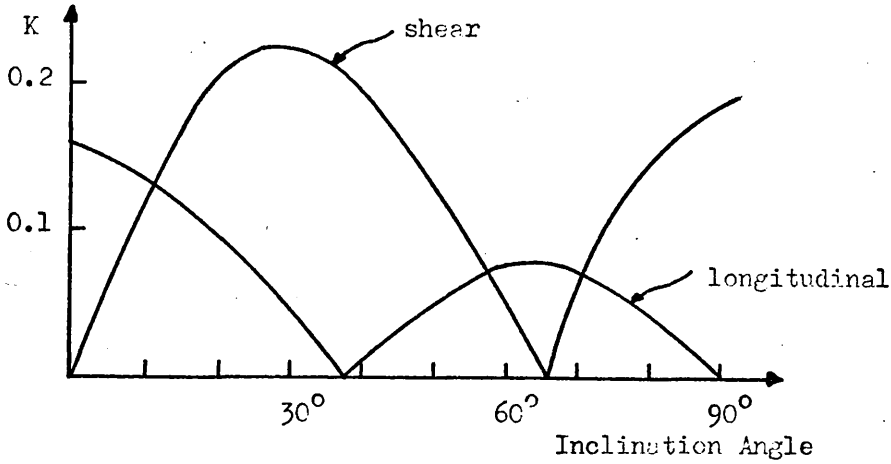

Figure 7 Variation of thickness longitudinal and thickness shear coupling constants for CdS, with tilting c-axis.

vapour beams mingle at the substrate[30]. The latter "co-evaporation" technique produces very highly ordered films, because of the slow deposition rate (10Å/min), but only films with the c-axis perpendicular to the substrate may be grown[28]. The direct evaporation technique gives a much higher rate of deposition (greater than 0.1μ/min if required), and so produces films which have less well ordered structures[28]. Direct evaporation has the advantage however, that if the deposition rate is high, and the CdS is evaporated at an angle to the substrate, the crystalline c-axis grows towards the direction of evaporation, and not perpendicular to the substrate[11]. A method is therefore available for tilting the c-axis to 38.5° to the normal, so that pure shear waves can be generated.

When CdS is deposited at an angle, the first layers to be deposited always have the c-axis perpendicular to the substrate[31].

On metallic and amorphous substrates, the c-axis bends towards the direction of evaporation only after a finite thickness of material has been deposited[31]. Thus any shear evaporated transducer has a base layer in which the structure is varying, and the thickness of this layer puts an upper frequency limit on efficient shear mode generation. Efficient operation (less than 10dB insertion loss) of shear transducers has not been reported above 600 MHz[11]. A technique has been developed for extending the frequency range of efficient generation by shear transducers. The region in which the c-axis is bending is rendered inactive as a transdcuer by cadmium doping, and the high resistivity top layer of the CdS film, which has the suitably tilted structure, is then the resonant transducer. The upper frequency limit, for efficient operation of fundamental mode shear transducers, will then be determined by the acoustic loss in CdS, but X band operation should be possible.

In this chapter, most of the work described was performed with longitudinal CdS transducers, deposited by the "direct evaporation" technique. * A theoretical full mode analysis of transducer operation, experimental measurements and analysis of structural properties, and measurements of the acousto-electric properties of transducers, are presented.

2.2. Transducer Deposition Procedure.

A direct evaporation technique was used, and the apparatus, shown diagrammatically in figure 8, is basically that described by

* By Mr. R. H. Hutchins of these laboratories.

Foster[11]. It is contained in a 12" bell jar, on a liquid nitrogen trap and oil diffusion pump. The substrate holder is an aluminium block, drilled to accept two substrates, and mounted on two coaxial thin walled stainless steel tubes, 16cm above the evaporation source. The block was heated by two 65W heaters, and the temperature of the substrate holder was monitored and controlled by a Honeywell control unit, using an iron-constantan thermocouple. During evaporation the substrates were maintained at the required temperature within $\pm$ 1^{0}C, and evaporation did not commence until a period of two hours had elapsed, after the substrate temperature reached the required value. The films were evaporated in a residual gas pressure of less than 2×10^{-5} torr, and the source material was either New Metals and Chemicals "Electronic grade" CdS powder, or A.E.I. "Ultra Pure" CdS This was evaporated from a tubular quartz crucible overwound with a platinum heater, and the source temperature was also monitored and controlled by a Honeywell control unit. Two additional source crucibles were inserted, to evaporate cadmium and sulphur independently and a filament was included for the coevaporation of doping metals. The rate of evaporation depends on the source temperature, and temperatures between 600^{o}C and 800^{o}C were used. The thickness of the CdS films was monitored by an AT cut quartz crystal located on the substrate holder, adjacent to the substrates[28]. The crystal monitor was calibrated by an optical interferometer, as a function of frequency change against thickness of deposited CdS.

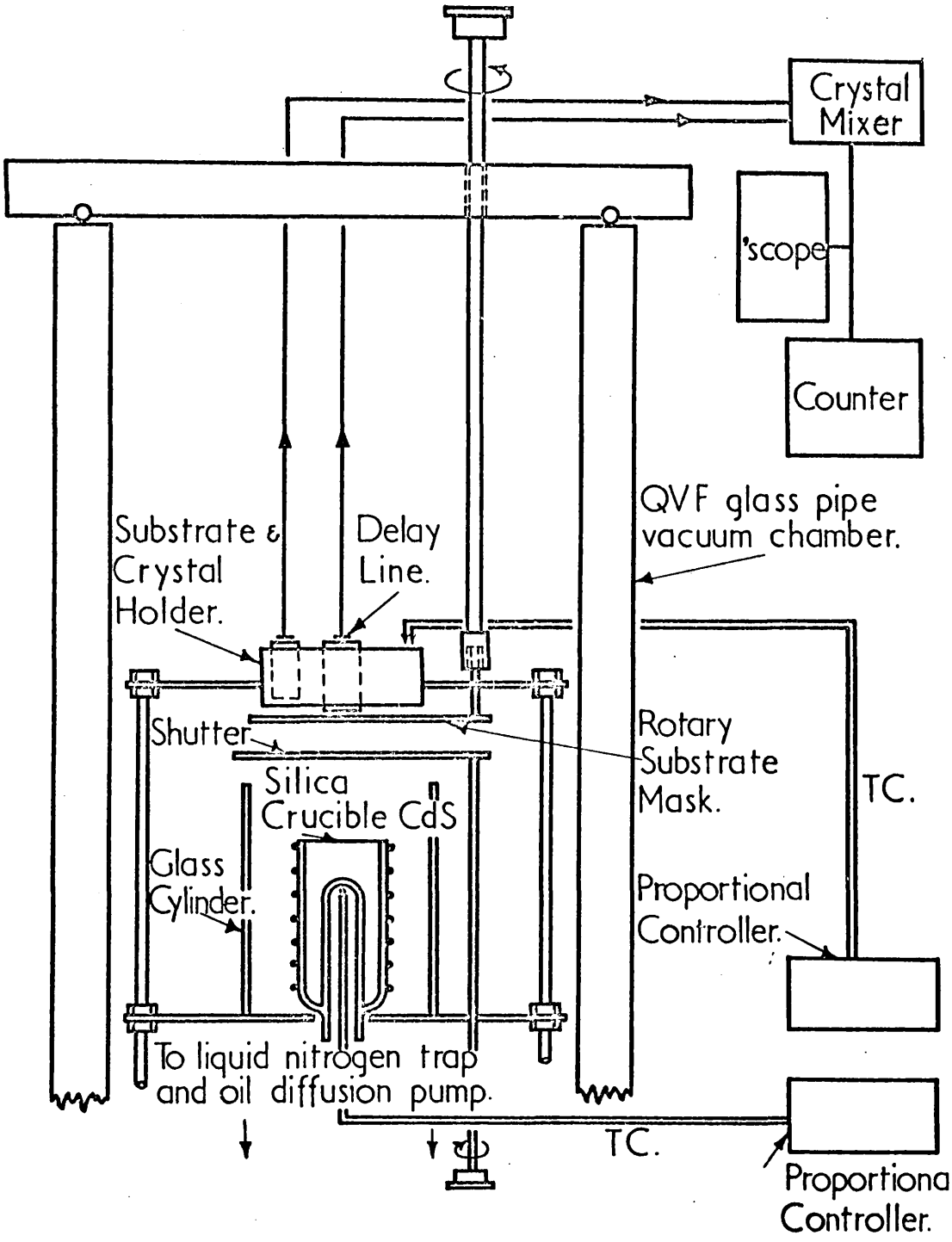

FIG. 8. SCHEMATIC DIAGRAM OF THE CdS DEPOSITION APPARATUS.

Single crystal sapphire rods, 1.0cm in diameter, and 2.5 cm long were used as substrates. These rods were oriented with the c-axis parallel to either the rod diameter or the geometric axis. After intensive chemical cleaning in "aqua regia" and alcohol vapour, the rods were inserted into the substrate holder. Metal layers, usually gold, were deposited on the sapphire rods, before the deposition of CdS.

The substrate holder could be tilted, so that the angle of incidence of the CdS vapour beam on the substrate could be varied, in order to produce shear transducers.

Longitudinal transducers were made by evaporating CdS at 600°C or less, and doping with silver or sulphur as required, on to a substrate at 200°C. Shear transducers were fabricated as double layers of CdS, with the vapour beam at 40° to the substrate. The bottom layer of highly conducting material was deposited at a rate in excess of 0.1μ/min, and with a source temperature of 700°C, and coevaporating cadmium at 240°C, on to a substrate at 100°C. The top layer, of high resistivity material, was evaporated at 600°C, with coevaporation of sulphur at 110°C, on to the substrate at 200°C.

2.3 Transducer Theory

2.3.1 Introduction

The analysis presented here was carried out to predict the behaviour of evaporated CdS transducers resonant in the frequency range 500 MHz to 10 GHz. The bandwidth and insertion loss characteristics of piezoelectric transducers are usually calculated from equivalent circuits, in which the mechanical elements are transformed into electrical elements[32,46]. The treatment given here does not use an equivalent circuit for the transducer. Starting from the equations of state for a piezoelectric medium, the impedance represented by the transducer is evaluated, by considering the properties of the acoustic waves excited in the transducer by an applied field. This analysis is based on work by Greebe[33], and the system considered is shown in figure 9.

The transducer layer is sandwiched between two metal layers, so that an electric field can be developed perpendicular to the substrate. The thickness of the metal layers is comparable with a wavelength, at the frequencies of interest, and they therefore have an effect on the transducer

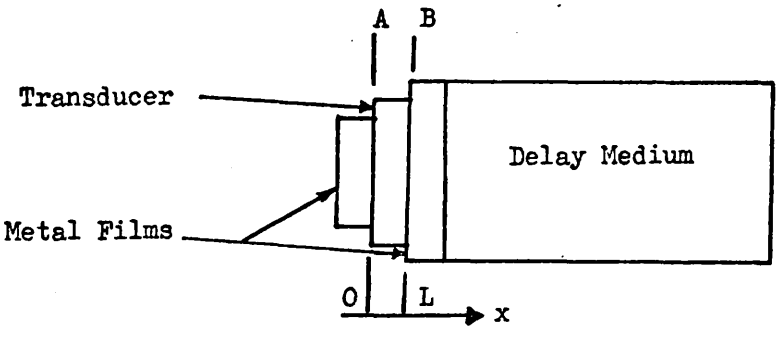

Figure 9 Transducer on Delay Line

response. The acoustic load on each side of the transducer was evaluated by treating the metal films and the delay medium as acoustic transmission lines. Digital computation was used to calculate the transducer impedance and insertion loss as functions of frequency.

2.3.2 Assumptions

a) The transducers are considered to be uniform and homogeneous in structure. In practice, it was found that the evaporated transducers were very uniform in thickness, and that the same conversion efficiency (within the limits of experimental error) could be obtained at different points on the same transducer. The degree of structural order is a function of thickness (see section 2.5.2), and transducers more than 1 μ thick are quite highly ordered.

b) It is assumed that mechanical losses in the transducer and metal layers can be ignored. Extrapolation of lower frequency measurements in CdS, suggests that the acoustic loss at 1 GHz is around 80dB/cm.[69] It can be shown from the following calculations, that this loss in the transducer becomes important, only if there is a gross impedance mismatch between the transducer and its mechanical load, a situation which is not considered here. Extrapolation to higher frequencies of acoustic loss measurements in metals made at 10 to 40 MHz[46], assuming that the loss increases as the square of the frequency, suggests that the loss at 1 GHz is of the order of 1dB/μ. In practical transducers, the behaviour of which is to be compared with the predictions of the following theory, the metal layers were normally less than 0.5μ thick, and so mechanical losses can

be ignored.

The absence of mechanical loss implies that all the mechanical impedances are wholly real, and all the propagation constants are wholly imaginary. The media are also considered to be non-dispersive.

c) The delay medium is considered to be infinite. These calculations were performed to make comparisons with transducer insertion loss measurements made by a pulse echo technique, in which pulses shorter than the round trip delay time were used. It is not necessary therefore to consider a reflected wave in the delay medium, at the metal delay medium interface.

d) Wave propagation in the transducer is considered to be one dimensional, so that the equations of state can be written accordingly.

2.3.3 Acoustic Waves in the Transducer

The piezoelectric equations of state are

$$T = c.S - e.E \qquad 1$$

$$D = e.S + \varepsilon.E \qquad 2$$

where T is the stress, S is the strain, E is the electric field strength, D is the electric displacement, c, e and ε are the appropriate elastic, piezoelectric and dielectric constants. D and E are parallel to the x direction.

The strain S is given by

$$S = \frac{\partial u}{\partial x} \qquad 3$$

where u is the particle displacement, and variations in T,S,D and E occur in the x-direction.

If the transducer is of high resistivity material, interaction with free carriers can be neglected, and Poisson's equation reduces to

$$\frac{\partial D}{\partial x} = 0 \qquad 4$$

Newton's second law gives

$$\frac{\partial T}{\partial x} = M \cdot \frac{\partial^2 u}{\partial t^2} \qquad 5$$

where M is the mass density of the transducer. These form a set of linear equations, and the solutions are considered to be plane waves with space and time dependence of the form

$$\exp\,(j\,(kx - \omega t)\,). \qquad 6$$

Combining equations 1 to 6 and rewriting them gives

$$T \quad -jk.c.u + e.E = 0 \qquad 7$$

$$jkD \quad = 0 \qquad 8$$

$$D \quad -jk.e.u - \varepsilon.E = 0 \qquad 9$$

$$jkT \quad +\omega^2 M.u = 0 \qquad 10$$

Equations 7 to 10 are four homogeneous equations in four unknowns. A non-trivial solution exists if the determinant of the coefficients is zero.

$$\begin{vmatrix} 1 & 0 & -jkc & e \\ 0 & jk & 0 & 0 \\ 0 & 1 & -jke & -\varepsilon \\ jk & 0 & \omega^2 M & 0 \end{vmatrix} = 0$$

$$\therefore jk\varepsilon c\,(1 + K^2).\,(k^2 - {}^{\omega^2 M}/_{c(1 + K^2)}\,) = 0 \qquad 11$$

where $K^2 = \frac{e^2}{\varepsilon.c.}$ is the electromechanical coupling constant.

The solutions given by equation 11 are

$$k = 0$$

$$k = \pm \left(\frac{\omega^2 M}{c(1 + K^2)}\right)^{\frac{1}{2}}$$

$$= \pm \omega/v_s \, (1 + K^2)^{\frac{1}{2}}$$

since the acoustic velocity $v_s = \sqrt{c/M}$

The solutions correspond to two acoustic modes, one propagating in the forward or positive x direction, and the other in the reverse or negative x direction, and a uniform electromagnetic mode. None of these modes is being attenuated, and since $K^2 << 1$ in CdS and other piezoelectric semiconductors, the dispersion of the piezoelectrically coupled waves is small. The forward and reverse acoustic modes, and the uniform mode, are denoted by the subscripts 1, 2 and u respectively.

2.3.4 Effect of Free Carriers on Acoustic Propagation

If free carriers are present in the transducer lattice, the equations 1 to 5 no longer describe the conditions. The equation of charge continuity

$$\frac{\partial J}{\partial x} = q \cdot \frac{\partial n_s}{\partial t} \qquad 12$$

and the current $J = q.\mu. (n_o + n_s).E + q.D_n \frac{\partial n_s}{\partial t}$ 13

must be introduced. n_s is the space charge density, n_o the mean electron density, μ the carrier mobility, D_n the diffusion constant, and q the charge on an electron.

Poisson's equation becomes

$$\frac{\partial D}{\partial x} = -qn_s \qquad 14$$

The same method of algebraic solution for k gives five solutions; a uniform mode and two acoustic modes as before, and two carrier modes. Greebe [33] has shown that carrier modes are heavily damped, and may be neglected when $\omega << \omega_D$. In CdS thin films, at the lower microwave frequencies, this condition applies, because of the low carrier mobilities (section 2.5.2).

The propagation constants of the acoustic modes, when diffusion effects can be neglected, are

$$k_1 = -k_2 = {}^{\omega}/_{v_s} \left(1 + {}^{jK^2}/\left(\frac{\omega_c}{\omega} + j\right)\right)^{\frac{1}{2}} \qquad 15$$

If the conductivity is large, $\omega_c = {}^{\sigma}/_{\varepsilon}$ is large, and the dispersion and coupling are small. If $\omega_c > \omega$ the conduction current in the transducer is greater than the displacement current. ω and ω_c become comparable in CdS at microwave frequencies, when the resistivity is $10^3 \Omega$ cm or less. Qualitatively, $\omega_c > \omega$ means that the electrons can move fast enough to cancel out the piezoelectric field, and inhibit the transducer action. The piezoelectric field is "shorted" by conduction.

2.3.5 Transducer Input Impedance.

The schematic representation in figure 10 is used in the discussion.

The metal films are represented by transmission line equivalent circuits, and the delay medium, which is effectively infinite, is represented by its characteristic acoustic impedance. A series resistance R_c is included to account for contact effects. No contact capacitance is included, because the depletion layer set up between a metal and a semi-

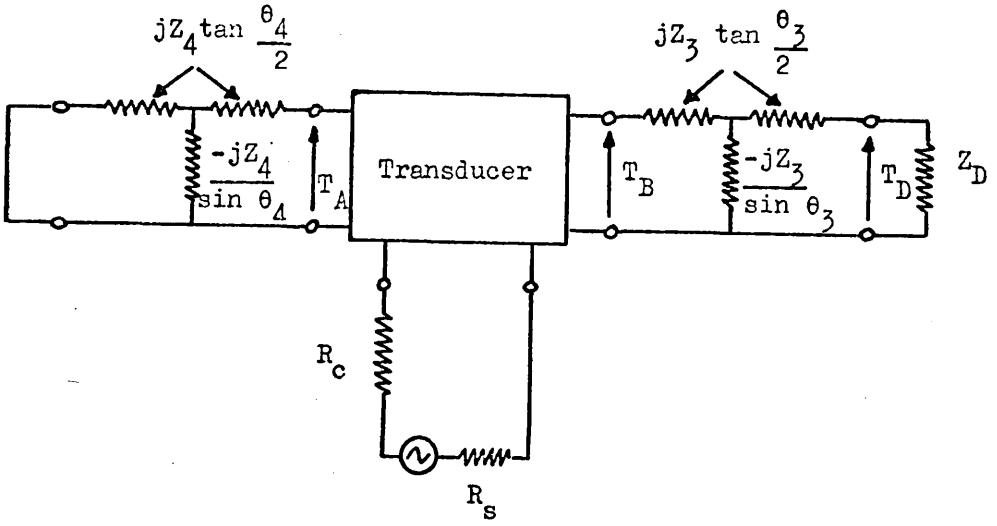

Figure 10 Schematic representation of transducer

conductor with free carriers is of the same order of width as a resonant transducer at microwave frequencies.[34] This effect is therefore more accurately represented by a double layer transducer with layers of different resistivity, than by a simple series capacitance. A depletion layer is of high resistivity, and so if the transducer itself is made of high resistivity material the capacitance can be ignored (page 93).

The total voltage V across the transducer is given by

$$V = E_u.L + \sum_{i=1}^{2} . \int_0^L E_i . e^{jk_i.x} \, dx,$$

where L is the transducer thickness, and i = 1 or 2.

$$\therefore V = E_u.L + \sum_{i=1}^{2} (E_i . (e^{jk_i.x})/jk_i) \Big|_0^L \qquad 16$$

Substituting equation 10 in 7 gives

$$T_i + jkc . \frac{jk}{\omega^2 M} . T_i + eE_i = 0$$

$$T_i = -e.E_i/(1 - \frac{k_i^2 c}{\omega^2 M}) \qquad 17$$

An expression must be derived for the current flowing in the transducer.

Maxwell's equations give

$$\text{curl } H = J + \frac{\partial D}{\partial t}$$

$$\text{div (curl } H) = 0$$

$$\therefore \text{ div } (J + \frac{\partial D}{\partial t}) = 0 \qquad 18$$

Equation 18 is valid for the whole system of transducer, electrodes and leads, and within the transducer, the equation is valid for each mode of propagation.

$$\therefore \frac{\partial}{\partial x} (J_i + \frac{\partial D_i}{\partial t}) = 0 \qquad 19$$

since propagation is one dimensional.

For any mode which has a dependence $e^{jk_i.x}$ on x, equation 19 leads to

$$j.k_i (J_i + \frac{\partial D_i}{\partial t}) = 0$$

$$\therefore \text{ either } k_i = 0 \text{ or } (J_i + \frac{\partial D_i}{\partial t}) = 0$$

For the acoustic modes $k_i \neq 0$, so $(J_i + \frac{\partial D_i}{\partial t}) = 0$.

but for the uniform mode $k_i = 0$,

hence $$(J_u + {}^{\partial D_u}/_{\partial t}) \neq 0$$

The external current I is therefore carried by the uniform mode.

$$\therefore \qquad I = A (J_u + \frac{\partial D_u}{\partial t}) \qquad 20$$

where A is the active area of the transducer.

From equations 2 and 5, $D_u = \varepsilon.E_u$

Also $J_u = \sigma.E_u$,

where σ is the conductivity of the transducer material.

$$\therefore \quad I = A\,(\sigma - j\omega\epsilon).E_u \qquad 21$$

The negative sign in equation 21 arises from the sign convention chosen in equation 6, where the variation with respect to time is $e^{-j\omega t}$. The transducer impedance $Z = V/I$ is obtained from equations 16 and 21. It is necessary therefore to express E_i in equation 16 in terms of E_u, which is done by using equation 17, and the boundary conditions, to express T_i in terms of T_u.

2.3.6 Boundary Conditions.

Acoustic propagation velocities in the positive x direction are considered positive, and in the negative x direction are considered negative.

At the interface A in figure 9.

$$T_1 + T_2 + T_u = T_A \qquad 22$$

The continuity of particle velocity $v = \frac{\partial u}{\partial t}$, at a slip free boundary, requires that

$$v_1 + v_2 = v_A \qquad 23$$

Since mode 2 is propagating in the negative x direction $v_2 = -T_2/Z_0$, where Z_0 is the acoustic impedance of the transducer medium. If the medium on the negative x side of A was infinite, then the transmitted signal would clearly propagate in the negative x direction.

Hence $v_A = -T_A/Z_A$

$$\therefore \frac{T_1}{Z_0} - \frac{T_2}{Z_0} = -\frac{T_A}{Z_A} \qquad 24$$

Similarly at interface B

$$\frac{T_1}{Z_0} \cdot e^{jk_1L} - \frac{T_2}{Z_0} \cdot e^{jk_2L} = \frac{T_B}{Z_B} \qquad 25$$

$$- T_1 \cdot e^{jk_1L} + T_2 \cdot e^{jk_2L} + T_u = T_B \qquad 26$$

By eliminating T_A and T_B from equations 22 to 26, T_1 and T_2 can be expressed in terms of T_u. Z_A and Z_B can be evaluated by means of the equivalent circuits given in figure 10.

2.3.7 Transducer Insertion Loss

Due to leakage resistance and contact effects, there are two aspects to the evaluation of transducer insertion loss. There is loss due to reflection from the transducer, and loss due to internal dissipation. The power absorbed by the device is determined from a knowledge of the input impedance, by calculating the reflection coefficient W, of the transducer, with respect to the impedance of the energising system.

Hence $P_{absorbed} = P_{incident} \times (1 - |W|^2)$

The fraction of the absorbed power which is converted into acoustic power is obtained by evaluating the ratio $P_{acoustic}/P_{absorbed}$.

The transducer insertion loss which is actually measured is

$$\frac{P_{acoustic}}{P_{absorbed}} \times \frac{P_{absorbed}}{P_{incident}} = \frac{P_{ac}}{P_{ab}} \times (1 - |W|^2) \qquad 27$$

The power absorbed by the transducer is I^2. Re (Zin)

$$\therefore \quad P_{absorbed} = \frac{V^2}{|Zin|^2} \times \text{Re (Zin)}$$

The acoustic power into the delay medium is $\frac{T_D^2}{Z_D} \times A$, where T_D is the stress produced in the delay medium, at the boundary. Hence the transducer insertion loss in dB is

$$10.\log_{10}(P_{ac}/P_{incident}) = 10.\log_{10}\left(\frac{T_D^2 . A}{Z_D} \times \frac{|Zin|^2}{V^2 . Re(Zin)} \times (1 - |W|^2)\right)$$

T_D is evaluated in terms of T_B, and T_B can be expressed in terms of V from equations 16, 17 and the boundary conditions.

It can be shown that when there is no contact resistance, and the transducer is insulating, (i.e. $R_c = 0$ and $\sigma = 0$) the ratio P_{ac}/P_{ab} is unity. The above theory can be reduced to the equations normally used to describe transducer equivalent circuits (Appendix A1).

2.3.8 Computer Programme

An Algol computer programme was written to calculate the theoretical performance of transducers. Most of the computations were carried out for CdS transducers, with gold electrodes, on sapphire delay rods, since this was the structure of most experimental transducers. The data used was taken from published measurements of the basic acoustic and electrical constants of single crystal CdS[35], sapphire[36] and metals.[32]

Longitudinal CdS transducers were studied principally, and the appropriate electromechanical coupling constant is designated K_t, where

$$K_t^2 = \frac{e_{33}^2}{C_{33}^D . \varepsilon_{33}^S}$$

Mason[2] has demonstrated that this is the appropriate coupling constant for a thin plate, resonant in its thickness mode, with the 3 axis (the

c-axis in CdS) parallel to the thickness. This relationship is valid when there is no strain in the plane of the plate perpendicular to the 3-axis.

2.3.9 Theoretical Transducer Behaviour

In this section results are presented for various transducer configurations. A shortened notation is used to describe the structures; for example, a longitudinal CdS transducer, tin bonded to a sapphire delay rod, with an aluminium backing layer is described in the notation as Al-CdS-Sn-Al_2O_3 (long.) Computed results are presented for the condition in which the transducer is energised directly from a 50Ω system, and not through any tuning or matching network. This was done in order to investigate the performance of the transducer alone, since a tuning system has a bandwidth which would be superimposed on the transducer response.

In figure 11 is given the calculated insertion loss versus frequency characteristic for the system CdS-Au-Al_2O_3 (long.) i.e. without a backing layer. The CdS transducer and gold layer were 0.5λ thick at 1 GHz (= f_o, where λ is the acoustic wavelength). The transducer was considered to be insulating, and to have no contact resistance, and the acoustic beam area used was 3.10^{-6} m^2. It is significant that the minimum insertion loss of 18dB occurs at 500 MHz, which is where the transducer is 0.25λ thick. The shape of the harmonics is very similar to that of the fundamental, and the minima occur at frequencies where the transducer is nλ thick (where n is an integer). In this condition there is minimum stress at the transducer metal layer interface. Below $0.5f_o$

the insertion loss increases as the frequency falls. The bandwidth is about 40% at $0.5f_o$ and consequently very broad bandwidths will be available from transducers which are fundamentally resonant at higher frequencies (say X band). It was shown in sections 2.3.3 and 2.3.4 that the dispersion of the coupled acoustic waves is insignificant, and consequently the transducer response is determined by the mismatches between the transducer and the electrical energising system, and between the transducer and its acoustic load. The latter mainly determines the shape of the response.

The longitudinal acoustic impedances of CdS, gold and sapphire are $20.7.10^6$, $62.5.10^6$ and $45.2.10^6$ $kgm/m^2sec.$ respectively. Gold is clearly a very poor acoustic match between transducer and delay rod, and if tin, with longitudinal impedance of $24.6.10^6$, is used in place of gold, the transducer response becomes single peaked, with the peak close to the $\lambda/2$ frequency. The response of CdS-Au-Al_2O_3 (Shear) has the same shape as figure 11, for the same conditions, but the level of insertion loss is different, since the coupling constant K_{15} is different from the constant K_t.

In figure 12 is shown the effect of varying the gold bond thickness in the system of figure 11, over a limited frequency range. The minimum insertion loss is obtained by using a gold bond 0.5λ thick, but the difference in shape produced by varying the gold bond from 0λ to 1.0λ is very small. A subsidiary resonance begins to appear at f_o as the gold bond thickness is increased. If the bond is made of a material which is a good acoustic match between transducer and delay rod, varying the thickness has a marked effect on the shape of the response.

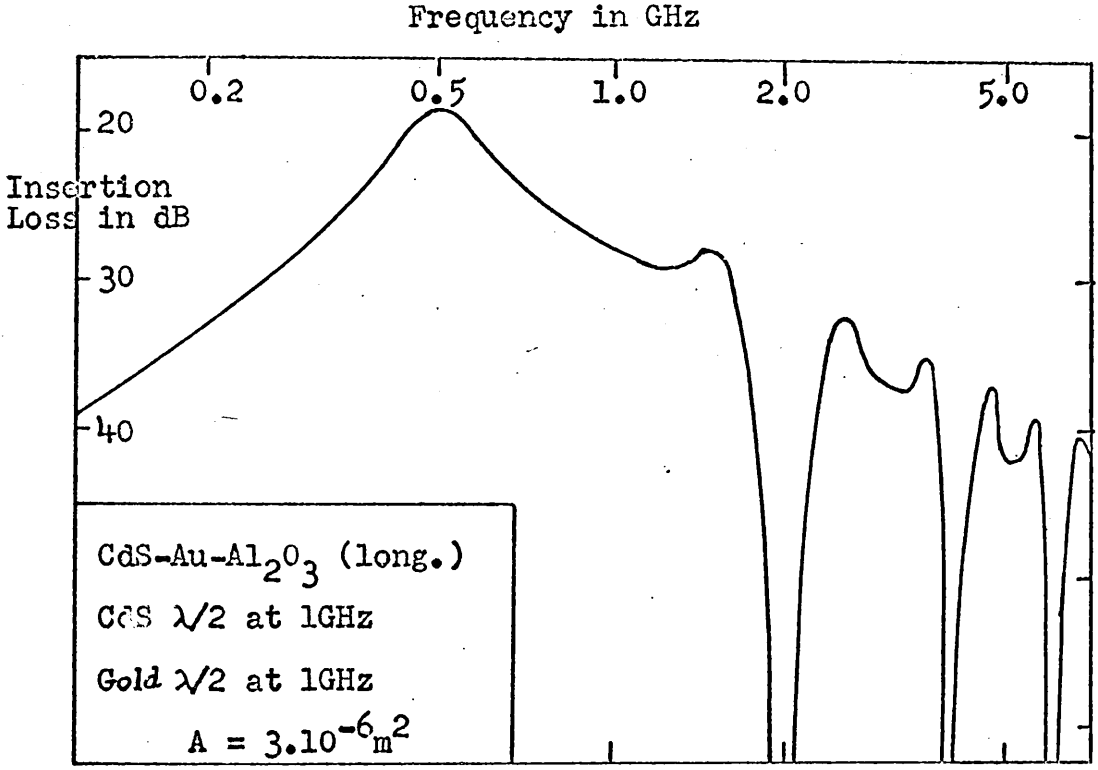

Figure 11. Untuned frequency response of a longitudinal CdS transducer.

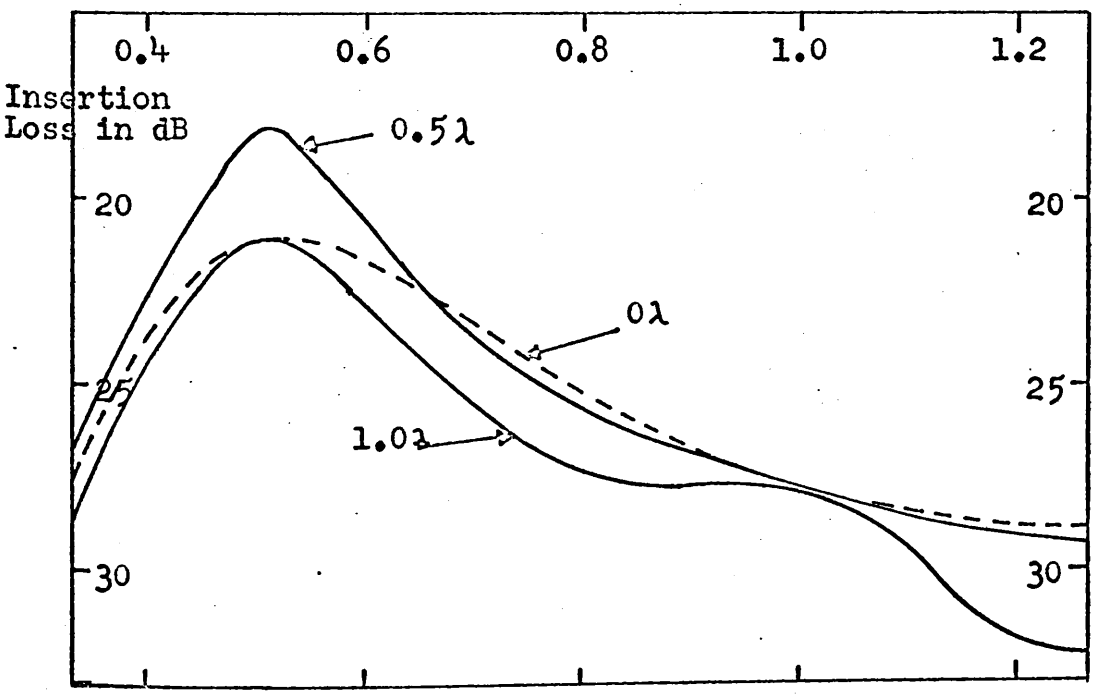

Figure 12. Effect of varying bond thickness on the frequency response of a longitudinal CdS transducer.

The thickness of the bond layer does, however, have a significant effect on the phase response of the transducer. The phase of the stress launched in the delay rod with respect to the voltage applied to the transducer, for CdS-Au-Al_2O_3 (long.) is given in figure 13, for a number of bond thicknesses. For signal processing, it is essential that the phase response of the device should be either constant, or smoothly varying, with frequency. A smooth variation in phase can be removed by the use of a corrective electrical network. In figure 13, for most bond thicknesses, there are regions, up to 400 MHz in width, in which the phase response varies smoothly. By using different bond and backing materials the phase response can be modified, and the phase response for the structure CdS-Sn-Al_2O_3 (long.) is shown in figure 14. This has a smoothly varying response, which is particularly good for the case of a 0.5λ bond.

A transducer acts as an impedance transformer between the acoustic and electrical systems. Since it is a passive device, it can be argued that it has a reciprocal conversion efficiency between the two systems.

Figure 15 shows that a backing layer, which is a significant fraction of a wavelength, has a marked effect on the response of a transducer. The response is for the structure Au-CdS-Au-Al_2O_3 (long.) with a 0.5λ gold bond, and the effects of gold backing layers of 0.25λ and 0.5λ are shown. Although the overall shape of the responses with backing layers, is very similar to that for the unbacked case, the whole response has been shifted down in frequency. Increasing the backing

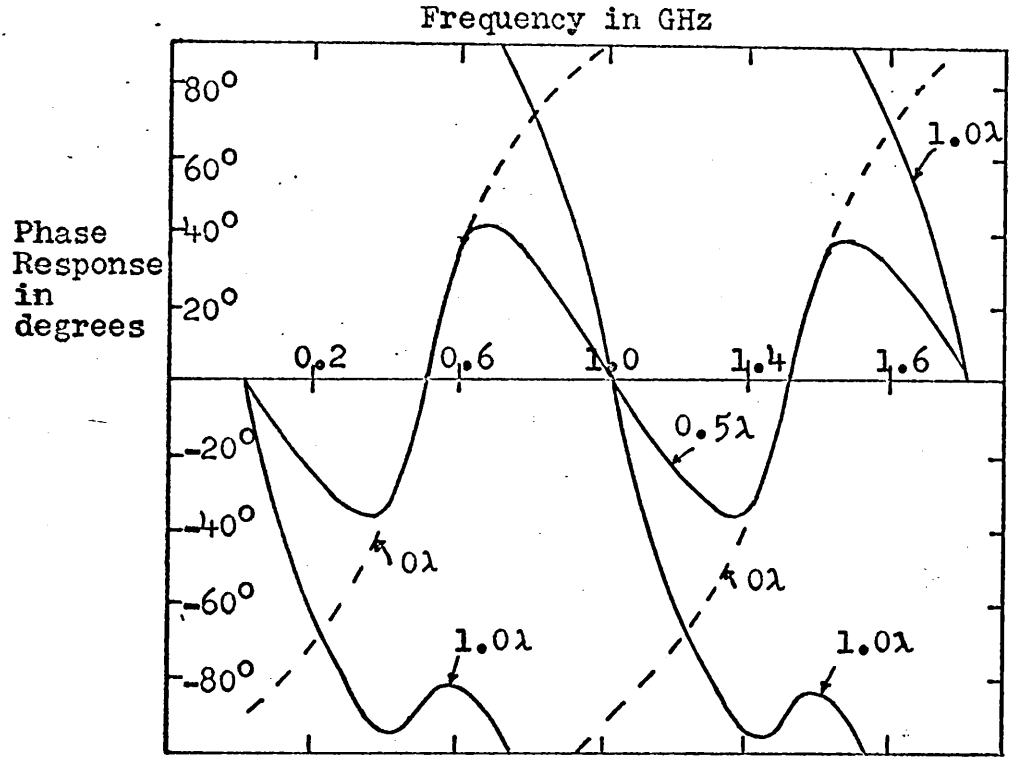

Figure 13. Phase response of CdS-Au-Al_2O_3 (long.) for variable bond thickness.

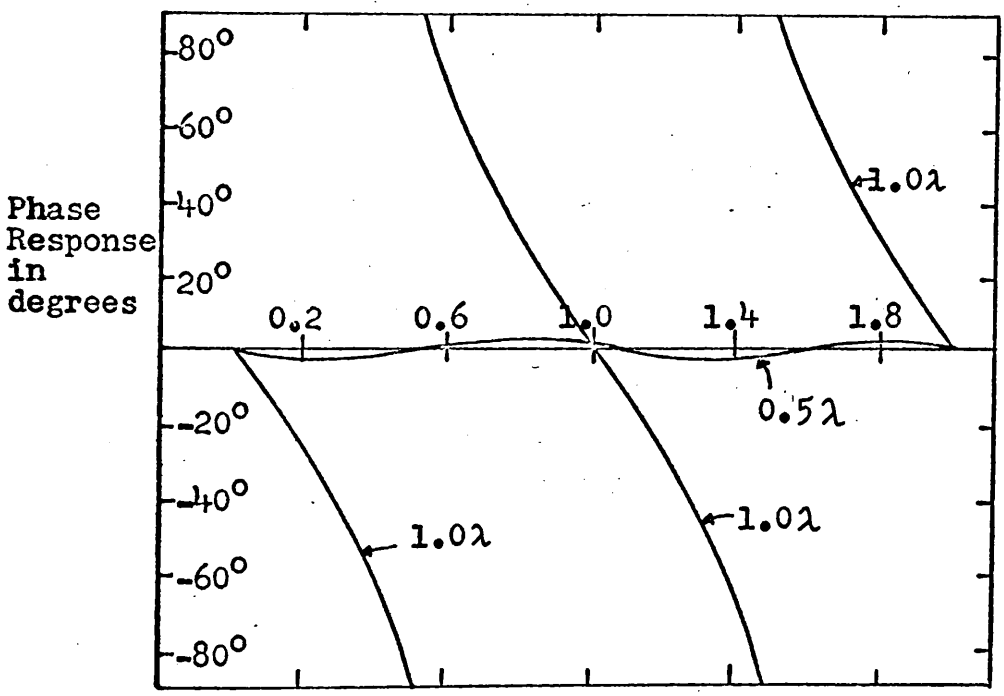

Figure 14. Phase response of CdS-Sn-Al_2O_3 (long.) for variable bond thickness.

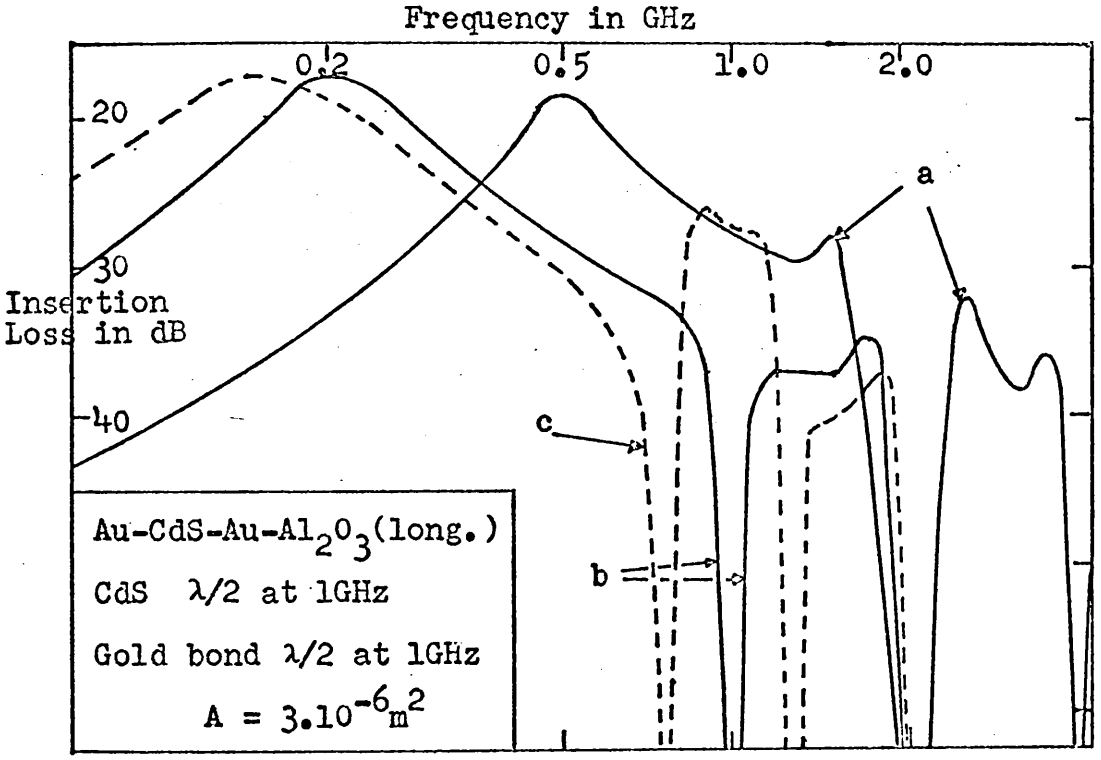

Figure 15. Effect of backing layer on transducer response, a) 0λ, b) 0.25λ, c) 0.5λ thick layer.

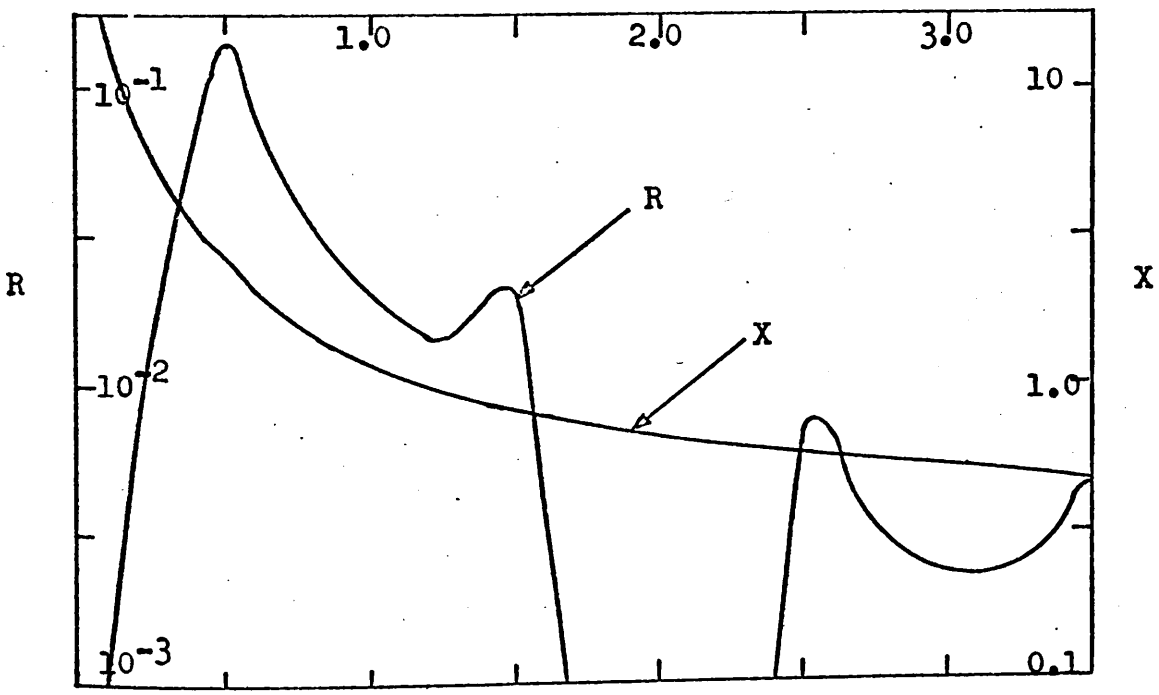

Figure 16. Input impedance (R + jX) of unbacked CdS transducer with insertion loss shown in Fig. 11.

thickness shifts the response even further down in frequency, so that a 1.0λ thick backing layer reduces the frequency of minimum insertion loss to 0.1 f_o.

Basically, this transducer analysis evaluates the input impedance, and figure 16 gives the series impedance (R + jX), presented by the transducer whose frequency response is given in figure 11. The real part is highly resonant, and the reactive part behaves as a capacitance, except for a slight distortion at the principal ($\lambda/4$) resonant frequency. Since $K^2 << 1$, the real part of the impedance will be small, and for most of the frequency range the impedance is less than (0.1 - j2)Ω, which is a gross mismatch to 50Ω, thus accounting for the high values of insertion loss. At resonance the impedance is (0.17 - j 2.68)Ω. The transducer impedance is inversely proportional to its active area (equation 21), assuming that there is no fringing, and the active area, corresponding to the acoustic beam area used in the calculations, was 3.10^{-6} m^2. This was the nominal beam area in the experiments described below. The transducers are normally excited in coaxial mounts, in which the centre conductor has a smaller area than the transducer. In the absence of a backing layer, the centre conductor is assumed to define the active area. It should be possible to evaluate an optimum beam area to give the best matching conditions to a 50Ω system, without any electrical matching. For the conditions used to evaluate figure 11, this area was predicted to be 10^{-7} m^2. The input impedance of the same system for this area, at the $\lambda/4$ resonance is (5.1 - j 80.4)Ω . At beam areas less than the optimum value, the insertion loss is worsened, and the frequency response is flatter. The theoretical

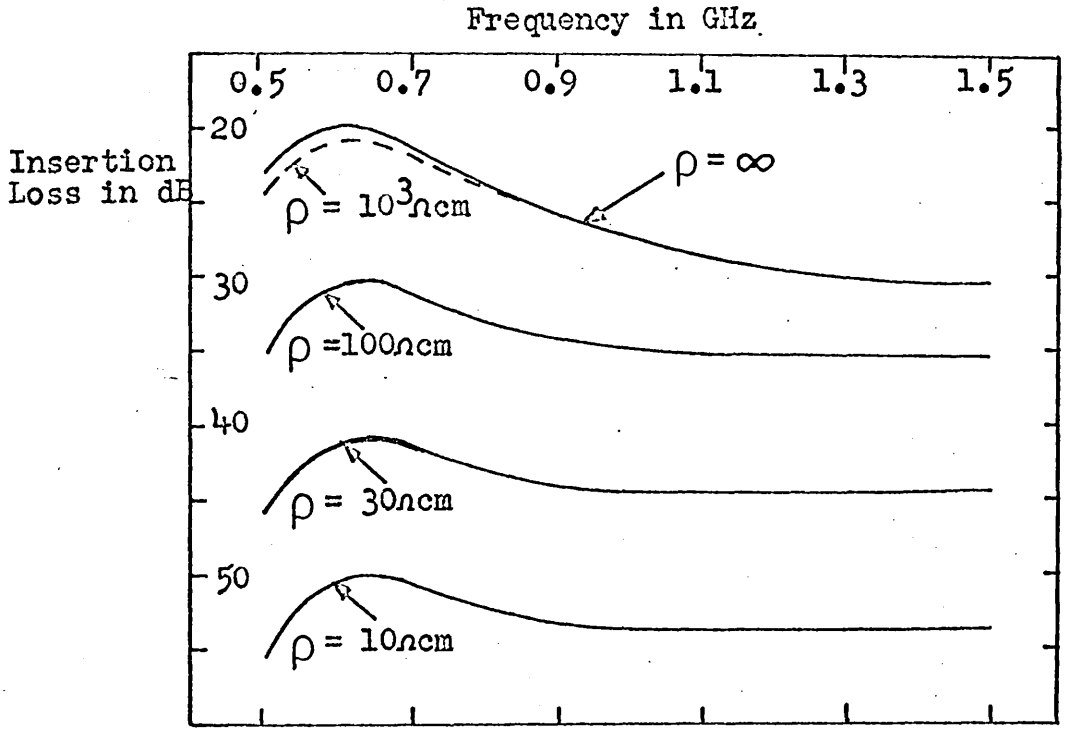

Figure 17. Effect of transducer resistivity on insertion loss.

improvement in insertion loss which can be achieved by reducing the beam area from 3.10^{-6} m^2 to 10^{-7} m^2 is 11dB, at the $\lambda/4$ frequency. As the operating frequency rises, the beam area for matching falls.

It was demonstrated in section 2.3.4 that free carriers in the transducer can inhibit its action, and will cause a conduction current to flow. The coupling to acoustic waves is reduced, and the leakage path provided by the carriers shorts out the real impedance presented by the transducer, hence the conversion efficiency is reduced. Figure 17 shows the effect of transducer conductivity on the insertion loss. When the resistivity is 10^3 Ωcm, the effect is almost negligible, and so if the resistivity is 10^4 Ωcm or higher, conduction effects can be neglected. This graph is for the structure CdS-Au-Al_2O_3 (long.), with the $\lambda/2$ frequency for CdS and gold at 1.2 GHz, and a beam area of 3.10^{-6} m^2.

If there is a series resistance in the transducer thin film metal contacts, or mounting jig, the impedance loading the energising system will be changed, and the insertion loss increased.

2.3.10 Conclusion

Since the electromechanical coupling constant of CdS is small, the impedance presented by a microwave CdS transducer is a bad mismatch to a 50Ω energising system. These transducers therefore tend to have high insertion losses, if operated without a matching system, but do have large fractional bandwidths. The shape of a transducer frequency response is determined mainly by the acoustic impedances of the materials mechanically loading the transducer. Several factors, such as the electromechanical coupling constant, the conductivity, contact resistance and active area of the transducer, affect the absolute level of the insertion loss.

2.4 Acoustic Measurements on CdS Transducers

2.4.1 Measurement Technique

Acoustic measurements were made in the frequency range 0.9 to 2.0 GHz. All the transducers were deposited on metal films on sapphire substrates. The metal was normally gold, and the sapphires were single crystal delay rods, polished flat to one quarter of a fringe of sodium light, and parallel to better than 6 seconds of arc. The transducer and delay rod were held, for acoustic wave excitation, in the 50Ω coaxial brass mount shown in figure 19. The centre conductor of the mount was an indium tipped brass post, lightly spring loaded to make contact with the transducer. Most films did not have a backing layer acting as a top electrode. The outer conductor of the mount made good electrical contact with the metal layer between the CdS and sapphire. In this configuration the electric field was perpendicular to the substrate, and parallel to the c-axis in

films deposited normal to the substrate, thus generating longitudinal waves. Pure shear waves are generated by an electric field normal to the substrate, when the c-axis of the CdS is inclined at 38.5° to the normal.

The measurement system is shown as a block diagram in figure 20. A C.W. signal generator and a travelling wave tube constituted the r.f. source, and had an available C.W. power output of 1W. The output was pulsed by a PIN diode modulator, with a pulse width of 1μsec, and a repetition rate of 1 msec. The pulses were coupled to the transducer via a three port circulator, and the reflected delayed pulses were passed, via a blanking PIN diode modulator, to a superheterodyne receiver with a sensitivity of - 90dBm. The receiver output was displayed on an oscilloscope. To obtain accurate measurements of both the transducer conversion loss, and the acoustic attenuation in the sapphire delay rod, a comparison circuit was included. A signal was tapped off the main signal generator output, via a coupler and precision attenuator (accuracy $\pm$ 1dB), passed through a PIN diode modulator providing variable delay, and returned to the main circuit via a 20dB coupler. The observed echo pattern from the transducer and delay rod decayed exponentially, and the acoustic attenuation due to the sapphire delay rod was obtained from the difference in amplitude of successive echoes. The total loss incurred in conversion from an electromagnetic to an acoustic signal, propagation in the delay medium, and reconversion to an electromagnetic signal, was measured by comparing the amplitude of the first echo with that of the incident pulse, using the comparison circuit. Hence the difference between the measurement of total loss and the acoustic loss in the delay

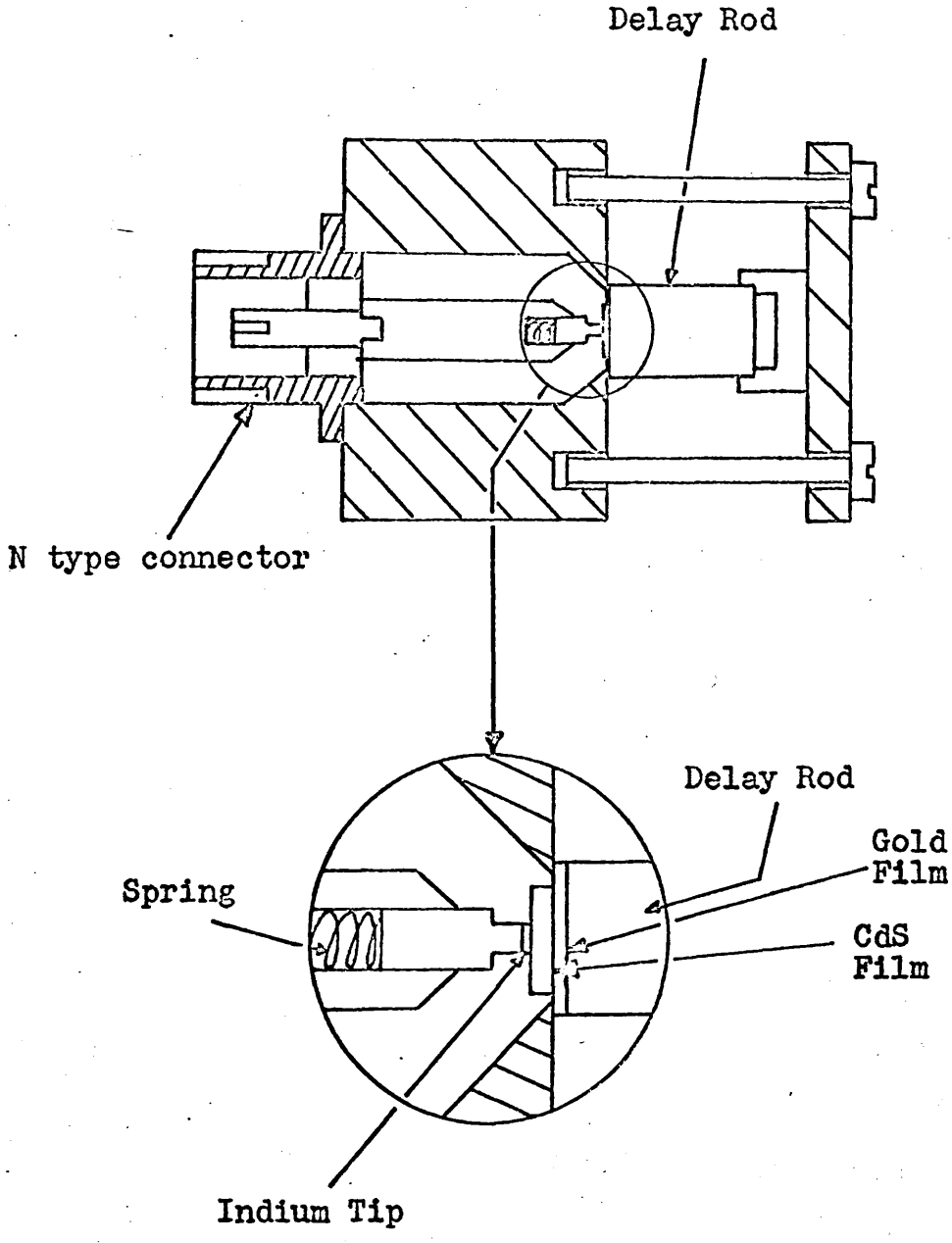

Figure 19. Transducer mount and coaxial exciter.

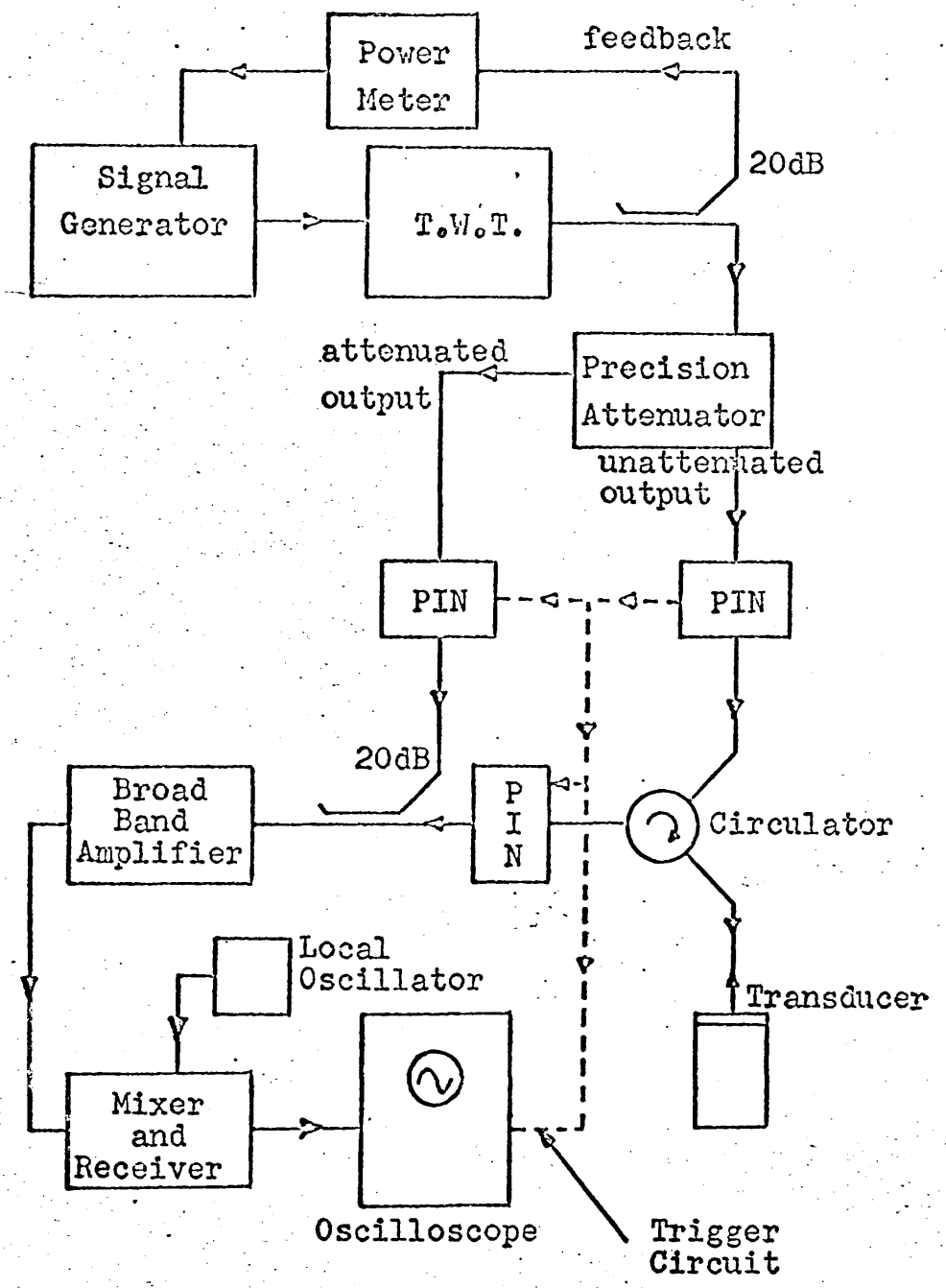

Figure 20. Schematic diagram of transducer test apparatus.

rod, is twice the one way transducer conversion loss.

2.4.2 Acoustic Loss

The acoustic loss in sapphire was measured for both shear and longitudinal waves. At room temperature the longitudinal acoustic loss, between 1 and 2 GHz was found to be very similar to the measurements published by Fitzgerald, Chick and Truell[37], for their normal specimens of sapphire. They also present lower loss measurements on samples which they claim to be almost perfectly pure, and attribute the higher loss in normal specimens to impurity scattering. The accustic loss was found by them to vary as (frequency).$^{1.7}$

De Klerk[38] has published acoustic loss measurements for shear and longitudinal waves in sapphire at 1 GHz. He observed a loss of 0.2 dB/cm and 0.6 dB/cm for longitudinal and fast shear waves respectively, at room temperature. The sapphire used in the experiments described here had acoustic losses of 0.63 dB/cm and 1.9 dB/cm for longitudinal and fast shear waves respectively, under the same conditions of frequency and temperature. The ratio of fast shear to longitudinal acoustic loss was the same as found by de Klerk[38], and the frequency dependence of the loss was found to be around (frequency)$^{1.7}$ for both modes.

2.4.3 Typical Experimental Results and Comparison with Theory

Before transducer behaviour is discussed in greater detail, the actual frequency responses of two evaporated transducers, with the structure CdS-Au-Al_2O_3 (long.), are presented in figure 21, to illustrate

the relevance of the theory. The gold bonds were 0.3μ thick, and the centre post of the coaxial mount was 3.10^{-6} m^2 in area. Both responses were measured with the transducer untuned, so that direct comparison can be made with the theory. The half wavelength resonant frequency f_o, is marked on the graphs, and it can be seen that there is reasonable agreement in shape with figure 11 over the same range of frequency. The absolute level of insertion loss for the experimental measurements is different from that predicted by the theory, which is to be expected, since the theoretical curves were evaluated using the data for single crystal CdS.

These results are fairly typical of those obtained from transducers. If the transducer has a significant conductivity, the absolute level of insertion loss is much greater, although the shape of the response is similar.

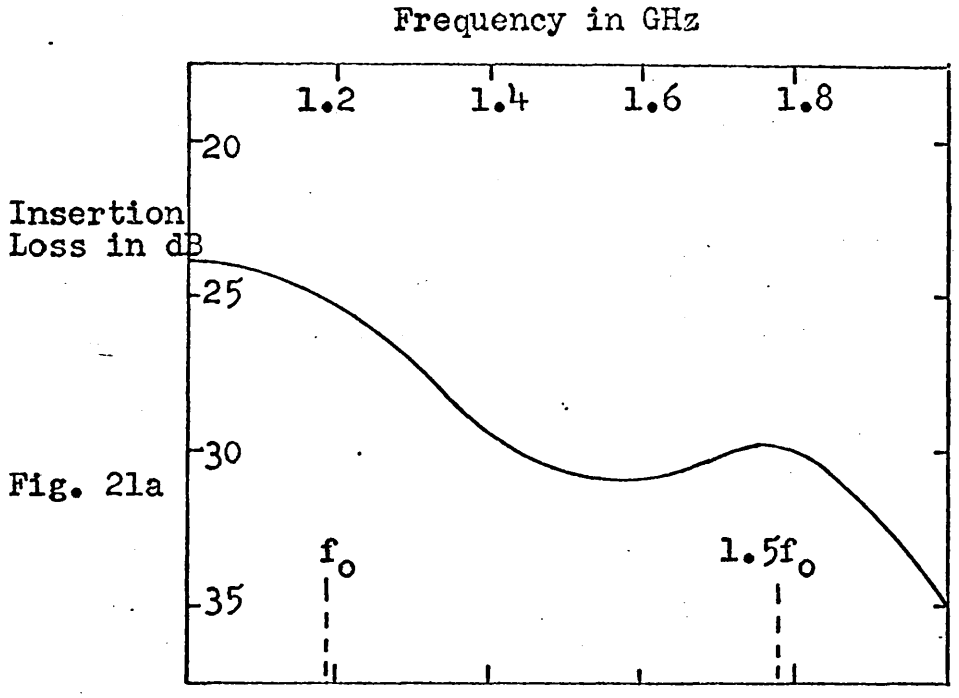

Fig. 21a

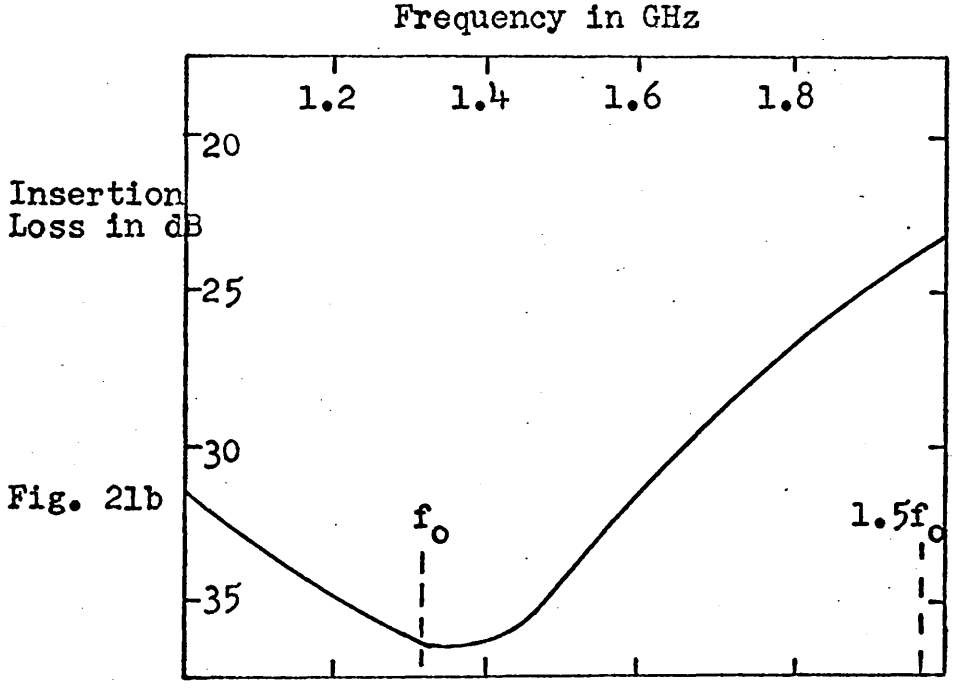

Fig. 21b

Figure 21. Untuned insertion loss against frequency for CdS transducers; a) 1.8μ thick, b) 1.65μ thick.

2.5 Transducer Properties

The measurements and discussion of transducer behaviour are presented under three headings; crystallographic structure; resistive properties and compensation techniques; and the use of transducers in microwave circuitry.

The basic properties of a CdS transducer which affect its conversion efficiency are the crystallographic structure and the resistivity. A review of the literature[28] on CdS deposition shows that with standard evaporation techniques, and using heated substrates, CdS films are deposited as hexagonal phase crystallites, preferentially oriented with the c-axis perpendicular to the substrate. The films are frequently sulphur deficient leading to low resistivities, and film resistivities ranging from 10^{-1} to 10^{12} Ω cm have been reported.[28] Attempts have been made to compensate for this lack of stoichiometry by coevaporation of sulphur, or metallic dopants such as silver or copper, during growth. Many post evaporation treatments are reported[28], mainly annealing procedures, and diffusion of metal compensators. The annealing procedures frequently resulted in the c-axes of many of the crystallites tilting away from the normal, so that these films could not act as single mode transducers. There are relatively few publications in which the crystal structure of CdS films is related to their behaviour as acousto-electric transducers[38] (mainly for the longitudinal mode), and only Foster has studied the structures of CdS films acting as shear mode transducers.[31]

The work described in this section, on the structural

properties of transducers, is concerned with finding suitable structures for efficient longitudinal and shear transducers, for microwave frequencies, and evolving compensation procedures to give these transducers high resistivities. The structure, and degree of order, of the evaporated CdS films were determined by X ray analysis. A new method of compensation, by thermal neutron bombardment, to introduce trapping sites in the CdS lattice, was investigated with significant results.

As demonstrated in section 2.3 the insertion losses of untuned CdS transducers tend to be high at microwave frequencies, due to the impedance mismatch between the transducer and energising system. Impedance measurements were made on transducers to investigate this effect, and any other sources of loss.

2.5.1 Crystallographic Structure of CdS Thin Films.

a) General Observations

X ray diffraction was used to structurally analyse CdS thin films. The analysis was performed by a technique which is commonly used for examining powdered specimens of crystalline material.[39] If a collimated beam of monochromatic X rays is incident upon a random polycrystalline powder, cones of diffracted X rays are produced at the appropriate Bragg angles, defined by $n\lambda = 2d \sin \theta$. (where n is an integer, λ the wavelength, d the spacing between planes, and θ the Bragg angle.) If the polycrystals have a preferred orientation, the diffracted rays comprise only segments of cones. Evaporated CdS films are known to be polycrystalline, with crystallites, usually about 1000Å in diameter,[31] which tend to grow with the hexagonal c-axis perpendicular to the substrate.

These films can then be analysed by treating them as polycrystalline powders, whose crystallites possess a preferred orientation. The natural tendency of the crystallites to grow with the c-axis perpendicular to the substrate, means that it is relatively easy to produce longitudinal CdS transducers by direct evaporation. As discussed in section 2.1, it is possible to produce evaporated shear transducers by tilting the c-axis of the CdS film at 38.5° to the substrate normal, and X ray analysis can be used to determine the required conditions for deposition of pure shear mode transducers.

CdS commonly occurs in the hexagonal crystalline form, but it can also exist in a cubic form.[40] In table 2 are given the reflecting planes, with their corresponding Bragg angles for Cu Kα radiation, and normalised integrated reflection intensities, for random powders of cubic and hexagonal phase CdS. (A.S.T.M. Index). Cu Kα radiation has two closely spaced wavelengths, and the Bragg angles are given for the lower wavelength. It can be seen that all the cubic reflections, excluding the (200) and (400), are virtually coincident with hexagonal reflections. There are, however, several hexagonal reflections which do not coincide with cubic reflections. Unless the cubic (200) and (400) reflections are observed, the cubic phase of CdS cannot be positively identified by X ray diffraction.

The principle of the diffractometer is illustrated on page 62. The detector and specimen are rotated so that the incident X ray beam, and the detector axis, are always at the same angle with respect to the substrate normal. The diffractometer thus records only the reflection from planes which are parallel to the film surface and the substrate,

Hexagonal			Cubic		
hkl	Bragg Angle	I/I_1	hkl	Bragg Angle	I/I_1
100	12.43°	75	-	-	-
002	13.20°	59	111	13.26°	100
101	14.10°	100	-	-	-
-	-	-	200	15.36°	40
102	18.28°	25	-	-	-
110	21.88°	57	220	22.02°	80
103	23.85°	42	-	-	-
200	25.48°	17	-	-	-
112	25.91°	45	311	26.04°	60
201	26.43°	18	-	-	-
004	27.17°	4	-	-	-
202	29.14°	7	-	-	-
104	30.31°	2	-	-	-
-	-	-	400	31.98°	20
203	33.36°	15	-	-	-
210	34.69°	6	-	-	-
211	35.48°	11	331	35.24°	30
114	36.10°	7	420	36.30°	10
105	37.58°	11	-	-	-
204	38.85°	1	-	-	-
300	40.19°	8	422	40.43°	30
213	41.62°	12	-	-	-
302	43.20°	8	333	43.47°	30

Table 2. Observed planes with Bragg angles and normalised reflection intensities for random powders of hexagonal and cubic phase CdS.

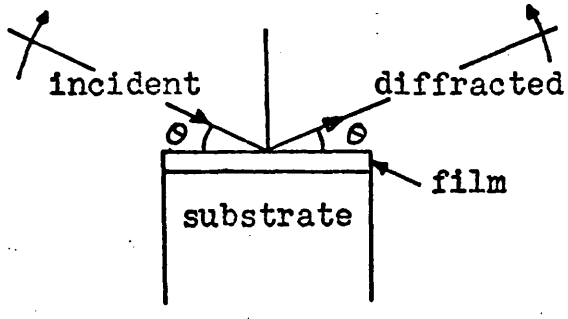

Operation of X ray diffractometer.

when Bragg's law is satisfied for these planes. The presence of reflections other than the (002) and (004) in CdS, shows that the c-axes of some of the crystallites are tilted away from the normal. This technique does not give a complete picture of how the crystallites are tilted, since reflections appear only when the crystallites are inclined such that sets of planes are parallel to the film surface. There are regions in which no reflections appear, and on which there is therefore no information. The diffractometer sweeps in one plane, perpendicular to the substrate, and so the detector axis cuts the arc of the cone of diffracted rays in only one point. This limitation can be overcome by taking glancing angle Laue photographs of the thin films. The incident X ray beam is perpendicular to a photographic plate, and the CdS film is rotated in the beam. With filtered radiation, the reflections again identify those planes which are parallel to the film surface, but since the diffracted beam is recorded in two dimensions, the whole diffracted arc is recorded, and a measure is obtained of the degree of misorientation of the crystallites.

b) Measurement Technique

The CdS films which were structurally examined were deposited on sapphire substrates, usually with gold bonding layers, so that the transducer action of the films could be observed and correlated with the crystalline structure. X ray analysis was performed on a Phillips diffractometer, with nickel filtered, Cu Kα radiation, and pulse height discrimination. Each diffraction line was scanned, and the integrated line intensity was obtained from a digital counter linked to a Geiger

counter detector; allowance being made for background radiation. With this procedure, the maximum deviation of the integrated intensity, over six successive runs, was no greater than 5%, when the reflection intensity was more than five times the background radiation intensity. Only one longitudinal CdS transducer was analysed by the glancing angle technique*, also using Cu Kα radiation.

c) Results

Measurements were made on a large number of transducers, and the following series of tables details the observations made on a representative sample of longitudinal and shear evaporated CdS transducers.

Table 3 gives the structure of six longitudinal CdS transducers, evaporated on to gold layers on sapphire substrates, with the direction of evaporation normal to the substrate, except for specimen A6 which was deposited by the coevaporation technique.** The normalised intensities of the observed diffracted lines, and the transducer thicknesses, are recorded. For comparison the normalised intensities of the diffracted lines from a random powder, and the angles between the observed planes and the (002) plane, are given. In table 4 similar information is presented for transducers in which the c-axis was bent away from the normal by oblique evaporation, at 40° to the substrate normal, and at a higher rate of deposition. These transducers generated both shear and longitudinal waves unless the axis was tilted very close to the required 38.5° (see figure 7). The observed diffraction intensities in table 4 have been

* By Miss B.R. Brown of A.E.I., Rugby.

** By Mr. R.W. Harcourt of S.T.L., Harlow.

normalised, and each divided by the normalised intensity of the same line for a random powder, so that the most predominant planes are readily distinguished. The data for transducers B4 and B7 is presented in graphical form in figure 22b to illustrate how the structure has tilted.

Several different longitudinal transducers were doped with cadmium or silver, and one of the silver doped films developed a strong subsidiary orientation with the (103) plane parallel to the substrate.

All the transducers described up to this point were deposited on gold layers, on sapphire substrates. The gold films were found to be highly oriented with the (111) planes parallel to the substrate, and frequently a subsidiary orientation with the (200) planes parallel to the substrate was found. Since this highly oriented base layer probably influences the initial growth of the CdS,[28,31] several films were deposited on other substrates, with a low rate of deposition, and the results are summarised in table 5. Aluminium substrates can produce strong misorientation, and silver can prevent the development of preferred orientation. CdS is deposited, on almost all substrates, with the (002) close packed planes parallel to the substrate. All the cubic metals used as substrates, except silver, were found to deposit with the (111) plane parallel to the substrate, and the hexagonal metals had the (002) planes similarly oriented.

In several CdS films, some diffraction lines were observed which could not be identified as belonging to either phase of CdS, or to the substrate materials. The Bragg angles are listed in table 6, and it was found that integral multiples of the interplanar spacing d,

Plane	Angle w.r.t. (002) Plane	Intensity in a Random Powder	A1	A2	A3	A4	A5	A6
			2.7μ	1.8μ	1.8μ	1.08μ	0.3μ	0.4μ
002	0°	59	59	59	59	59	59	59
004	0°	4	4.7	3.9	3.7	4.7	3.5	3.2
105	20.8°	11	-	-	-	2.5	20	0.1
104	25.4°	2	-	-	-	-	-	-
103	32.4°	42	-	-	-	1.2	64	0.4
114	39.0°	7	-	-	-	-	5	-
101	62.3°	100	-	-	-	-	27	-
100	90.0°	75	-	-	-	-	6	-

Table 3. Measured thicknesses of, and normalised reflection intensities from observed planes in, longitudinal CdS transducers. (Specimens A1 to A5 deposited by direct evaporation; A6 by coevaporation.)

Plane	Angle w.r.t. (002) Plane	Intensity in a Random Powder	B1	B2	B3	B4	B5	B6	B7
			1.5μ	2.1μ	2.5μ	3μ	9μ	11μ	18μ
002	0°	59	1	1	1	1	1	1	1
004	0°	4	1.25	0.95	0.82	1.25	1.3	0.8	1.03
105	20.8°	11	1.53	1.04	0.45	0.36	1.94	0.96	4.93
104	25.4°	2	-	-	-	-	1.75	0.3	-
103	32.4°	42	0.14	0.86	2.73	1.26	0.31	0.1	20.7
114	39.0°	7	-	1.09	-	12.4	-	-	4.53
102	43.5°	25	-	0.02	-	-	-	0.02	0.42
203	51.8°	15	-	-	-	-	0.04	-	2.1
112	58.3°	45	-	0.19	0.15	-	0.06	-	-
101	62.3°	100	0.03	-	-	-	-	-	-
302	70.6°	8	-	-	-	-	0.26	-	-
100	90.0°	75	-	-	0.11	-	-	0.01	-

Table 4. Measured thicknesses of, and reflection intensities (normalised w.r.t. intensities in a random powder) from observed planes in, obliquely evaporated CdS transducers.

corresponding to these angles, accurately gave simple combinations of the lattice constants of CdS. The intensities of the diffraction lines from these stacking faults were relatively weak.

There are several reports in the literature of a type of stacking fault, found in both thin film and single crystal CdS, in which adjacent regions have the c-axis oppositely directed.[42,43] Several films were etched with hydrochloric acid vapour, but no evidence of large scale stacking faults was seen.[44]

Figure 22a is a glancing angle Laue photograph of a longitudinal CdS transducer, 2.3μ thick, on a gold layer and sapphire substrate. The spots come from the single crystal sapphire, the two dark arcs from the gold layer and the short inner arc from the CdS. The gold lines are from the (111) and (200) planes, and the CdS line from the (002) plane. The (002) diffraction line is spread 10 to 15° on either side of the axis, indicating the spread in the orientation of the crystallites in the CdS film.

d) Discussion

When an X ray beam penetrates into a material, the radiation is scattered, absorbed or diffracted.[45] The beam intensity thus decreases with penetration, and most of the diffracted radiation comes from the upper layers of a specimen. In CdS, with Cu Kα radiation, it can be shown that 63% of the diffracted radiation comes from the 1μ layer on the surface, and that the beam intensity has decayed to 1% of its initial value on penetrating 4.7μ.

If the measurements made on specimens A1 to A5, in table 3, are examined, it can be seen that the degree of structural order increases

Substrate	Evaporation Direction	Principal CdS Planes Observed
Sapphire	Normal	002
Aluminium	Normal	002, 103
Sapphire	45°	002
Glass	45°	002
Silver	45°	All planes
Chromium	Normal	002

Table 5. Structure of CdS films deposited on non-gold substrates.

Observed Bragg Angle θ	Sin θ	Equivalent d spacing $d=n\lambda/2\sin\theta$	Composition c cubic h hexagonal	n
3.88°	0.0678	11.38n	$a_h + c_h$	0.96
7.90°	0.1374	5.61n	$2a_h + 3c_h$	5.08
11.95°	0.2071	3.73n	$2a_h + c_h$	4.02
17.01°	0.2926	2.63n	$2a_c + c_h$	6.99

Table 6. Stacking faults in CdS films.

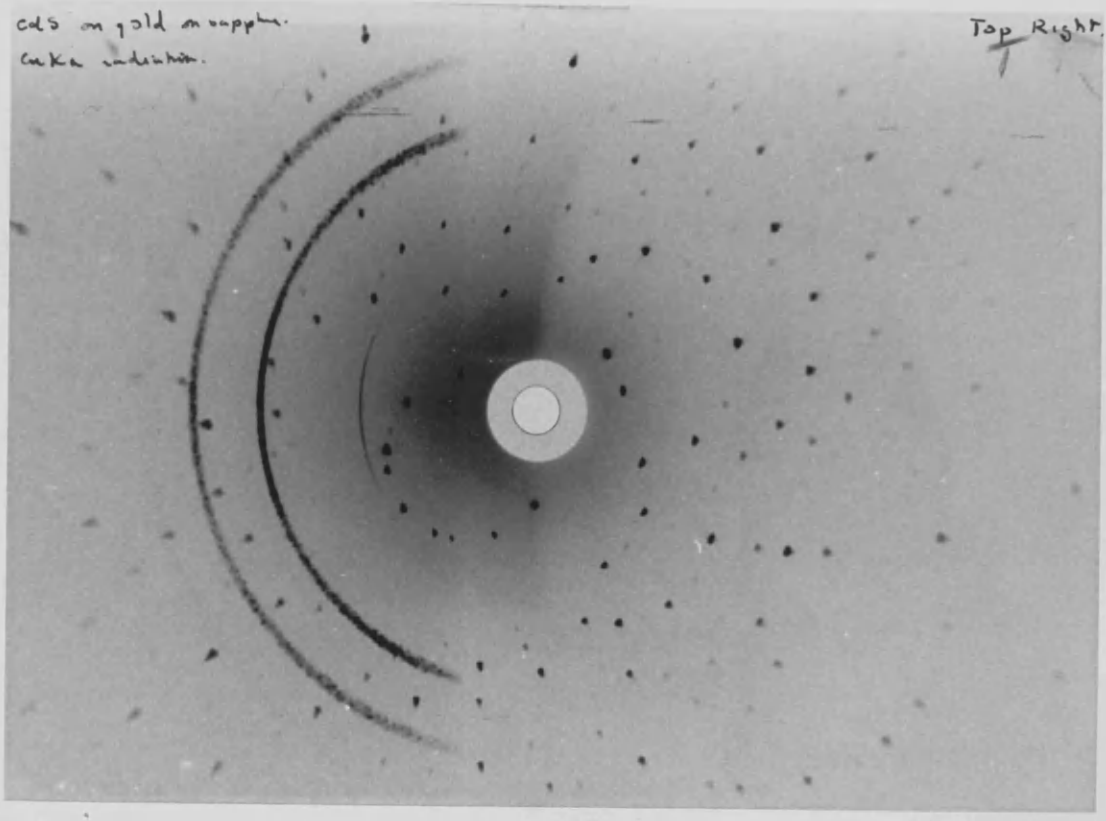

Figure 22a. GLANCING ANGLE LAUE PHOTOGRAPH OF LONGITUDINAL CdS TRANSDUCER ON A GOLD LAYER AND SAPPHIRE SUBSTRATE.

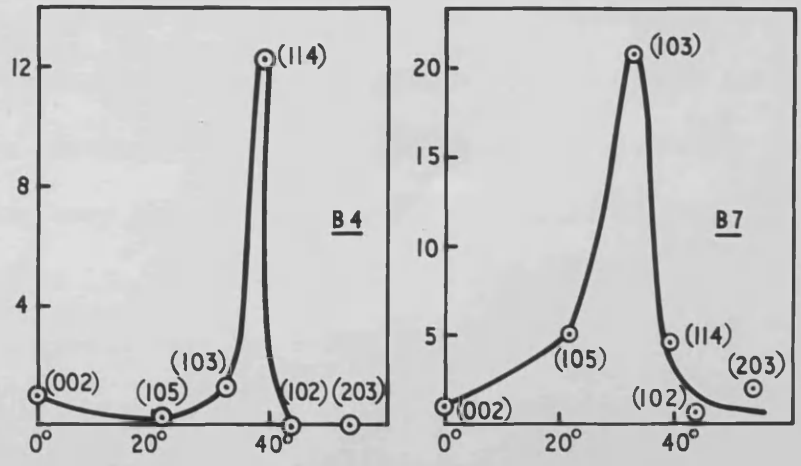

Figure 22b. X-RAY DIFFRACTION DATA FOR SPECIMENS B4 AND B7.

with thickness, and that the preferred orientation is with the (002) planes parallel to the substrate. Even the thickest film (A1), is completely penetrated by the X rays. In specimen A4, crystallites with the c-axis tilted 32.4° away from the normal are present, but the normalised intensities of the reflections from these crystallites are very weak, so that only a small proportion of the film is misoriented to this extent. No reflections are obtained from planes tilted at less than 20.8° to the (002) plane, since the possible planes (106), (107) etc. are planes with low packing densities, and so give very weak reflections. Thus the diffractometer will not detect a c-axis spread of less than 20.8°. This requires a Laue photograph (such as figure 22a), which shows that a film 2.7μ thick has a c-axis spread of ± 10 to 15°.

An interesting comparison can be drawn between the measurements on specimens A5 and A6, which were almost the same thickness, and were deposited by the direct evaporation and coevaporation techniques respectively. Specimen A5 has no preferred orientation, whereas specimen A6 has a clearly preferred orientation, with the (002) planes parallel to the substrate even at a thickness of 0.4μ. Coevaporation is clearly to be preferred for making very thin films, but has the disadvantage of a very slow growth rate (around 10Å/min) compared with the direct evaporation technique, in which the growth rate can exceed 0.1μ/min.

From the results shown in table 4, it can be seen that the growth direction of evaporated CdS films can be tilted, by evaporating at an angle to the substrate. The measurements on transducers B1 to B4 show that the c-axis tilts gradually, as the thickness increases,

towards the direction of evaporation, which was 40° to the normal for this series of transducers. The ideal shear evaporated CdS transducer has the c-axis tilted at 38.5° to the substrate normal, and would give a pronounced (114) diffraction line, since the (114) plane is at 39° to the (002) plane. A film thickness of 3μ seems to be adequate to tilt the axis to nearly 40°, but the procedure is not easy to reproduce, due to its complexity, and the need to maintain a high rate of deposition. Sometimes the c-axis develops a preferred orientation different to that required (e.g. B7), or possibly no preferred orientation at all. (e.g. B5 and B6). Figure 22b shows the distribution of crystallite orientations for specimens B4 and B7. In general, it was found that transducers which were over 4μ thick, had the c-axis tilted sufficiently well to give efficient shear wave generation, and reasonable discrimination over the longitudinal mode.

These observations differ from those of Foster[31], who found that the c-axis would only bend to 38.5° if the angle of evaporation was increased to 45°, and that it was impossible to tilt the c-axis if the substrate was a gold film. Bending of the axis was observed when the substrate film was of some other metal, or of amorphous gold.

The (004) reflection noted in tables 3 and 4 is simply obtained from the (002) plane, when n = 2 in Bragg's law, and since it gives weak reflections, the intensity cannot be measured accurately, which is also the case for other low intensity reflections.

It can be seen from table 5 that on most substrates, under most evaporation conditions, CdS films grow with the c-axis perpendicular to the substrate. Aluminium and silver are exceptions, and the effect

they have on the growth of directly evaporated CdS has been observed by other workers.[31,34] Foster[31] attributes the effect of a silver substrate to the presence of an oxide of silver, formed when the film is exposed to the atmosphere before CdS deposition. The silver film used here was exposed to the atmosphere. The measurements made on the 0.3μ thick, directly evaporated film A5, show that the nucleation of the film was not determined by the highly ordered gold substrate. De Klerk[28] has found distinct evidence of epitaxial growth in coevaporated, slow growing CdS films on sapphire substrates. The a-axes of the crystallites were aligned parallel to the c-axis of the sapphire, and the c-axes were normal to the substrate. To summarise; it appears that the crystalline nature of the substrate strongly influences coevaporated films, but rarely influences directly evaporated films, which are deposited at a higher rate.

De Klerk[28] showed, by electron diffraction, that the a-axes of the crystallites in coevaporated longitudinal CdS transducers were all parallel. The X ray diffraction technique used here does not give this information, which is not important, since the acoustic properties of CdS are the same in any direction in the basal plane.[15]

No large scale stacking faults were observed, but the faults recorded in table 6 indicate that there are regions in some films in which the normal stacking is disturbed. The diffracted lines from these faults had a low intensity, at most about ten times the background radiation level. In the transducers in which these faults occurred, no unusual acoustic behaviour was noted, and so this type of fault cannot comprise

a large part of the CdS film. Similar faults have been observed in cadmium selenide[41]. The fault with the 17.01° Bragg angle is accounted for by using the lattice constant for cubic CdS in the summation. This was the only evidence found of the formation of cubic CdS. Escoffery[40] has obtained cubic CdS in thin films by annealing at 400°C for several days. The properties of the cubic phase have not been thoroughly investigated, but cubic materials with the same Sphalerite structure ($\bar{4}3m$) as CdS, such as GaAs and InSb, have smaller electromechanical coupling constants than hexagonal materials like CdS and ZnO.[26] The presence of cubic phase CdS in thin films could then reduce the overall coupling constant.

e) Conclusions

X ray diffraction is a useful method of analysing the structure of evaporated CdS transducers, and has given information on nucleation, and preferred growth directions in CdS thin films. Suitable structures for shear mode generation by CdS transducers have been determined by comparing X ray and acoustic data. Coevaporated films have been shown to have a much higher degree of structural order than directly evaporated films.

2.5.2 The Resistivity of CdS Films and Compensation by Neutron Bombardment.

a) Introduction

As discussed in the transducer theory (section 2.3), the efficiency of CdS transducers depends upon their resistivity. It was shown that if the resistivity of the CdS was around 10^4 Ωcm, then the shunting effect of the free carriers on the acoustic radiation resistance could be ignored. This figure of 10^4 Ωcm has been quoted by other workers.[31] Evaporated CdS films tend to be non-stoichiometric, with an excess of cadmium atoms acting as shallow donors, so that the films are n-type, and can have resistivities as low as 0.1 Ω cm.[31] The excess donor electrons can be compensated by the addition of a suitable impurity, such as silver, by either coevaporation or diffusion.[11]

The recent work of Chester,[47] and Oswald and Kikuchi,[48] on compensation of bulk n-type CdS by irradiation with thermal neutrons, seemed to indicate that this method could be applied to thin films.[63] The latter investigators showed that the mechanism whereby compensating defect centres are introduced into CdS, is that associated with the recoil energy of a ^{114}Cd isotope, when it emits γ radiation. The relevant nuclear reaction is

$$^{113}Cd + {}^{n}th \longrightarrow {}^{114}(Cd)^{*} \longrightarrow {}^{114}Cd + \gamma$$

and the recoil energy of the ^{114}Cd isotope is 143 eV. From the measured values of the threshold energy for displacement of cadmium and sulphur atoms in CdS, which are 7.3 and 8.7 eV,[50, 51] respectively, and using a mean energy of displacement of 8 eV, the expected number of atomic

displacements is 9 per thermal neutron absorbed. The relative number of displacements produced by thermal neutrons, as compared with fast neutrons, has been shown by these workers to be

$$R = \frac{1.8 \cdot \phi_{th}}{\phi_f}$$

where ϕ_{th} is the thermal neutron flux, and ϕ_f the fast neutron flux. For their experimental conditions, R was 18, and the dominant effect on the resistivity was that due to the high value of atomic displacements per thermal neutron absorbed.

This investigation was undertaken to examine the effect of thermal and fast neutron irradiation on the acoustic generation of longitudinal CdS transducers, evaporated on low loss, single crystal, sapphire delay rods, operating in the frequency range 0.9 to 2.0 GHz. Since the delay rod is an integral part of the acoustic system, the dependence of the acoustic attenuation on neutron bombardment was investigated. It was considered that the large number of atomic displacements might affect the basic structural constants of the CdS, and results are presented on the effect of high energy particles on the electromechanical coupling constant (K^2) of single crystals of CdS, as a means of assessing the structural damage caused by bombardment. In view of the importance of the orientation and resistivity of the films, X ray diffraction and resistivity measurements were made, in an attempt to correlate these properties with the acoustic data. The nature of the damage induced by bombardment can be further investigated by annealing irradiated material. Therefore the CdS films and single crystal samples used in the investigation

were annealed, and their properties remeasured, after the changes caused by neutron bombardment had been assessed.

b) Experimental Procedure.

The CdS films used in these experiments were longitudinal mode transducers, deposited as described in section 2.2, on gold layers on polished sapphire substrates. The acoustic measurements were made in the frequency range 0.9 to 2.0 GHz, using the 50Ω coaxial mount, and measurement technique, described in section 2.4.

The resistivity measurements were carried out on CdS films which were typically 1 cm long and 0.5 cm in width. The films were deposited directly on to polished sapphire rods, identical to those used in the acoustic work, and a resistivity specimen was deposited simultaneously with a corresponding acoustic specimen. Current and voltage contacts were made to the film by deposition of indium strips at room temperature, the voltage contacts being 3 mm apart. With this arrangement the film resistivity was measured parallel to the surface and the contacts were ohmic within 5%.

The crystal structures of both acoustic and resistivity specimens were examined by X ray diffraction (as in section 2.5.1).

The electromechanical coupling constant was measured in bulk samples of CdS, using the resonance anti-resonance technique.[52] Figure 23a is a schematic diagram of the measurement apparatus, and the constant K_{31} was measured on bars 1 cm long and 0.3 cms wide, with both length and width perpendicular to the c-axis, as illustrated in figure 23b. The thickness of the bars was about one quarter of the width, and the a-axis of the crystal was parallel to the 0.3 cm dimension. A one micron thick

layer of aluminium was deposited on the faces perpendicular to the c-axis, so that the applied electric field was parallel to the c-axis, and the specimen was resonant in a longitudinal expander mode. The piezoelectric polarisation is thus in the basal plane, and a typical resonance anti-resonance curve is shown in figure 23c (f_R and f_A are the resonant and anti-resonant frequencies respectively). Electrical contact was made to the aluminium films with thin wires and small drops of silver paint, so that the bars were effectively freely vibrating. During measurements, the bars were in a light tight container, so that the CdS resistivity was high, and did not damp the resonance. The container was placed in an ice water mixture at $0^{o}C$, to eliminate small temperature changes which can cause the resonance to change in frequency during a measurement. The penetration depth of thermal neutrons in pure cadmium is approximately 0.5 mm,[53] and it is unlikely that the penetration depth in bulk CdS is less than this. To remove the possibility of incomplete penetration in the CdS, all samples were thinner than 1.0 mm.

c) Irradiation Procedure

The neutron irradiation was carried out in the core of a 100 kW reactor, where the thermal neutron flux was 10^{12} neutrons per cm^2 sec, the ratio of thermal to fast neutron flux was slightly less than 5 to 1, and the gamma ray intensity was 2 M rads/hour. Fast neutron irradiation was carried out in the same position by covering the samples with cadmium sheet, and so suppressing the thermal neutrons, but leaving the fast neutron flux constant. Gamma irradiations were carried out by using a ^{60}Co source. It was not possible to conduct an experiment solely with thermal neutrons,

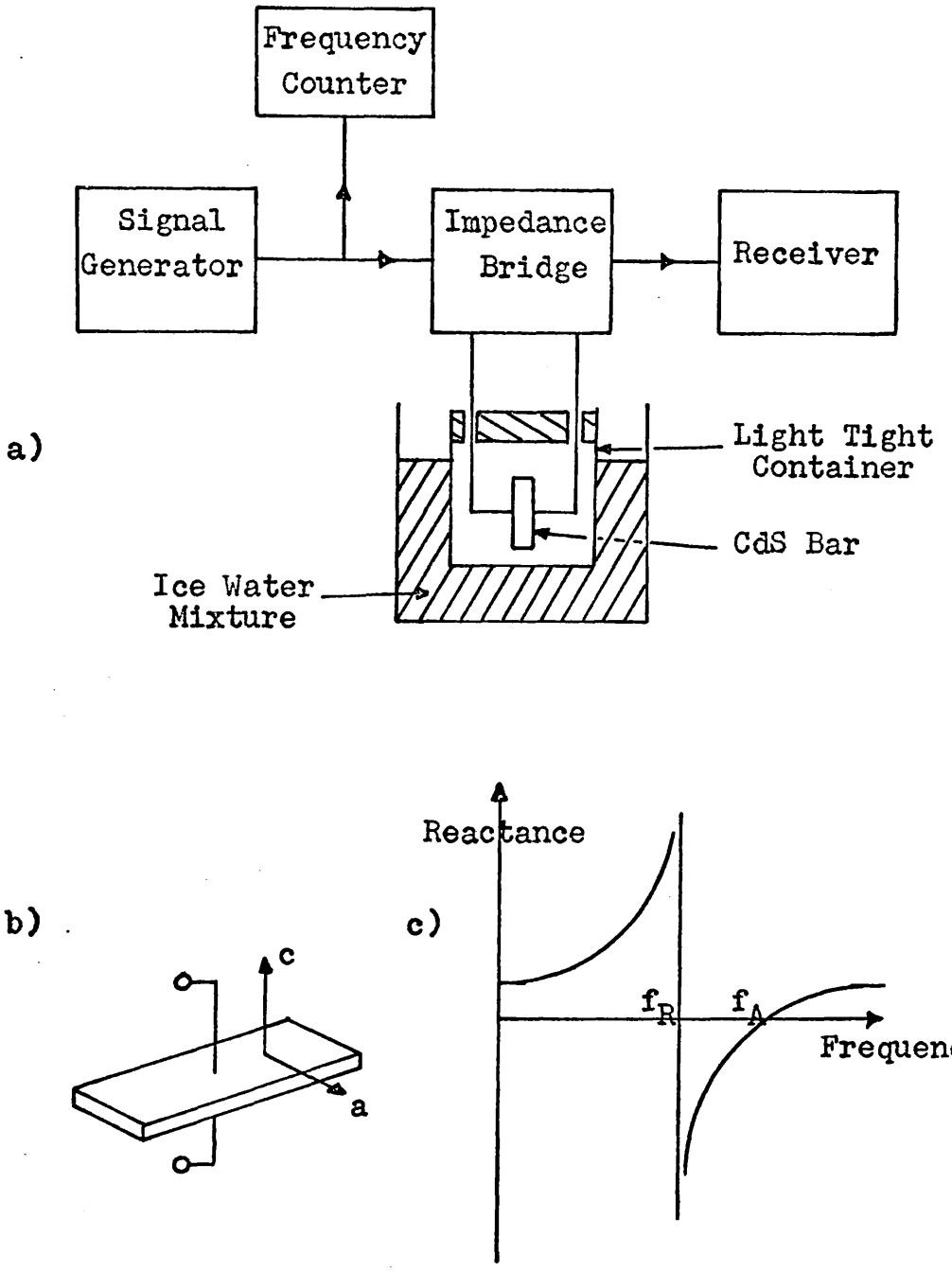

Figure 23. Resonance anti-resonance measurements on CdS.

a) Schematic diagram of measurement apparatus.
b) Bar used for measuring K_{31}.
c) Resonance anti-resonance curve.

as the suitable sites in the reactor had a very low flux density, and the exposure times would have been prohibitively long. The sample temperature during irradiation was no greater than 50°C, and the radioactive level immediately after irradiation was 30 mR/hour at contact. Consequently, the specimens were left for several days, until the activity level was less than 1 mR/hour at contact.

d) Results

The results obtained from measurements of the effect of neutron bombardment and subsequent annealing, on transducer loss, X ray diffraction intensity and film resistivity, for four CdS films, are presented in this section. Measurements are also included for two films which were silver doped by a coevaporation process. Measurements on the effect of neutron irradiation, and annealing, on the electromechanical coupling constant of bulk CdS are also presented. Samples for acoustic and resistivity measurements were always deposited simultaneously, and the acoustic specimens have been labelled, A, B etc. and the corresponding resistivity specimens A', B' etc.

The one way transducer loss of specimens A, B, C and F was measured by the technique outlined previously, and results are shown as a function of frequency in Figs. 24, 25, 26, and 27 respectively. In each case the loss, as evaporated, exhibits a resonance behaviour with a minimum loss ranging from 33 to 42 dB, and an off resonance value of 50 dB. Samples A and B were $\lambda/2$ and $\lambda/4$ transducers respectively, whereas C and F were respectively $3\lambda/4$, and $3\lambda/2$ and $5\lambda/2$ resonances. The latter two show a more marked resonance behaviour than the former two, in their frequency

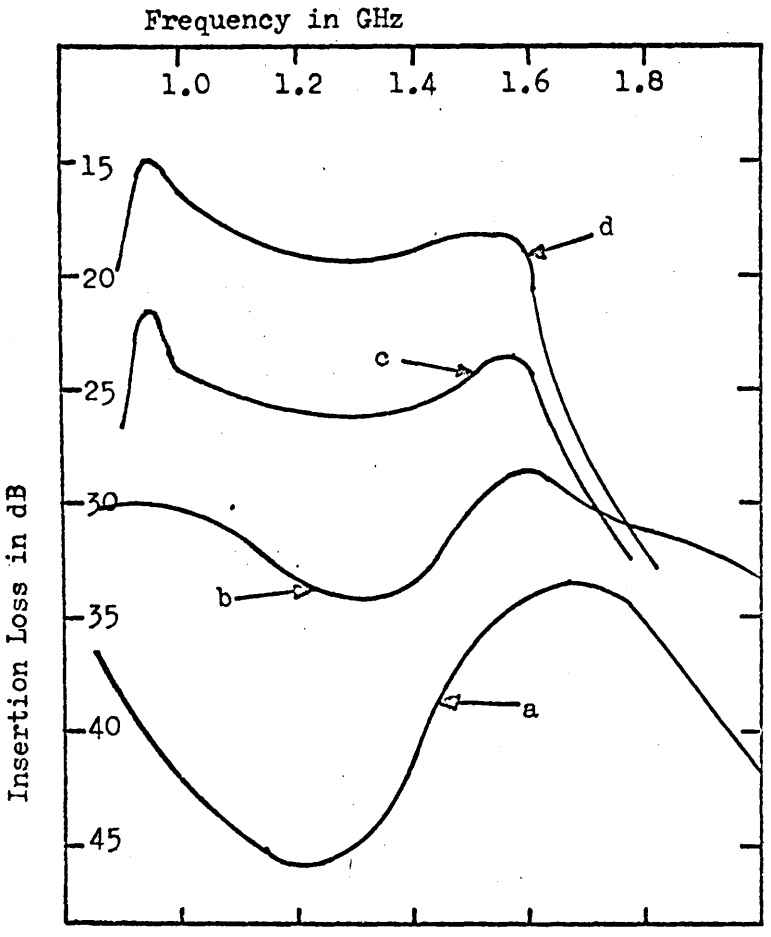

Figure 24. Specimen A

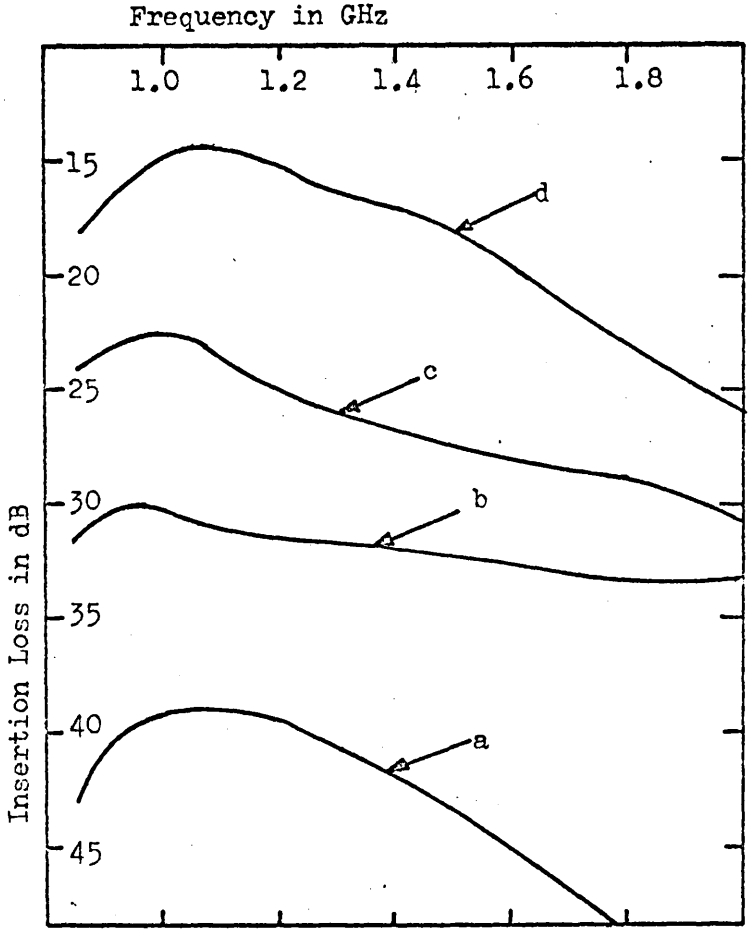

Figure 25. Specimen B

Insertion Loss against frequency for CdS transducers;
a) as evaporated,
b) after 6 hours irradiation,
c) after 2 hours annealing at 350°C,
d) stub tuning in condition c.

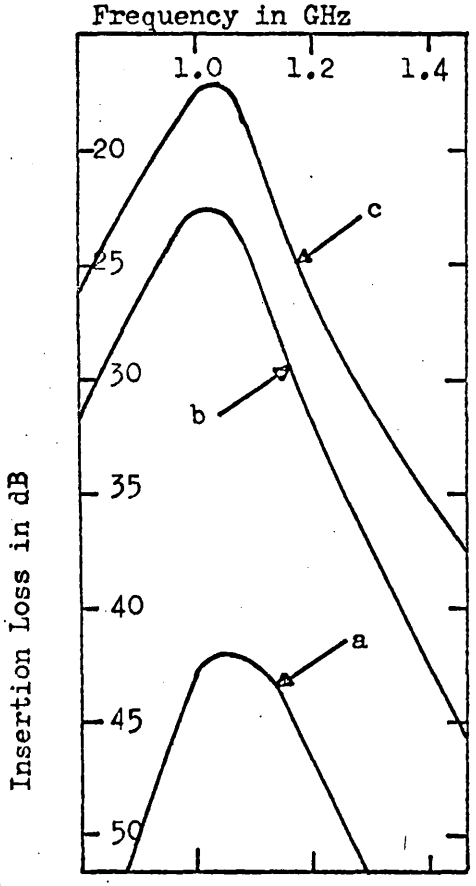

Figure 26. Insertion loss against frequency for specimen C;
a) As evaporated.
b) After 6 hours irradiation
c) Stub tuning in condition b

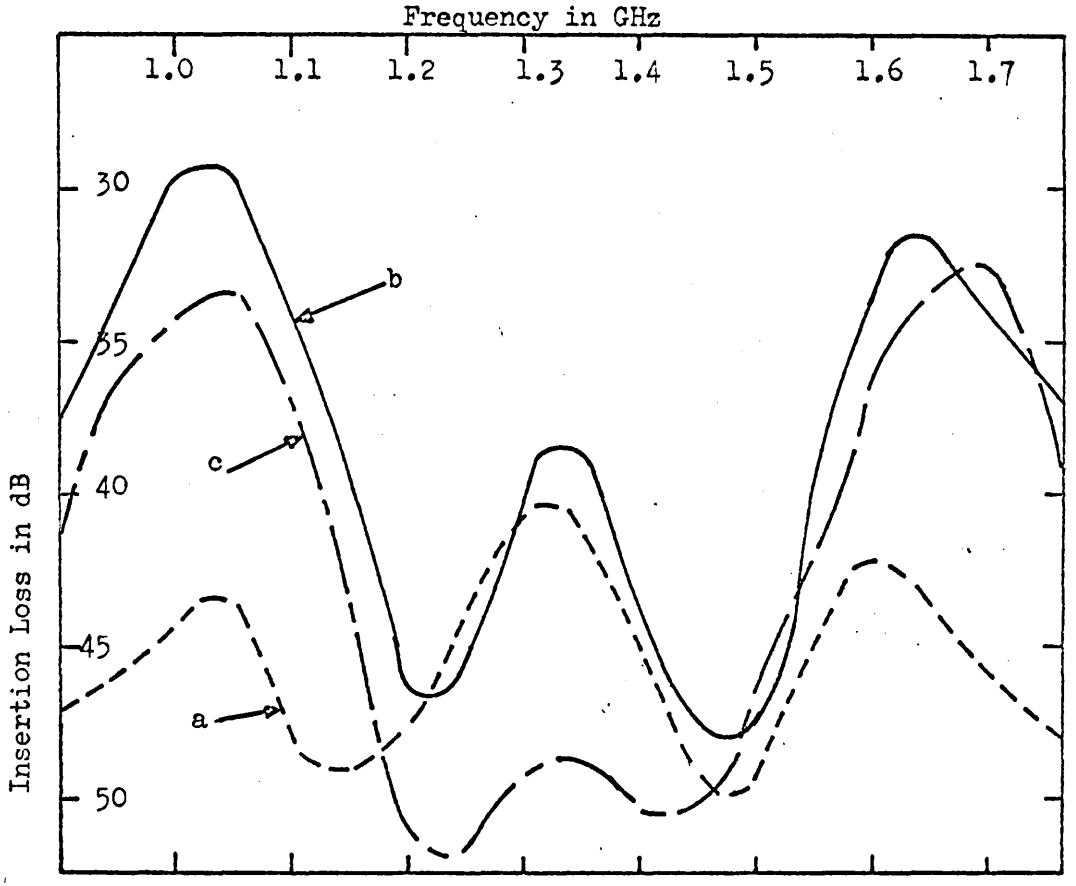

Figure 27. Insertion loss against frequency for specimen F;
a) As evaporated.
b) After 7 hours irradiation.
c) After 13 hours irradiation.

response. Irradiation in each case by thermal plus fast neutrons, for 6 hours, produced a marked reduction in the transducer loss. In samples A and B the improvement was 10 dB, and the frequency response was significantly broadened, and for samples C and F, the improvement was 20 dB and 15 dB respectively, although the shape of the frequency response was essentially unchanged for the overtone transducers. Since there are three sources of loss in the system, (a) the transducer, (b) the delay medium, (c) the gold film, it is important to distinguish between the effects of irradiation on one or all of these. Utilising the fact that the loss in the delay rod can be obtained from the amplitude of successive echoes of an exponential decay pattern, the loss in the sapphire was determined prior to, and after, irradiation, and no change in the acoustic loss was observed. Further to this, some sapphire rods were irradiated for upwards of 30 hours and no change was observable in either the acoustic loss, or the delay time of the echoes, within the limits of experimental error. Several resistivity specimens were tested in a 1 GHz tuneable cavity with the electric field parallel to the surface of the film and so generating shear waves.[19, 38] After a six hour exposure to thermal plus fast neutrons, the improvement in transducer loss was similar to that observed with the longitudinal mode transducers, which had a gold backing contact. Both specimens A and B were annealed for two hours at 350°C in vacuum, and the loss was subsequently found to have been reduced in each case. It is important to note that annealing of pre-irradiated films had no effect on the transducer performance. Electrical matching of both transducers with a double stub tuner resulted in a further improvement of the loss; the minimum loss was now slightly less than 15 dB. The measurements with the stub tuner were

made at 50 MHz intervals and the full curve, (d), in figures (2) and (3) is a composite curve of these spot frequencies. This reduction in loss was achieved at the expense of the bandwidth, which is determined by the stub tuners, and is of the order of 5%. It should be pointed out here that electrical matching reduces the transducer loss of any of the curves (a), (b) and (c) shown in figures 24 and 25. For the purpose of clarity, the results of matching have only been shown for specimens A and B after annealing. Specimen F was irradiated for seven hours under similar conditions to the other films, and in this case the resulting improvement in the one way transducer loss was 15 dB. Upon continued irradiation of specimen F for a further six hours the minimum loss increased by 5 dB over the previously irradiated value; the overall improvement now being 10 dB. As in the case of specimen C no heat treatment was carried out on this film at any stage in the procedure. Specimens A and B were also irradiated for a further three hours after annealing, and the transducer loss was degraded by approximately 3 dB over that shown in curve (c) of figures 24 and 25. On re-annealing these two films however, the loss corresponding to curve (c) in these figures was obtained. Two additional transducers were irradiated for six hours by fast neutrons alone, and the one way transducer loss was degraded by 3 to 4 dB over the frequency band, but after annealing the resulting loss did not differ from the value prior to irradiation within the limits of experimental accuracy. Another two transducers were irradiated by a ^{60}Co source and received a radiation dose of 5.3 M rads, which marginally degraded the insertion loss, but the initial value was reproduced by annealing.

It was mentioned previously that compensation of n-type CdS

can be carried out by coevaporation of silver, and the frequency dependence of the transducer loss for two such films is shown in figure 28. These were specimens D and E, which were doped with 0.47% and 1.4% of silver respectively. Although both transducers have a comparable minimum loss, the frequency responses of these transducers, which were both operated on the $\lambda/4$ mode, are markedly different, and a similar heat treatment procedure to that used with the post-irradiated films had no noticeable effect on the transducer loss.

Measurements are presented in table 7 of the dark resistivity, film thickness, and X ray reflection intensity from the (002) plane for films A', B' and C' and the silver doped films D' and E'. The dark resistivities of the former three films, after a six hour irradiation by a thermal plus fast neutron flux (thermal to fast ratio 5:1) are also listed there. In table 8 the X ray measurements made on specimens A, B, C, D and E (as evaporated), are presented, in the format used in section 2.5.1. The same relationship, as before, was observed between film thickness and degree of structural order, except in the silver doped film E, which had a strong reflection from the (103) plane. After irradiation, weak reflections from the (103) and (105) planes were observed in specimen C. Comparison of the X ray diffraction intensities from the acoustic specimens and the corresponding resistivity specimens, i.e. a comparison between A and A' etc, did not reveal any significant differences.

Resonance anti-resonance measurements are presented in Table 9 of the electromechanical coupling constant K_{31}^2 in single crystals of CdS. The specimens were cut from three different boules, and specimens

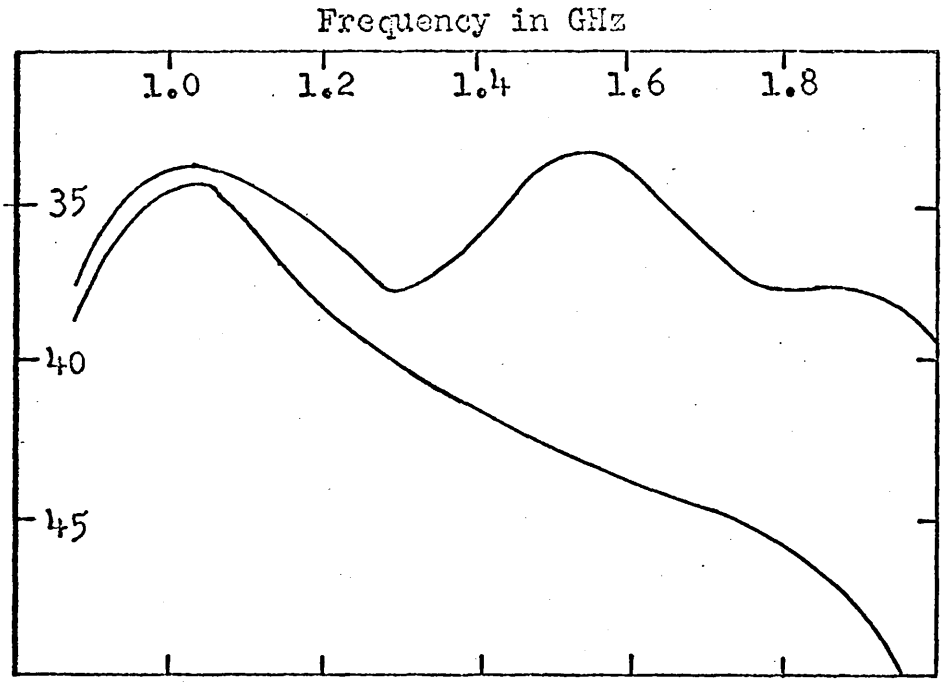

Figure 28. Insertion loss against frequency for silver doped transducers; curve a, specimen E; curve b, specimen D.

	(002) Reflection Intensity normalised w.r.t. sample E'.	Film Thickness (microns)	Dark Resistivity (Ωcm)	
			As Grown	After 6 hours Irradiation
A'	8.8	1.8	$1.1.10^{4}$	$5.0.10^{4}$
B'	3.1	1.08	$1.1.10^{5}$	$2.6.10^{6}$
C'	15.4	2.7	$1.8.10^{3}$	$4.4.10^{3}$
D'	5.9	1.1	-	-
E'	1.0	1.05	$2.3.10^{5}$	-

Table 7. Measured values of reflection intensity from the (002) plane, specimen thickness and dark resistivity before and after irradiation, for specimens A',B',C',D' and E'.

Plane	Angle w.r.t. (002) Plane	Intensity in a Random Powder	CdS Films				
			A	B	C	D	E
002	0	59	59	59	59	59	59
004	0	4	3.9	3.5	4.7	3.4	3.2
105	20.8°	11	-	2.5	-	-	5
104	25.4°	2	-	-	-	-	-
103	32.4°	42	-	1.2	-	-	22
114	39.0°	7	-	-	-	-	-

Table 8. Basic structural data for hexagonal CdS, and normalised diffraction intensities from planes observed in specimens A,B,C,D and E.

Crystal	K_{31}^2		
	Pre-irradiation	After 18 hours irradiation	After 6 hours annealing at 350°C
I	0.0123	0.0070	0.0095
II	0.0122	0.0093	0.0104
III	0.0110	0.0091	0.0109
IV	0.0113	0.0088	0.0109

Table 9. Electromechanical coupling constant K_{31}^2 of the pre-irradiated, irradiated and annealed crystals. Specimens I and II were irradiated by thermal plus fast neutrons, and specimens III and IV by fast neutrons alone. (I and III were supplied by the Eagle Picher Corporation, and II and IV by A.E.I. Ltd.)

II and IV came from the same boule. Samples I and II were irradiated for 18 hours by thermal plus fast neutrons (thermal to fast ratio 5:1), and specimens III and IV were irradiated for the same time with the same fast neutron flux. In each case the value of K_{31}^2 decreased quite significantly with irradiation, but on annealing for six hours at 350°C in a nitrogen atmosphere, the coupling constant for samples III and IV rose to almost the original value, whereas that for samples I and II did not. Repeating the annealing procedure had no further effect on K_{31}^2.

Several samples of CdS, cut from one boule, were subjected to the same irradiation and annealing procedure as the resonance anti-resonance specimens. After each stage, one piece was powdered and examined by X ray diffraction. The object of this procedure was to determine whether or not the disordering by bombardment, and subsequent annealing of the crystal lattice, had resulted in the formation of the cubic phase. No evidence was found to suggest that cubic CdS had been formed.

e) Discussion

The observations which have been made, on the effect of neutron bombardment on the acoustic loss and velocity in single crystal sapphire rods, indicate that any defects produced in the sapphire rods have an insignificant effect on the acoustic propagation in sapphire. It was also observed that the shear wave acoustic specimens, without gold films, displayed the same type of behaviour with irradiation as the longitudinal acoustic specimens, which had gold backing films. These results therefore suggest that improvements in the insertion losses of the transducers are due entirely to neutron bombardment induced effects in the CdS transducers.

It was previously stated, that during irradiation of the CdS films and single crystals in the reactor, the specimens were exposed to gamma rays in addition to the neutrons. It is known that irradiation of solids with gamma rays can produce a high density of defects [54] which can, under certain conditions, bring about changes in resistivity [47] and the elastic constants.[55] Although the transducer performance was degraded by exposure to gamma rays from a ^{60}Co source, which was equivalent to the gamma flux in the reactor, the change was sufficiently small to be neglected. When the transducers were irradiated by fast neutrons the deterioration in performance was approximately 4 dB. This constrasts with the 10 to 20 dB improvement in transducer loss when the transducers were irradiated with thermal plus fast neutrons, indicating that the thermal neutrons alone are responsible for the improvement in performance. This is also consistent with the corresponding increase in film resistivity after exposure to the same thermal plus fast neutron fluence (fluence = flux x time). To check conclusively the effect of thermal neutrons alone on the CdS transducer would have required locating the specimens in an environment where the thermal to fast neutron flux ratio was an order of magnitude greater than that used here. This however, would have entailed prohibitively long exposure times due to the relatively low thermal flux in such positions.

It was shown from the results of annealing of post irradiated films, annealing prior to irradiation having no affect on the transducer loss, that heat treatment plays an important part in this work. No matter whether the films were irradiated with thermal plus fast neutrons, or

only fast neutrons, a further improvement was always observed after annealing. Thus some defect centres are introduced in the lattice which degrade the transducer performance, and which may be wholly or partially removed by annealing. This is confirmed by the results obtained on specimen F, shown in figure (6), which show an initial 15 dB improvement on irradiation for seven hours with thermal plus fast neutrons. Upon further irradiation for six hours the loss worsened by 5 dB , resulting in an overall improvement of 10 dB. A somewhat similar result was found in the case of specimens A and B which were re-irradiated after annealing and found to have a 3 dB increase in their loss, which was offset by further annealing. Now the film resistivity was found to be constant after the initial irradiation, and remained unchanged after annealing, hence the increased loss observed with continued irradiation is not associated with a resistive effect. It would appear that the associated decrease in efficiency with continued irradiation, and the effect of annealing, can be attributed to changes in K^2. This is confirmed by the observed decrease in K^2 in bulk crystals brought about by bombardment with both fast, and thermal plus fast neutrons. Irradiation with fast neutrons markedly reduces K^2, but annealing in an inert atmosphere removes the defects to such an extent that the pre-irradiated value is almost exactly obtained. On the other hand, with a similar annealing procedure carried out on crystals irradiated with thermal plus fast neutrons, the value of K^2, although it improves significantly, is noticeably less than the pre-irradiated value.

The overall effect of irradiation with thermal and fast neutrons on the transducer loss is that a considerable improvement is brought about,

due to the increase in resistivity associated with the defects produced by the thermal neutrons. This compensating effect is attributed to the creation of a new trapping site 0.5eV below the conduction band. [48] The thermal and fast neutrons give rise to defect states which reduce the electromechanical coupling constant, and although the fast neutron defects are apparently amenable to annihilation by annealing, the corresponding defects created by the thermal neutrons would appear to be unaffected by the heat treatment used here.

There is no evidence to suggest that the 0.5eV trapping level in CdS is the result of transmutation of a cadmium atom to a lower valence atom. This level has been tentatively associated with an interstitial cadmium atom.[48] In CdS the dominant neutron capture is due to the ^{113}Cd isotope, which decays to the stable ^{114}Cd isotope. All other isotopes of cadmium and sulphur have a relative neutron capture cross section at least four orders of magnitude down on that of the ^{113}Cd isotope, and their transmutation products should have no significant effect on the resistivity of CdS.[48] It can be shown that the defect density introduced into CdS by a thermal neutron flux of 10^{12} neutrons/cm^2sec is $1.29.10^7/cm^2$sec. Thus in 18 hours of bombardment a defect density of $8.36.10^{11}/cm^2$ is produced. The atomic density in the (002) plane is $5.86.10^{14}/cm^2$, so that the lattice damage is still relatively small. Investigations of the thermal neutron damage rate associated with the (n, γ) recoil, in a variety of elements,[56] have shown that this is particularly high for ^{113}Cd. Hence it may be expected that annealing at these relatively low temperatures would not be wholly effective in removing the thermal neutron induced defects in CdS.

It is believed that irradiation with fast neutrons gives rise

to clusters of defects,[57] which are randomly distributed throughout the lattice. In general, fast neutron induced defects are annealed out[54] at similar temperatures to that used here, and from the results of the electromechanical coupling constant, and transducer loss measurements, it would appear that these defects are annealed out in the case of CdS.

The results presented in table 9 for the electromechanical coupling constant K_{31}^2 summarise the resonance anti-resonance measurements made on the thin CdS bars. Measurements of this constant were made because of the relative simplicity of the technique using rectangular specimens. High Q resonances are produced, and the length extensional resonance, which is the fundamental resonance of the bar, is very distinct, and isolated in frequency from any other dimensional resonances. The piezoelectric polarisation produced via K_{31} is perpendicular to the direction of propagation.[2] Figure 23c shows a typical resonance anti-resonance curve, from which it is possible to deduce not only K^2, but the appropriate dielectric constant ε, and elastic constant c. At frequencies well away from resonance, the measured reactance is simply the capacitance of the CdS slice, hence ε can be obtained. The resonant frequency f_R, is dependent on the acoustic velocity in the resonance direction, $v_S = \sqrt{c/\rho}$, and hence c can be obtained.

$$K_{31}^2 = \frac{e_{31}^2}{\varepsilon^T_{33} \cdot c^E_{11}} = \frac{\pi^2}{4} \times \frac{f_A - f_R}{f_R}$$

$K_{31}^2 = 0.0142$ according to published measurements[35] and so the values obtained here are slightly low.

The accuracy of the measurement system was such that K_{31}^2,

ε^{T}_{33} and c^{E}_{11} were obtained with accuracies of $\pm$ 3%, $\pm$ 5% and $\pm$ 2% respectively. In the samples examined ε^{T}_{33} and c^{E}_{11} varied only slightly, within the limits of experimental accuracy, after 18 hours of bombardment. The large change in K_{31}^{2} was therefore due to changes in the piezoelectric constant e_{31}. The large changes in K_{31}^{2} resulted from 18 hours bombardment, and so the 2 or 3 hour exposures required to raise the resistivities of thin films, enough to remove the shunting effect on the radiation resistance, should not markedly reduce the coupling constant.

X ray results showed that there were no significant structural differences between A and A' etc. Although the resistivity measurements made on the films, as evaporated, varied from 10^{3} to 10^{5} Ωcm. the inefficient acoustic behaviour of the corresponding films suggested much lower resistivities. Comparison with the the theory suggests resistivities between 10 and 50Ωcm (see section 2.3).

It has been shown by Berger[49], that evaporated films of CdS consist of highly oriented single crystals in a matrix of disordered CdS. Also, according to Foster[31], and as noted in section 2.5.1, during the early stages of evaporation the (002) planes are oriented in a random manner, and, as the evaporation continues, these planes tend to orient themselves parallel to the substrate surface. Consequently, as the film thickness increases the (002) planes become preferentially oriented parallel to the substrate surface. Berger[49] has also pointed out that the resistivity of the crystalline CdS within the film is less than that of the disordered material. Therefore any measurement of film resistivity will be dependent on the respective resistivities of the disordered and crystalline material,

and their respective concentrations. Further to this, Vergunas, Mingagin, Smirnova and Abdiev[58] found that the resistivity of evaporated CdS films decreased with increasing film thickness, for films ranging in thickness between 1 and 5 microns. This result of Vergunas et al[58] is in agreement with the results listed in Table 7, which show that the resistivity decreased by two orders of magnitude for films A', B' and C', which were evaporated under similar conditions, and whose thicknesses ranged from 1μ to 2.7μ. Further, the reflection intensities from the (002) planes increased by a factor of five, for a less than three fold increase in thickness, indicating an increase in the degree of orientation with increasing thickness.

If it is assumed that the carrier mobility is dominated by lattice scattering, i.e. it is independent of the concentration of impurities, then the resistivity is inversely proportional to the excess free electron concentration.[18] If N_D and N_A are the concentrations of donors and acceptors in the lattice, respectively, then the excess electron concentration is $(N_D - N_A)$. For a given neutron fluence, implying a specific increase in N_A, the inverse relationship between $(N_D - N_A)$ and the resistivity means that the increase in resistivity will be greater the more highly resistive the film. Then for a film whose effective resistivity is dominated by the disordered material the effective value should be high, and should show a large increase in effective resistivity for a specific neutron fluence. Correspondingly, a film whose effective resistivity shows considerable dependence on the crystalline material, would show a smaller change in resistivity for the same neutron fluence. The measurements of

film resistivity as a function of film thickness and irradiation time, in table 7, support this argument, that the greater the film resistivity, the greater the increase for a given neutron fluence.

The Hall mobility of electrons was measured at room temperature in a 1.5μ thick cadmium doped CdS film, of resistivity 0.5Ω cm, and found to be 10 cm^2/V sec. This figure will also be an effective value for crystalline plus disordered material, but agrees well with published values.[49,59]

Transducers D and E were doped with silver by coevaporation during deposition. Silver acts as an acceptor, and thus reduces the electron concentration. The silver atoms may lie in cadmium sites, since they are introduced during growth, and the atoms are a similar size. These transducers were unaffected by annealing, and so it is unlikely that the silver atoms lay in interstitial sites.

The values of insertion loss obtained (figure 28) were inferior to those obtained by irradiation and annealing of undoped transducers. Accurate compensation by this method is unlikely, as it is an empirical approach, which may produce either an n-type or p-type film, and the resulting efficiency is dependent on the evenness and accuracy of the doping. X ray evidence for specimen E suggests that undesirable growth directions may develop in silver doped films. D.C. resistivity measurements suggested that silver doped films had higher resistivities than undoped films, and the lower efficiency may possibly be due to greater disorder in the lattice, and uneven doping.

Pizzarello has shown that the response of a low resistivity

transducer need not be so simple as predicted in the theory. If the metal contact films produce Schottky barriers with the semiconducting CdS, these barriers will be of the order of microns in thickness. There will therefore be two regions, of different resistivity, in the transducer, and the high resistivity barrier layer should dominate the acoustic response. Gold forms such a barrier with semiconducting CdS, and it becomes difficult to predict the acoustic response of such transducers. They have high insertion losses in practice, and are therefore only of academic interest. A D.C. bias applied to these transducers varies the barrier width, and alters the insertion loss.

It is therefore not meaningful to draw detailed comparisons between the frequency responses of the low resistivity transducers discussed here, and the theoretical responses, since gold was used as the bonding metal. After compensation, when the transducers are in the high resistivity condition, comparisons may be drawn, and most of the frequency responses can be fitted to parts of the theoretical response of a CdS-Au-Al_2O_3 (long.) transducer given in figure 11.

f) Conclusions

Irradiation of evaporated CdS transducers with thermal plus fast neutrons gives rise to two opposing mechanisms which influence the transducer loss.[63] The resistivity is increased due to the introduction of compensating defects in the lattice which reduce the ohmic loss contribution to the transducer insertion loss. The electromechanical coupling constant is reduced by defects induced by both thermal and fast neutrons, and although the defects caused by fast neutrons can be annealed out at

350°C so that they do not significantly affect K^2, those caused by thermal neutrons are not fully amenable to heat treatment at this temperature.

It has been shown that measurements of film resistivity are effective values for the disordered and crystalline CdS which make up the film, and that the measured resistivity decreases as the film thickness, and degree of structural order, increases. Thin films, of the order of 1μ thickness, therefore have a resistivity which is dominated by the resistivity of the disordered material. A measured value of film resistivity could give a misleading estimate of the efficiency of a transducer, since the resistivity of the crystallites, which is the significant quantity, may be masked by that of the disordered material.

2.5.3 The Transducer as a Circuit Element.

a) Introduction

Since CdS transducers are links between electrical and acoustic systems, the power transferred depends upon the matching between each system and the transducer. It was shown in the transducer theory (section 2.3) that the shape of the frequency response of a transducer was mainly determined by the acoustic loading. It was also demonstrated that the principal source of loss in a normal transducer, was the mismatch between the transducer impedance, and the impedance of the energising electrical system. The main factors determining the impedance presented by a transducer are its resistivity, electromechanical coupling constant, contact resistance, active area and acoustic impedance. In this section the factors influencing electrical and acoustic matching, and the use of transducers in practical

delay lines, are discussed, and experimental measurements are presented.

b) Impedance Measurements.

The electrical impedance presented by a CdS transducer was measured by the "double power point" technique, between 1 and 2 GHz, on a 50Ω standing wave indicator.[60] This method, outlined in appendix A2, gives reasonably accurate measurements of VSWRs greater than 10, which is not possible if the standing wave indicator is used in the normal manner. The impedances of several CdS transducers, on sapphire delay rods, were measured by matching them to the 50Ω measuring system, with a 5Ω coaxial quarter wave line. A much larger and easily measured impedance, was thus presented to the standing wave indicator, and the transducer impedance was then obtained by calculation.

Without the 5Ω matching system, the impedances of several transducers were measured directly on the 50Ω standing wave indicator. The results had no similarity to the theoretical transducer impedance computed for the same geometry. In a typical case, the measured reactance was virtually constant over the frequency range, although it was of the correct order of magnitude. There was no resonance in the measured resistance, and the value was an order of magnitude high. The VSWRs were greater than 20, but were within the sensitivity of the technique. The frequency dependence of the insertion loss of this transducer agreed well with the theory, both in shape, and in absolute value of insertion loss. It was a $\lambda/4$ transducer with a minimum insertion loss of 23dB at 1GHz.

Using the 5Ω matching quarter wave line, the impedances of

several transducers were measured at the minimum insertion loss frequency. The 5Ω line reduced the transducer bandwidths to between 100 and 150 MHz, but reduced the insertion loss by up to 10dB. A distinct pattern emerged in the results. For transducers with partially tuned insertion losses of less than 20dB, the measured impedances at resonance, were of the form (0.1 - j 1.0)Ω which agreed well with theory, but when the insertion loss was above 20 dB, the measured impedances were typically (2.0 - j2.5)Ω i.e. the real part of the impedance had increased, by an order of magnitude.

c) Discussion

1) Electrical Factors

The significant result in the impedance measurements is the appearance of an anomalously high resistance. Since the transducers were known to be high resistivity, this implies the presence of a contact resistance. In the transducers in which this contact resistance was detected, it appeared to limit the conversion efficiency.

Contact resistances of up to 2Ω were found, which is similar to measurements subsequently published by Bahr and Court[61] who worked, with the same technique, on transducers produced by coevaporation, between 0.4 and 1.0 GHz. The contact resistance may possibly arise in the jig, or the gold film, or between the jig and the thin films.[11]

The 5Ω line gave useful results about the performance of CdS transducers with fixed matching systems. The frequency responses were reduced in bandwidth, as expected, but it appears that with more elaborate

matching systems, reasonable insertion loss (say 10dB), and bandwidths of 250 MHz or more, could be achieved. Coaxial matching systems, with possibly four quarter wave sections are possible, but the impedances of the device and the measuring system are so widely different that a broad band filter with a very flat response would be unreasonably large. The transducer response is dominated by the capacitance, which means that most of the incident power will be reflected. Ideal matching would be achieved by introducing an inductance at the plane of the transducer. Attempts to do this, by introducing posts into the coaxial line beside the transducer, or by changing the line configuration at the transducer, have had only limited success. Stub tuners, which operate at a point away from the transducer, do not give perfect matching, because they have a resistance of the same order as the series resistance presented by the transducer.

62

2) Acoustic Factors

The impedance presented by a transducer is inversely proportional to its active area. Calculation showed that the optimum acoustic beam area, at 1GHz, for matching to 50Ω, was 10^{-7} m^2, assuming that the basic constants for thin films are the same as for single crystals of the same material. In the light of the measurements of the electromechanical coupling constant, K^2, in neutron damaged material, it appears that the coupling constant of imperfect, or damaged, structures will be less than that of perfect crystals of the same material. The K^2 of CdS films will be less than that of single crystals of CdS, hence the real part of the transducer impedance will be less, and the optimum matching area for

matching will be smaller than 10^{-7} m^2. In the experiments the nominal area of the centre post of the jig was 3.10^{-6} m^2, and it was found that the minimum insertion loss was achieved with an area of 10^{-6} m^2, although the results were only marginally better than those obtained with posts ranging in area from 3.10^{-8} to 6.10^{-6} m^2. On some transducers, aluminium contacts of varying area were evaporated on to the surface, to clearly define the area of excitation, but the results obtained were similar to those achieved with the posts. In general, the use of top contacts is to be avoided with thin film transducers, because of the danger of mechanical damage shorting out the transducer, and because a backing layer moves the response in frequency.

The active area of the transducer was always much less than the total area of the CdS film, but as the films were only 1 to 3 microns thick, fringing effects should be small. Reports from elsewhere have shown that when an acoustic beam is launched by a post 10^{-7} m^2 in area, the area of the beam in the delay rod (detected by Brillouin scattering[64]) is the same as that of the post.[66] The minimum values of insertion loss obtained from the longitudinal CdS transducers described in this chapter, using posts of 3.10^{-6} m^2 area, are the same as values reported in the literature using smaller post areas. The untuned insertion loss of CdS transducers, if excited by the optimum beam area, should theoretically be less than 10 dB above 1 GHz, at the $\lambda/4$ resonant frequency. There are no reports of performance as good as this, but untuned insertion losses less than 20 dB, above 1 GHz, have been observed in several transducers. No evidence was found of large scale stacking faults in the CdS films,

and the simplest explanation of the conflicting results is, either, that the posts did not always excite all the area which they covered, or, that the contact resistance effect varied with the post area. The former point could be clarified by Brillouin scattering experiments,[64] and the latter by combined insertion loss and impedance measurements with a variety of post areas.

In many applications, only single frequency operation is required, and a low insertion loss transducer can be made by using a bond material, between the CdS and sapphire, which is a worse acoustic match than gold. Tungsten is a possible material and could give an untuned insertion loss of 10 dB or less, with a very narrow bandwidth.

d) Delay Line Stability.

If acoustic delay lines are used as calibration devices in microwave circuitry, the stability of the delay, as temperature varies, is of the utmost importance. An experiment was performed on a CdS transducer and sapphire delay rod assembly, to investigate this property, using the apparatus shown in figure 29. The swept frequency input to the transducer was delayed in the sapphire rod, and on reconversion to electromagnetic energy mixed with the incoming signal, which was then at a higher frequency. The mixed frequency is constant, if the transducer phase response is linear over the swept range, and is a measure of the acoustic delay. It was measured by beating with a signal of known frequency from a stable source. A longitudinal CdS transducer on a 1.6 cms sapphire rod was used in the experiment, and with a sweep rate of 1.6 GHz/sec, centred on 1.5 GHz, the observed mixed frequency was 4.8 kHz. The

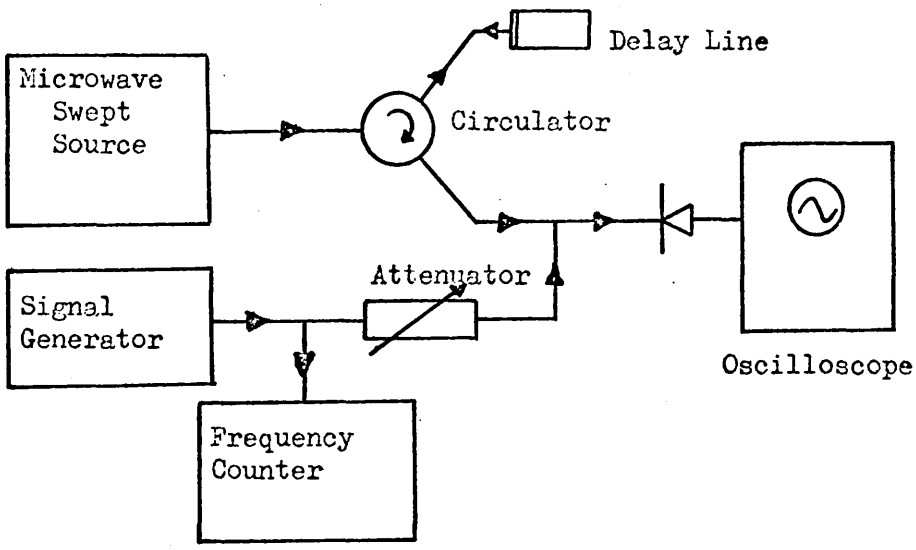

Figure 29, Apparatus for measuring delay line stability.

acoustic delay was 3 μsec. The transducer assembly was immersed in liquid nitrogen, and the beat, observed on the oscilloscope, did not change within 1 Hz as the delay rod cooled from room temperature. Several repetitions gave the same result, and so the delay was stable to within 1 Hz in 4.8 kHz between 77°K and 300°K i.e. a stability of 0.02%

e) Conclusions

The complete analysis of the behaviour of thin film CdS transducers requires the knowledge of several parameters, which are difficult to measure independently. These are the electromechanical coupling constant, contact resistance, acoustic beam area, and resistivity. Those films which were high resistivity, had only a small contact resistance, and whose frequency response corresponded well with theory for the same nominal acoustic beam area, could be presumed to have an electromechanical coupling constant K^2 of the same order as that for single crystal CdS, although K^2 for the film would be smaller, since it is a relatively disordered

structure.

CdS transducers are most suitable for use where a large bandwidth is important, and a low insertion loss is not, although single frequency insertion losses less than 10 dB, and probably as low as 3 dB, can be achieved by several means. The temperature stability of delay lines using CdS transducers, in the microwave frequency range, is very satisfactory.

2.6 Double Layer Transducers

a) Introduction

The aim of the transducer work was the fabrication of efficient shear wave transducers for microwave frequencies. Results have been presented above, and in the literature, showing efficient operation of fundamental mode longitudinal transducers in the frequency range 1-2 GHz. These transducers have also been operated at X band frequencies.[68] As regards the efficient operation of shear transducers, measurements have been presented by Foster,[65] showing that highly efficient fundamental mode shear transducers are limited to frequencies of the order of 600 MHz. Normally, longitudinal mode transducers operate with the r.f. electric field, and the crystalline c-axis, perpendicular to the substrate, whereas operation of shear transducers requires the c-axis to be inclined at a specific angle to the substrate normal, and the electric field. In the case of CdS, it has been shown that the required angle is 38.5°.[15,29] Foster[31] has shown that the conditions required to fabricate shear transducers are, a vapour beam incident upon a substrate at 45° to the normal, and a deposition rate greater than 0.1μ per min. Further, he has shown that the degree of crystalline order in the substrate has an influence on the

growth direction of the c-axis. When these conditions are fulfilled, the c-axis is tilted in the direction of the vapour beam, but this growth direction is not developed until the film is approximately 0.5μ thick. Consequently, there is an upper frequency limit to the efficient generation of shear waves, with strong discrimination over longitudinal waves, when the fundamental resonant thickness for shear waves is comparable to 0.5μ. The region in which the c-axis is bending will generate both modes.

The work described in this section is a development of the basic technique, which extends the frequency range of the fundamental shear mode, with good rejection of the longitudinal mode.[67,71] The new type of transducer is a two layer structure, Fig. 30. The base layer is the region in which the c-axis is bending, and the acoustic response is suppressed by cadmium doping the layer and making it highly conducting, with a resistivity of the order of 1Ωcm. The top layer has a high resistivity of the order of 10^4Ωcm or higher, with a well defined c-axis orientation. When an electric field is applied normal to the substrate, it will be developed across the well ordered high resistivity top layer, since the conducting layer acts as a short circuit. The sole purpose of the highly conducting region is to create a well ordered crystalline structure, with a specific orientation of the c-axis. This well ordered structure is preserved throughout the high resistivity top layer, which can be made much thinner than 0.5μ.

The frequency response of a double layer transducer is dominated by the top layer, but is perturbed by the acoustic loading of the bottom layer. This technique also lends itself to the fabrication of efficient

high frequency longitudinal transducers by the direct evaporation method. Theoretical and experimental results were first obtained on the behaviour of longitudinal double layer transducers in the frequency range 1 to 2 GHz, and the technique was then applied to shear transducers.

The method of deposition used for these double layer transducers was described in section 2.2, and the acoustic measurements were performed as outlined in section 2.4.

b) Theoretical Results

The theory in section 2.3 was slightly altered to take account of the additional layer in the transducer structure. Since this layer is highly conducting, $\omega_c >> \omega$ for microwave frequencies, where ω_c is the dielectric relaxation frequency. As discussed in section 2.3.4 the layer is rendered inactive as a transducer, and so the bottom layer was included in the theory by treating it as an acoustic transmission line. Calculations were performed only for double layer longitudinal transducers. The propagation of a shear wave in a medium with a tilting axis, means that the directions of polarisation, and propagation, with respect to the crystalline axes, are continuously varying. This presents an analytical difficulty to prediction of the behaviour of double layer shear transducers.

The acoustic attenuation in CdS at 1 GHz is around 80 dB/cm,[69] and so mechanical losses may be ignored in layers 10μ or less in thickness. Theoretical results are presented in figure 31 of the frequency response, between 1 and 2 GHz, of a double layer longitudinal CdS transducer, of the same dimensions as an experimental transducer, of 1.2μ on 8.5μ. Two graphs are given, for acoustic beam areas of 3.10^{-6} m^2 and 3.10^{-7} m^2.

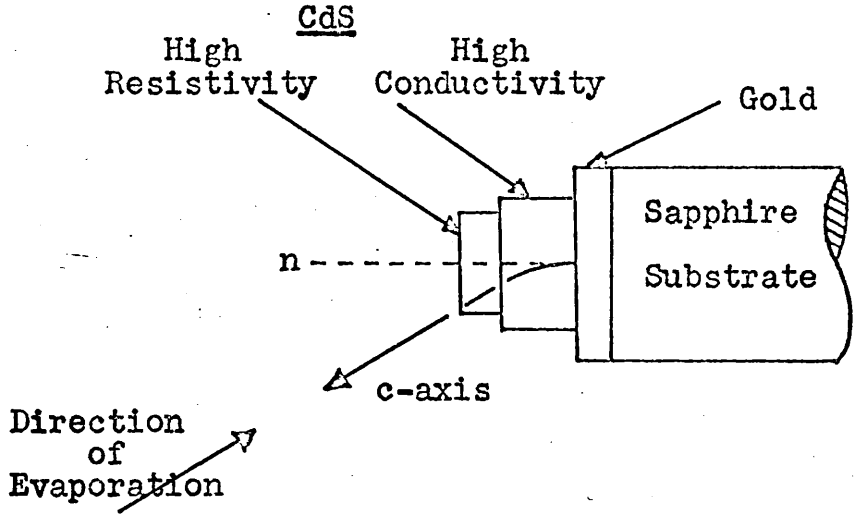

Figure 30. Schematic diagram of double layer shear transducer.

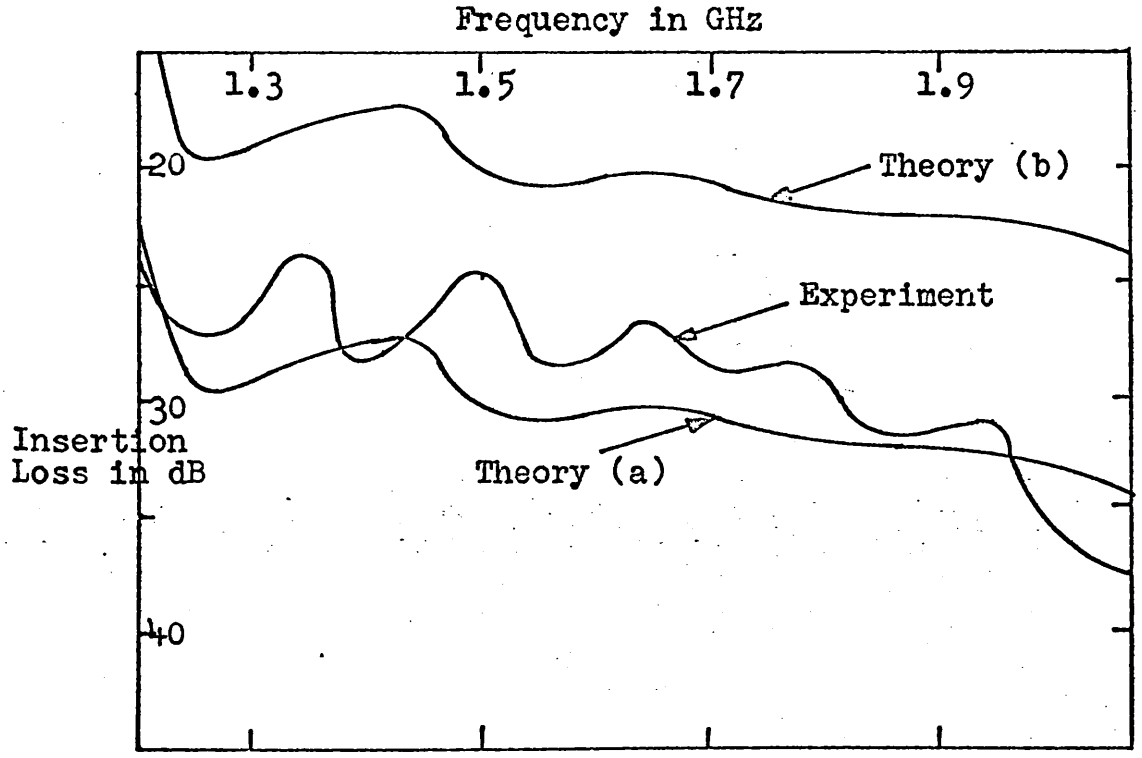

Figure 31. Untuned insertion loss of a double layer longitudinal CdS transducer. Theoretical curves a and b evaluated for acoustic beam areas of 3.10^{-6} m^2 and 3.10^{-7} m^2 respectively.

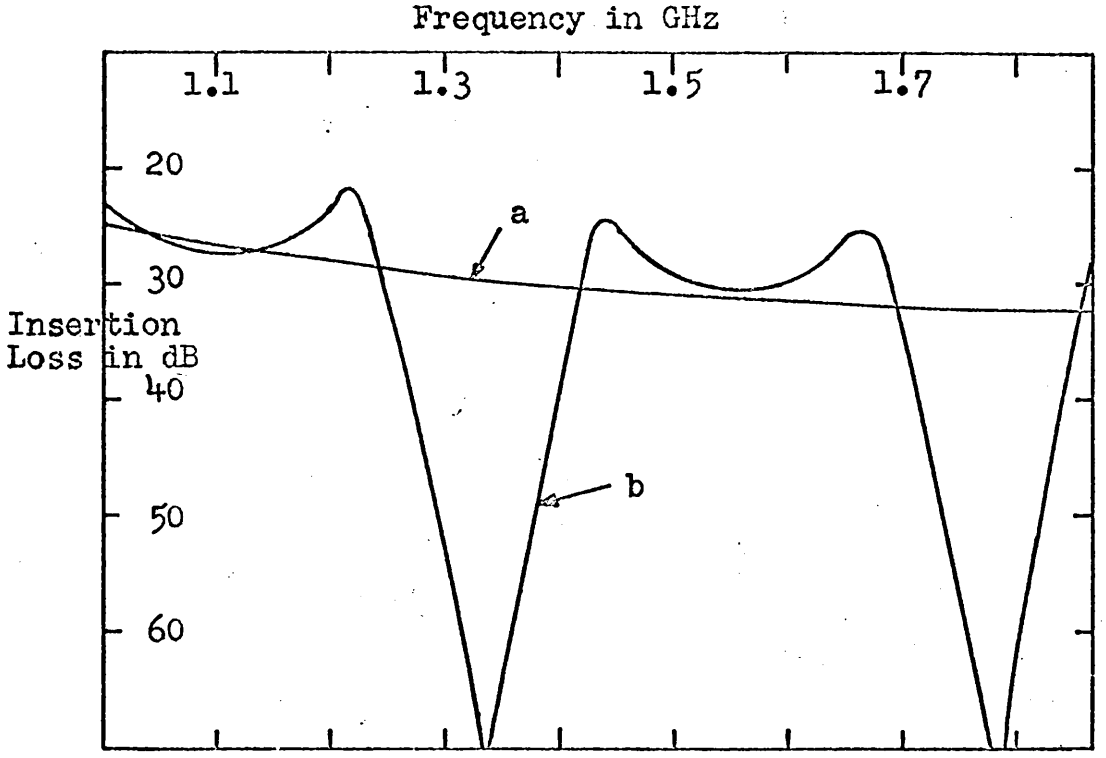

Figure 32. Theoretical untuned insertion loss for transducers; a) 1.2μ thick, b) 9.7μ thick.

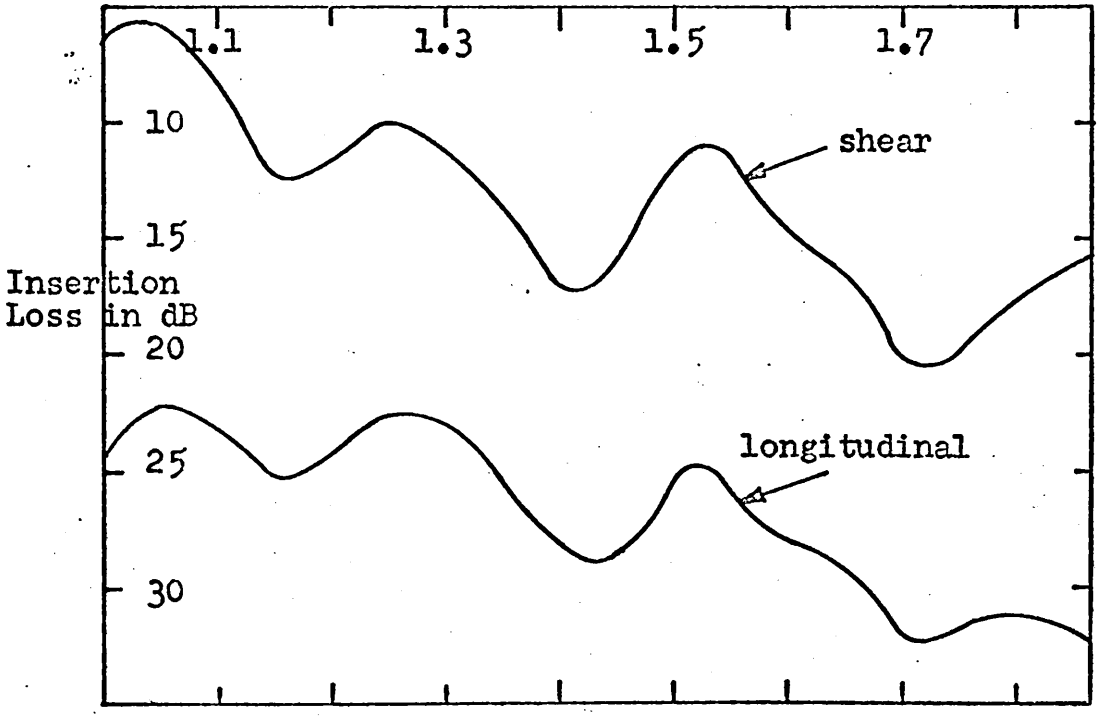

Figure 33. Tuned insertion loss of shear and longitudinal modes generated by a predominantly shear transducer.

In figure 32 are shown the calculated responses of fundamental mode longitudinal CdS transducers 1.2μ, and 9.7μ thick, over the same frequency range.

An interesting result is that the thickness of the gold bond affects the amplitude of the ripple on the response of a double layer transducer. A $\lambda/8$ bond minimises the ripple amplitude for the case of figure 31.

c) Experimental Results.

Measurements of the frequency characteristics of longitudinal and shear double layer transducers are presented in this section. In figure 31 is given the untuned frequency response of a longitudinal double layer transducer, with top and bottom layers 1.2 and 8.5 microns thick respectively, and it can be seen that the device has a broad band characteristic with a superimposed ripple. The quarter wavelength resonant frequency for the top layer is at 900 MHz.

The frequency response of a double layer shear transducer is given in figure 33, with top and bottom layers 1.05 and 3.6 microns respectively. Both shear and longitudinal waves were excited by the transducer, and there was reasonable discrimination throughout the band. These results are for the tuned condition, and the graphs are made up by joining together values measured at 50 MHz intervals. The bandwidth at each frequency is that of the stub tuner. The top layer is a half wavelength thick at 1020 MHz which is the peak of the frequency response, with 6 dB insertion loss, and the characteristics again have a superimposed ripple. The results in figures 31 and 33 are typical of those obtained

by this technique.

X ray diffraction measurements were made on shear transducers, and it was found that in efficient shear transducers, strong reflections were obtained from the (103) and (114) planes. These planes are inclined at 32.4° and 39° respectively to the (002) plane.

d) Discussion

It was stated earlier, that the overall film resistivity of the doped bottom layer, was of the order of 1 Ωcm. Since evaporated CdS films are a mosaic of disordered and crystalline CdS, the measured value is an average of the resistivities of both structures.[49] It has also been shown,[58,63] that the effective resistivity decreases with increasing film thickness, and in the limit of thick films, this effective value tends to the value of resistivity of the crystalline material. Hence the above measured value of resistivity of the doped layer will be greater than, or at best equal to, the resistivity of the crystallites. With this low value of resistivity, the resistance through this layer, short circuits the acoustic radiation resistance, and this layer will not operate as a transducer. Attempts to generate acoustic waves with these doped CdS layers alone were always unsuccessful. The sensitivity of the apparatus was such, that the one way conversion loss of these doped layers was greater than 60dB. The bottom layer can therefore be considered as an acoustic transmission line. The theoretical and experimental results for the longitudinal double layer transducer, shown in figure 31, indicate that there is good agreement as regards the shape of the frequency response. Further, the theoretical frequency characteristics for fundamental

resonance of the top layer alone, and of the combined structure, shown in figure 32, are widely different from the observed behaviour of the double layer transducer. This indicates that the top layer dominates the frequency response, and the bottom layer acts as an acoustic transmission line, which produces a ripple on the frequency response. (The double layer structure is in fact, working as expected).

The theoretical analysis of the double layer transducer is based on the assumption that the layers of CdS are perfectly crystalline, and the data used in these computations was that for single crystal CdS.[35] The layers, however, are decidedly polycrystalline, and so a calculation of the theoretical conversion loss of an evaporated transducer, should predict a lower loss than is observed in practice. It has been shown that induced structural disorder in CdS markedly reduces the electro-mechanical coupling constant, K^2.[63] Consequently, one would expect that the effective K^2 of a polycrystalline film would be less than that of a single crystal.

The theoretical results presented for different acoustic beam areas in figure 31 show that the absolute level, but not the shape, of the insertion loss characteristic depends upon the beam area. This parameter is not accurately known, and the values used for the calculations were $3.10^{-6}m^2$ and $3.10^{-7}m^2$; the area of the centre post of the coaxial exciter being $3.10^{-6}m^2$. These results imply that the active area of the transducer is less than the post area, since the theoretical result should be better than the experimental.

From the discussion of the factors which determine the absolute

level of insertion loss, in section 2.5.3, it is clear that no definite conclusions can be drawn from the relative amplitudes of theoretical and experimental curves. The significant results are, the similarity of the experimental and theoretical curves in figure 31, and the difference between the fundamental resonances of figure 32, and the frequency response of the double layer in figure 31. These prove that the high resistivity top layer dominates the transducer response.

The transducers discussed here were all deposited on gold films, highly oriented with the ⟨111⟩ direction perpendicular to the substrate. It has been mentioned, (section 2.5.1) that the c-axis of the CdS can be made to tilt to the required angle to the substrate normal, after approximately 4μ of CdS has been deposited. The thickness of the bottom layer of the shear transducer in figure 33 was only 3.6μ, and so the c-axis was probably tilted to less than the required 38.5°. A thicker bottom layer may have produced a transducer with better discrimination between modes.

Since the top layer has a well defined orientation throughout, it can be of any desired thickness, and very thin layers, fundamentally resonant at frequencies up to X band, can be deposited. The upper frequency limit, on efficient operation of these transducers, will then be determined by the acoustic loss in the layers of CdS and the metal electrode, particularly in the thicker bottom layer of CdS which must be as thin as possible.

e) Conclusions

A satisfactory technique for producing efficient shear mode

transducers, fundamentally resonant at frequencies above 1 GHz, has been developed. The transducers are double layers of CdS, and the bottom layer, in which the required structural orientation is developed, is cadmium doped, and does not act as a transducer. The top layer has a constant inclination to the substrate normal, is made of high resistivity material, and can be of any desired thickness. The frequency response is dominated by the top layer, and it should be possible to produce shear transducers with their fundamental resonant frequencies in X band. It may be possible to grow the top layer epitaxially, by the coevaporation technique, to produce a transducer with a well ordered structure, and maximum conversion efficiency.

CHAPTER 3

3. Experimental Techniques for the Construction of Microwave Acoustic Amplifiers.

3.1 Introduction

The acoustic amplifiers discussed in this chapter, and in chapter 4, consisted of a slice of CdS, which was the amplifier, sandwiched between two sapphire delay rods, each of which had a transducer on its end face. This configuration, shown in the sketch below, was chosen because the project was directed to producing a useful device; an amplifier with built in delay.

Although this device requires efficient acoustic bonds between the CdS and sapphire delay rods, it has several experimental advantages. The length of the CdS amplifier is, in practice, limited to about 2mm in order to keep the acoustic loss, and very large gain per unit length,[69] within reasonable limits, so that the full attenuation versus drift field characteristics can be measured. An amplifier without delay rods is therefore very short, has a very short delay, and short r.f. pulses (about 0.1μsec) must be used, thus increasing experimental difficulties. Also the sapphire rods, being insulators, isolate the

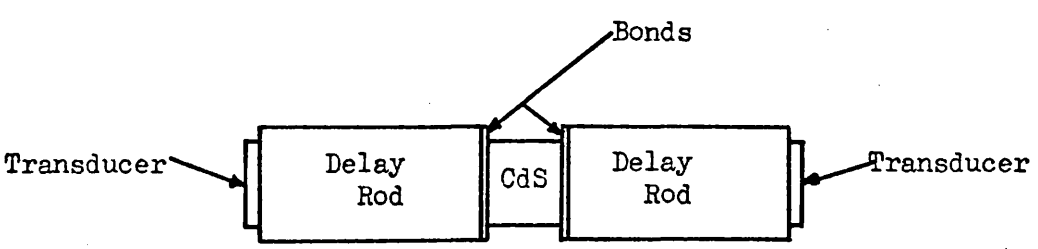

Schematic diagram of acoustic amplifier.

drift field from the transducers.

Several technological problems were encountered in fabricating these devices, the most intractable of which was the nature of the CdS crystals. It proved difficult to obtain crystals of suitable resistivity for microwave operation (10^3 Ωcm or less), and many of the CdS crystals had non-uniform properties. Some attempts were made to assess the material uniformity, and the temperature dependence of the basic parameters of CdS. Compensation of low resistivity CdS, by neutron bombardment, was investigated, to see if useful material could be produced. The formation of ohmic contacts to CdS proved difficult, and a technique was developed for making contacts by indium diffusion. Efficient acoustic bonds were produced by thermo-compression indium bonding, and as the extension of the technique to microwave frequencies is of value, representative measurements were made.

Before the double layer technique for making shear transducers for frequencies above 1 GHz was developed,[67] several other methods of shear wave generation were tried. Polished CdS transducers,[70] mode converters,[46] and cavity excitation of shear waves from CdS films with the c-axis perpendicular to, and the electric field parallel to, the substrate,[19,38] were all investigated, with varying degrees of success.

3.2 Formation of Ohmic Contacts to CdS

A relationship was observed between triangular etch pit densities on (100) faces of some single crystal CdS samples, and the relative difficulty encountered in making indium ohmic contacts to

these faces of the samples.[72] It was found that evaporation of metal films (such as silver, indium or aluminium) on to CdS, did not make ohmic contacts, which are essential if meaningful measurements are to be made on acoustic amplifiers.

Ohmic contacts were made by diffusion of indium into CdS at 425°C. The quality of the contacts was assessed by measuring the V-I characteristic of each sample. Good contacts produced a V-I characteristic which was symmetric, with linear ohmic regions, strong saturation, and a sharp "knee" between the ohmic and saturated regions.[73] The asymmetry of the contacts is defined by the ratio of the drift voltages at the "knees" in the forward and backward directions. The non-linearity of the ohmic region is defined by (mean deviation/mean value) expressed as a percentage.

It has been shown[74,75] that there is a close relationship between etch pit and dislocation densities in Cadmium Sulphide. The (100) faces of the specimens were optically polished, and etched for $2\frac{1}{2}$ minutes in dilute chromic acid at 80°C. The etch pit densities produced by this treatment are given in Table 10.

Ohmic contacts were made to Specimen A by vacuum evaporation of a 200Å layer of indium, followed by diffusion of the indium into the CdS, at 425°C, for 10 minutes, in a nitrogen atmosphere. This procedure did not produce good contacts to Specimen B, but by heating the specimen to 425°C during evaporation of indium, and allowing the indium to diffuse in for 10 minutes at this temperature, ohmic contacts were produced.

The latter procedure failed to produce good ohmic contacts to Specimen C. This sample had a very low triangular etch pit density, suggesting that the dislocation density was low. It was postulated that an important mechanism of diffusion might be via dislocations. The (100) faces of Specimen C were therefore abraded on silicon carbide (600 grade) to induce dislocations in the surface. The procedure used to make good contacts to Specimen B was then used successfully to produce ohmic contacts to Specimen C. Further examination of the abraded surface of Specimen C showed an etch pit density similar to that of Specimen A, although most of the etch pits produced were not triangular. The results are summarised in Table 10.

It was not possible to measure etch pit densities on (002) faces, where hexagonal etch pits form in one direction, since these pits grow very rapidly and overlap. The etching time required to produce hexagonal etch pits on Specimen C was such that the (002) faces of Specimen A were very strongly etched, and the true etch pit density was obscured.

No other Eagle Picher or Clevite specimens have been obtained with dislocation densities as low as $10^4/cm^2$. A.E.I. material appears to have this low dislocation density, but ohmic contacts were made to polished specimens by the technique used for Specimen B. Conceivably, the optical polishing induced dislocations into the surface.

The above measurements show that it is more difficult to make ohmic contacts to sulphur compensated than to uncompensated

Crystal [a] After Growth Treatment and Resistivity Range.	Contact Procedure	V-I Characteristic Asymmetry	V-I Characteristic Non-linearity	Etch Pit Density cm^{-2}
A No Sulphur Compensation 6kΩcm-1.3MΩcm	Indium evaporation and diffusion at 425°C in a nitrogen atmosphere.	1.05	1.2%	$1.1.10^{7}$
B Sulphur Compensated 35Ωcm-0.5MΩcm	Indium evaporation and diffusion at 425°C in a nitrogen atmosphere.	1.25	2.5%	$6.2.10^{5}$
	Indium evaporation on to CdS heated to 425°C in vacuum.	1.01	3.3%	
C Sulphur Compensated 1.7kΩcm-7.3MΩcm	Indium evaporation on to CdS heated to 425°C in vacuum;			
	before grinding,	1.28	4.9%	$4.4.10^{4}$
	after grinding.	1.01	3.7%	$1.0.10^{7}$

Table 10. Observed relationship between contact formation procedure, contact performance and etch pit density in CdS samples.

(a) Specimen A supplied by the Eagle Picher Corp. Specimens B and C supplied by the Clevite Corp.

material, and suggest that an important mechanism in contact formation is diffusion into dislocations.

3.3 Thermo-Compression Bonding.

a) Bonding Technique

Methods for making low transmission loss, metallic, acoustic bonds, for room temperature applications, have been developed up to 100 MHz.[76] Bonds made with evaporated metal films are of the same order of thickness as acoustic wavelengths, at microwave frequencies. Indium is the most commonly used bonding metal,[32] and melts at 153°C. It is essential to be able to make efficient bonds, for both longitudinal and shear waves, if the practicability of the acoustic amplifier as a device is to be determined.

The most important aspect of the bonding technique described here, is that the complete procedure is performed in vacuum, eliminating any problems which arise from oxidation of the evaporated metal films. Figure 34 is a photograph of the bonding apparatus, in which a sapphire delay rod is being bonded to a piece of CdS. The specimens were optically polished flat and parallel to the tolerances described above (section 2.4.1). The apparatus is rigidly constructed of steel, and stands on a throat suitable for mounting on a vacuum system. A bell jar, 18" long and 12" in diameter, contains the whole apparatus. The sapphire rod is held in an adjustable jig on a movable carriage, and the concealed end of the rod is held against a hardened steel thrust pad which rests on a conical tip. Another hardened steel pad supports the CdS slice, and it also rests on a conical tip. This bottom pad holds two 25W heaters

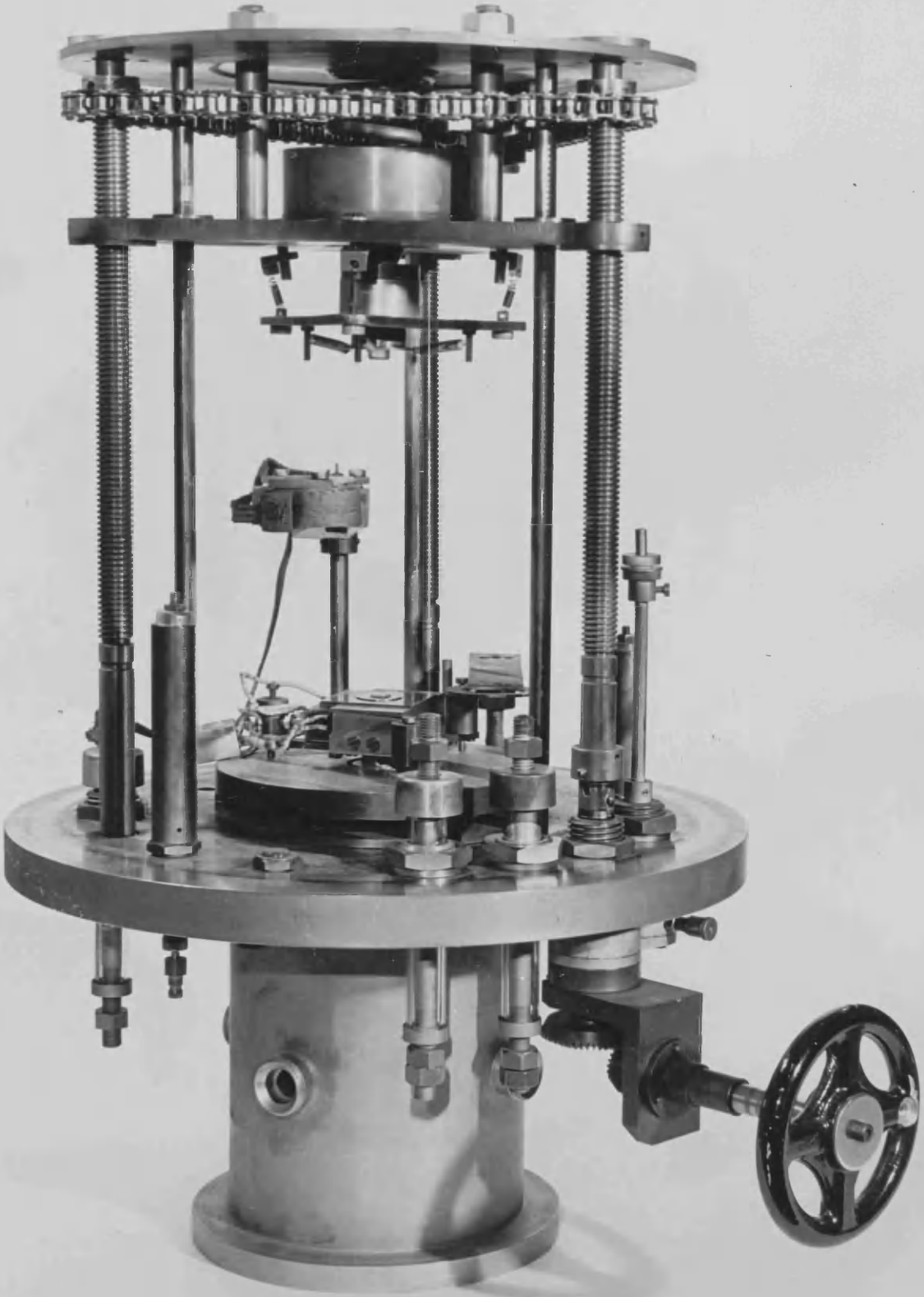

Figure 34. Vacuum bonding apparatus.

and a thermostat, and is steadied by three spring loaded pistons on extended arms. Both specimens are on the central axis of the jig, and can be mated and compressed by winding down the carriage. On compression, the upper specimen recedes into the carriage, compressing the spring which gives 50 lbs thrust per $\frac{1"}{8}$ compression.

The bonding metal is evaporated from a molybdenum gauze, mounted in pyrophilite rings, in an assembly, between the specimens, which can be rotated to the side of the apparatus. A gauze is used so that metal can be evaporated both up and down. A typical bond is made by first chemically cleaning the specimens, and then mounting and aligning them in the jig so that they mate evenly, and with the required orientation. The specimens are further cleaned by an ion discharge, and the carriage is then positioned so that the faces to be coated with the bonding metal are equidistant from the gauze. When the chamber has been pumped down to 2.10^{-5}torr the metal is evaporated. The gauze is rotated to the side, and the specimens brought together and compressed to about 400 lbs/in^2, and heated at a temperature just below the melting point of the bonding metal, for one day.

Almost all the bonds were made with indium, which meant that sapphire surfaces had first to be coated with chromium, to make the indium stick, and the heat treatment temperature was 150^{o}C. Some tin bonds were attempted, so that transducers could be deposited on sapphire delay rods, after assembly of the amplifier, since tin melts at 220^{o}C, which is higher than the substrate temperatures used for transducer deposition (section 2.2). The tin bonds were more difficult

to make, and had higher transmission losses, than the indium bonds. Acoustic amplifiers were therefore constructed using rods on which CdS transducers had already been deposited. Thrust pads with central recesses were used, so that a minimum of damage was inflicted on the transducers during amplifier assembly.

b) Bond Loss Measurements

The transmission losses of shear and longitundinal waves in indium bonds, made by the above technique, were measured between 1 and 2 GHz, using two sapphire rods bonded as shown in figure 35. A CdS transducer was deposited on one end of the longer rod, and the bond consisted of a layer of indium sandwiched between two 0.1μ thick layers of chromium.

A pulse input to the transducer produced reflections from the bond, and from the free end of the shorter rod. The rod lengths were such that the second echo, from the free face of the shorter rod, reached the transducer before the second echo from the bond. The relative amplitudes of the first three echoes were measured, and from these measurements, the reflection coefficients r, and the transmission loss, in the bond, were evaluated, as outlined in figure 35. An advantage of this method is that the transducer behaviour is unimportant, provided that it operates with reasonable efficiency over the frequency band of interest. An estimate of the bond thickness was made by doubling the measured thickness of the evaporated layer of indium, which does not take account of any changes produced by compression.

The transmission losses, in two different bonds, for longitudinal and shear waves, are given in figures 36a and 36b respectively. The

Path of Reflection

Power Level of Reflection

P_i

P_1 $\quad P_1 = |r_1|^2 . P_i$

P_2 $\quad P_2 = (1-|r_2|^2).(1-|r_1|^2)P_i$

P_3 $\quad P_3 = (1-|r_2|^2).(1-|r_1|^2).|r_2|^2.P_i$

$$P_2/P_1 = (1-|r_2|^2).(1-|r_1|^2)/|r_1|^2$$

$$P_3/P_2 = |r_2|^2$$

Figure 35 Technique for bond loss measurements.

bond thicknesses were 2x0.75μ and 2x0.2μ respectively. Using these dimensions, and known values of acoustic impedance for the materials,[32,36] the theoretical transmission characteristics of both bond structures were evaluated, and plotted on the same graphs. Internal losses were neglected in the case of the longitudinal bond, but an estimated loss of 5000 $dB/_{cm}$ at 1 GHz was included in the shear mode case. There is reasonable agreement between this simple theory and experiment for the longitudinal case, but for the shear case, agreement is not so good. A small error in thickness measurement in the shear case, of say 0.05μ, gives a large change in the calculated position of the resonance, as shown by the inclusion of the calculated result for a 0.5μ thick indium bond.

Further, since both experimental curves peak at lower frequencies than the calculated curves, the results imply that the acoustic velocities in these indium films are lower than the published values used in the calculations. The indium thickness was possibly reduced by compression, so that the theoretical response would have peaked at a higher frequency.

Good longitudinal bonds were made with indium thicknesses of 1.5μ and more, and with heating to 140°C, but in order to make good shear bonds, the indium had to be 0.5μ or less in thickness, and heated to 150°C. Shear bonds about 1.5μ thick had minimum transmission losses of about 10 dB, and the acoustic loss in indium thin films appears to be very high for shear waves, hence the above estimate of 5000 dB/cm.

These measurements were not performed to determine the transmission losses in bonds with great accuracy, but to obtain reasonable estimates. The accuracy of pulse height measurement was $\pm$ 1 dB, and as the final calculated losses are of this order, the accuracy is not sufficiently good to allow a very critical comparison with theory. r_1 and r_2 were usually in fair agreement, and their average was used in the calculations.

From figure 35, it can be seen that a perfect bond would produce only the second pulse, and so in practice, with highly parallel rods, when the second pulse is larger than the first pulse, the bond is clearly efficient. This situation existed, at most frequencies, for the longitudinal case, and at the minimum loss frequencies for the shear case. The transmission losses in tin bonds were measured only for longitudinal waves, and found to be between 5 and 10 dB at 1 GHz.

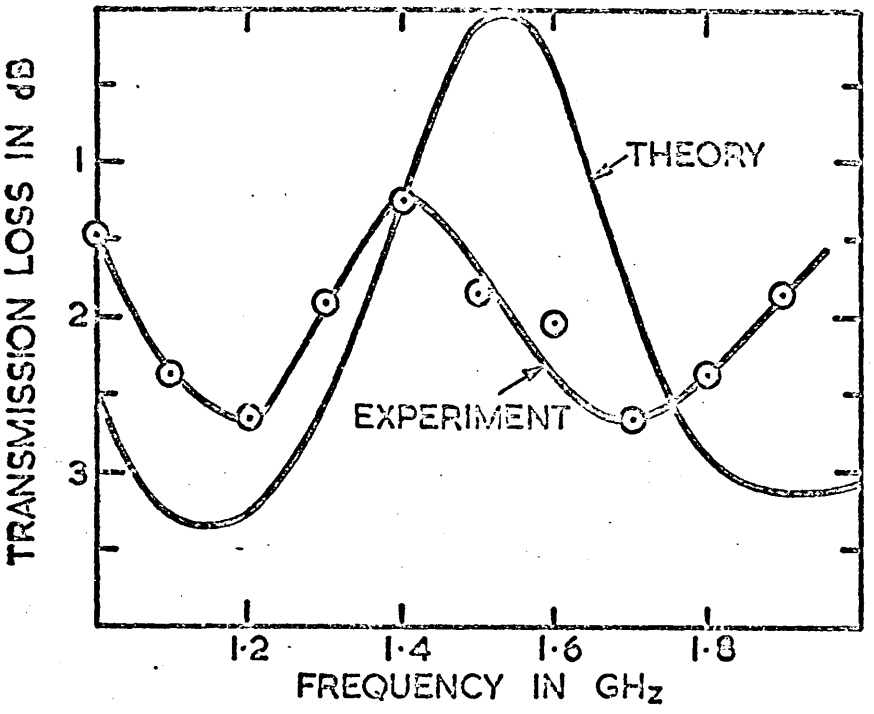

Fig. 36a. Transmission loss of longitudinal waves in a 2 x 0·75 μ thick indium bond.

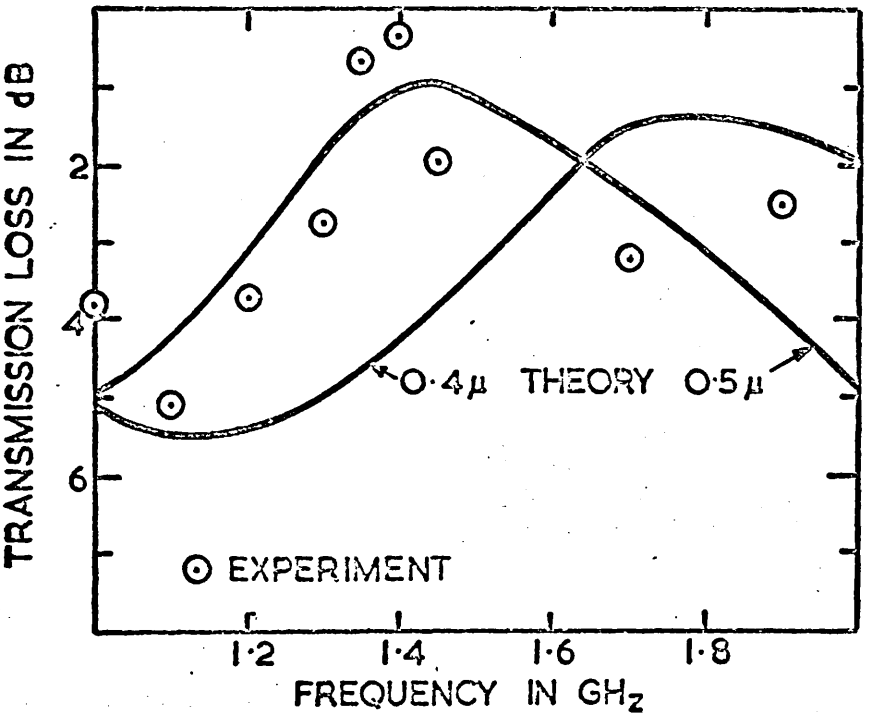

Fig. 36b. Transmission loss of shear waves in a 2 x 0·2 μ thick indium bond.

These measurements showed that efficient acoustic bonds could be made for microwave frequencies, using indium thin films.

3.4 Parameters of CdS

a) Observed Properties

The CdS used in the amplifiers was obtained from three sources; A.E.I. Ltd., the Eagle Picher Corporation and the Clevite Corporation.

The Eagle Picher samples had dark resistivities ranging from 10^5 to 10^7 Ωcm, and illuminated resistivities occasionally less than 10^3 Ωcm. The drift mobility of free electrons μ_d, was from 80 to 160 $cm^2/_{V\ sec}$, at room temperature, and fell with decreasing temperature to under 30 $cm^2/_{V\ sec}$ at 77°K. By probing the voltage distribution on 1 cm long samples, it was determined that the resistivity profile was uniform to within 10%. Measured electomechanical coupling constants K, were smaller than the published values.

Clevite material had higher drift mobilities, from 200 to 220 $cm^2/_{V\ sec}$, and a greater range of resistivity in any one sample, sometimes down to 500 Ωcm. The mobility increased as temperature fell, according to the relation $\mu_d = c.T^{-1.7}$ (where c is a constant) and measured K values were nearer published values. It was however, much less uniform material than Eagle Picher, and so the overall values of the parameters which were measured, do not adequately describe the material.

Only a limited amount of A.E.I. material was available, but

this proved to have K values very close to published values, and μ_d varied from 150 to 200 $cm^2/Vsec$. No measurements of uniformity, or of the variation of μ_d with temperature were made.

A simple, non-destructive, capacitive probing technique, which did not require contacts to be made to the CdS, was used to assess uniformity. Thin slices of CdS were placed between two sheets of Melinex insulation (0.0035" thick) on a flat polished steel plate. A steel probe (with a 3 mm diameter head) was allowed to rest on the upper surface, and the impedance between the probe and the steel plate was measured on a bridge. The measurements were reproducible, and gave the same information about the uniformity of the material as the voltage probing technique, without the complication of making ohmic contacts to the CdS.

The Hall mobility in CdS is about 300 cm^2/V sec, and the low measured drift mobilities are due to the presence of trapping sites.[23] Considerable effort has been devoted elsewhere to assessing the uniformity of CdS, [77,80,87] and the lack of uniformity in its properties is a major problem. Consequently the uniformity of Eagle Picher material is its one advantage, although reports have been made showing that A.E.I. material can be highly uniform.[78]

b) Selection of CdS Parameters

Single crystal CdS is grown from the vapour phase, and in practice it is more readily grown in the insulating state (dark resistivity greater than 10^6 Ωcm) or the semiconducting state (dark resistivity between 0.1 and 10 Ωcm), than for the intermediate resistivity range.[78] Resistivities of 10^3 Ωcm and less are of interest at frequencies above

1 GHz, since this is the resistivity required for maximum acousto-electric interaction as defined by $\omega^2 = \omega_C \omega_D$.[8] This resistivity range is normally obtained by illuminating higher resistivity CdS, but the technique of compensation by neutron bombardment, described in section 2.5.2, could be used to obtain suitable material, starting from semi-conducting CdS.

A test of this technique was carried out on a piece of CdS with a dark resistivity of 2.10^4 Ω cm (since semiconducting material was not available.) After measurement of the V-I characteristic,[9] to determine μ_d, the specimen was irradiated for one hour in the same thermal neutron flux of 10^{12} neutrons/cm^{2}sec. The dark resistivity rose to $1.7.10^5$ Ωcm, but μ_d did not change. μ_d was measured from the "knee" of the V-I characteristic, taken at the same conductivity as before irradiation. This technique can clearly produce CdS of the required resistivity, without altering the drift mobility. As previously discussed, annealing can remove the damage caused by fast neutrons, and the degradation of the electromechanical coupling constant should be only 2 or 3% after one hour of bombardment.

In cadmium, the penetration depth of thermal neutrons is about 0.5 mm,[53] and so this technique can only be applied to specimens 0.5 mm or less in thickness, in order to preserve a reasonably uniform resistivity profile. Such samples would be useful as oscillators.

3.5 Generation of Shear Waves

Before the development of double layer shear transducers,

were investigated.

a) Polished Transducers

Since a good bonding technique had been evolved, and precision polishing facilities were available, it appeared that transducers could be made by bonding CdS slices on to delay rods, and polishing the slices down to the required resonant thicknesses.[70] It was hoped that this method would give transducers with improved crystal structures, and has the advantage that any orientation of the CdS lattice, with respect to the substrate, can be chosen.

Two longitudinal CdS transducers were polished to 23 and 25μ thick respectively, making them resonant about 100 MHz. One was indium bonded, and the other cement bonded (Eastmann 910 cement), to a quartz delay rod. The indium bonded transducer looked more uniform, and had a minimum tuned insertion loss of 7 dB, whereas the cement bonded transducer had a 12.5 dB insertion loss. A shear transducer, on a sapphire delay rod, was polished down to a thickness of 9μ, and found to have a tuned insertion loss of 60 dB at 1 GHz where it would have been operating at a harmonic of the fundamental frequency. The performance at lower frequencies was also poor, possibly due to polishing damage extending throughout the slice of CdS. Broad band shear transducers for 1 to 2 GHz require to be 1μ or less in thickness, and so only a very small amount of surface damage can be tolerated. In the light of this poor result, it was decided to abandon this method, because of the technological difficulties.

b) Cavity Excitation of Shear Waves

As mentioned in section 2.1 shear waves can be excited in

CdS transducers deposited with the c-axis perpendicular to the substrate, by directing an electric field parallel to the substrate.[19, 38] CdS transducers were therefore deposited directly on sapphire delay rods, and energised in a simple tuned cavity, which developed an electric field parallel to the sapphire surface. The best conversion efficiency observed was 44 dB, which is too high for device operation. Several shear amplifiers were constructed with this type of transducer, but in only one case were transmitted signals detected. The complete assembly was very cumbersome, with cavities at each end of the amplifier.

c) Mode Conversion

Since efficient longitudinal CdS transducers were available for the frequency range of interest, they could be used as the starting point for shear mode generation in a mode converter,[46] as shown in figure 37.

A mode converter was made from sapphire, and the angle α was calculated, so that a reflected shear wave was produced at 90° to

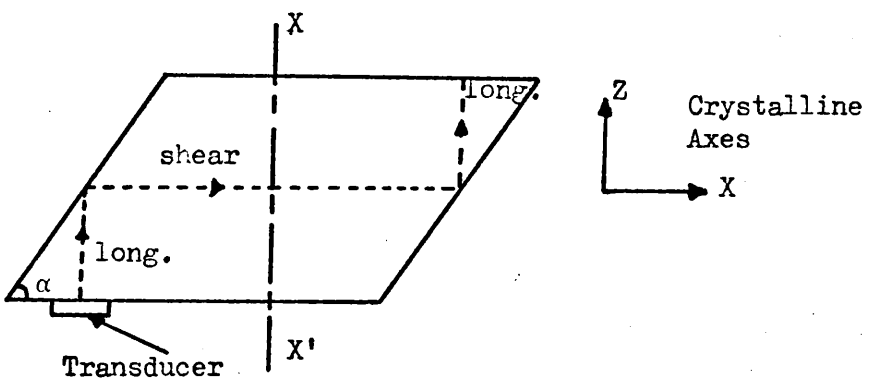

Figure 37 Sapphire Mode Converter.

the incident longitudinal wave. Two shear waves and a longitudinal wave are reflected from the surface, and so all the incident energy is not converted into the desired shear wave. In appendix A3, this situation is analysed, and the conversion loss is calculated.

It was proposed to cut the mode converter at right angles to the X axis, along the plane XX', and bond a CdS slice between the two halves. There would have been considerable technological difficulties in fabricating such an amplifier, but as the parallel work on double layer transducers produced results first, this approach was abandoned.

CHAPTER 4

4. Acoustic Amplification at Microwave Frequencies.

4.1 Introduction and Measurement Technique.

In this chapter measurements on the behaviour of CdS acoustic amplifiers, operating at 1 GHz and above, are presented and analysed. Both longitudinal and shear devices were constructed, using evaporated CdS transducers, in the configuration of figure 38, in which a slice of CdS is bonded between two sapphire delay rods.

The CdS slices were thin (2 mm or less) in order to minimise the effects of acoustic loss in the amplifier. Although this limits the maximum possible gain in the device, and prevents net gain being achieved, it allows the transmitted pulse to be observed in the maximum attenuation condition. The total transmission loss through an amplifier was usually between 80 and 90 dB, with no drift field on the CdS. The evaporated CdS transducers were produced by the techniques described in Chapter 2, and the amplifiers were pulse operated in order to reduce the power dissipation.

A coaxial jig was used to hold the amplifier, so that the centre posts on each of the transducers were accurately aligned. Electrical

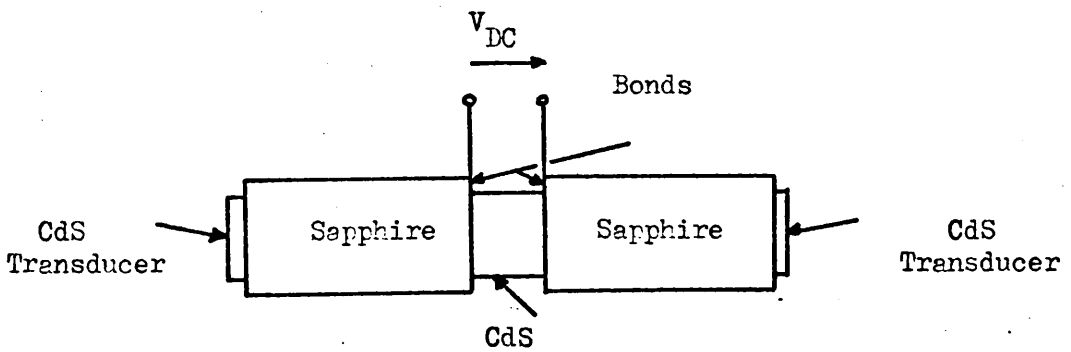

Figure 38. Acoustic Amplifier.

connections were made to the CdS slice by connecting wires to the indium bonds, with conducting silver paint. The 2.5 cm sapphire rods insulated the drift field from the r.f. system at the transducers, and 1000 pF capacitors were inserted into the 50Ω coaxial lines, on either side of the device, as further insulation.

The electrical system was virtually the same as figure 20, for transducer measurement, except that it was a two port system, without a circulator. D.C. pulses were produced by either a high power transistor amplifier, for voltages below 200V, or a thyratron switch, timed by a transmission line, for voltages up to 4kV. Focussed white light was used to illuminate the CdS, to reduce the resistivity. Several shear and longitudinal amplifiers were made, but results are presented only for representative devices.

4.2. Longitudinal Mode Amplifiers.

a) Measurements.

A 2mm thick slice of CdS (Eagle Picher No. 219) was used in a longitudinal mode amplifier. The c-axis of the CdS was in the direction of propagation, so that the appropriate electromechanical coupling constant was K_t^{52}. In figure 39a is shown the pulse pattern detected by the output transducer of the device. There are many reflections caused within the amplifier and delay rods, because of the mismatch between the acoustic impedances of the various media. Measurements were made on the first delayed echo, which had passed directly through the amplifier. A very strong double saturation was observed in the V - I characteristic (Figure 39b), and this type of saturation was not observed in any other longitudinal mode experiments. From the two

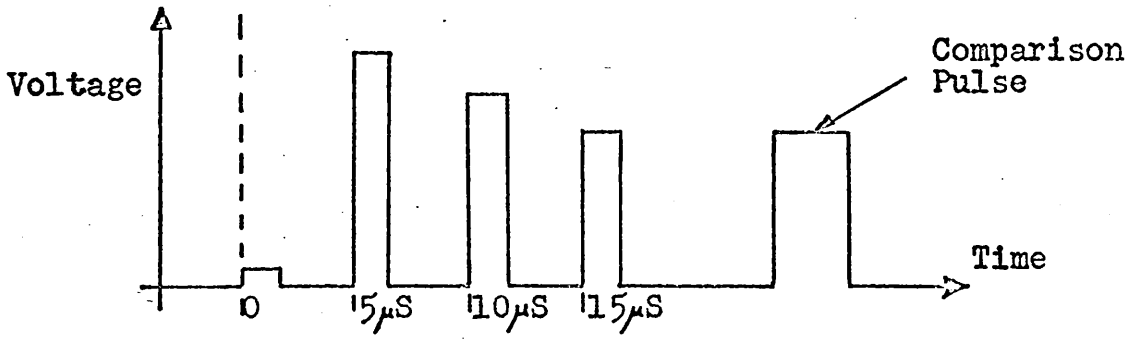

Figure 39a. Acoustic amplifier output.

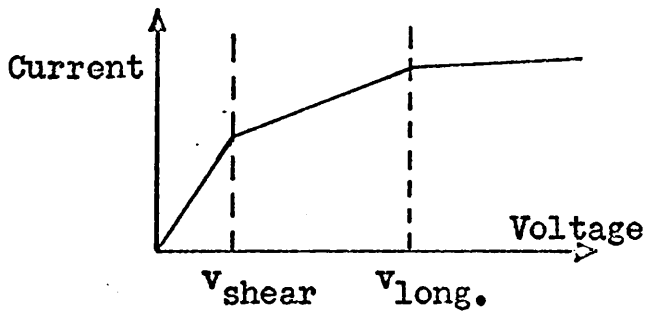

Figure 39b. V-I characteristic of 1st longitudinal amplifier

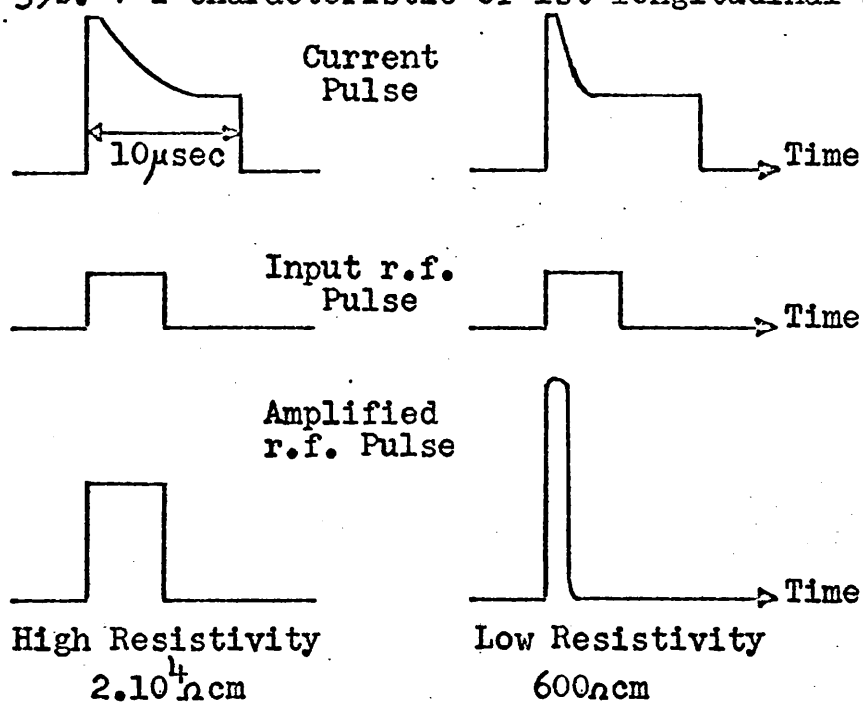

Figure 39c. Effect of resistivity change on the shape of the current pulse and the amplified r.f. pulse. (Drawings are not to scale.)

"knees" in figure 39b, the drift mobility for electrons was measured as 113 and 124 $cm^2/Vsec$, for shear and longitudinal waves respectively[9]. K_t^2 was measured in the absence of a drift field, by varying the illumination, and measuring the r.f. signal attenuation as a function of conductivity[5] (see equation 31 of Chapter 1). K_t^2 was 0.014, which is much lower than the published value of 0.024, but was typical of K_t^2 measurements made on Eagle Picher crystals.

A small acoustic gain of 20 dB/cm was observed at 1 GHz, which is much less than predicted by the White theory[8]. It was observed that varying the specimen resistivity, in the gaining condition, affected the shape of the current and r.f. pulses, as shown in figure 39c. When the resistivity was decreased, the current pulse saturated more quickly, and the width of the amplified pulse decreased, although the amplification increased. This amplifier did not give a full attenuation versus drift field characteristic, as the combined loss of the various components was high, and increasing the loss reduced the signal level nearly to noise level, so that measurements could not be made accurately. The amplifier was dismantled and the CdS sample was polished down to less than 1mm in thickness, but was broken before being assembled in another amplifier.

Another slice of the same CdS boule, 0.84 mm thick, was built into a longitudinal amplifier. K_t^2 was measured as 0.0145, and the V - I characteristic is sketched in figure 40 a. This is much more typical of longitudinal wave propagation in CdS, than figure 39 b. The measured drift mobility was 144 cm^2/V sec. Gain was observed from 1.0 to 1.8 GHz, and figure 41 is a plot of the attenuation versus drift field curve for this amplifier at 1.2 GHz. The theoretical curve,

evaluated for the measured drift mobility, resistivity and K_t is also included. 0 dB is the dark attenuation level. Maximum gain of 100 dB/cm was observed at 1.1 GHz. Figure 40b shows the current pulse, and the acoustic noise detected by the output transducer, produced by applying a rectangular voltage pulse to the amplifier, with no r.f. input pulse. The drift voltage pulse was greater than the voltage required to drift the electrons faster than the longitudinal velocity of sound, and was many times longer than the acoustic round

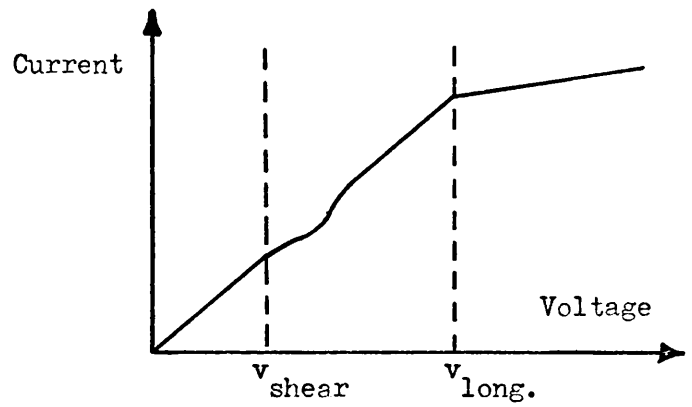

Figure 40a. V-I characteristic of second longitudinal amplifier.

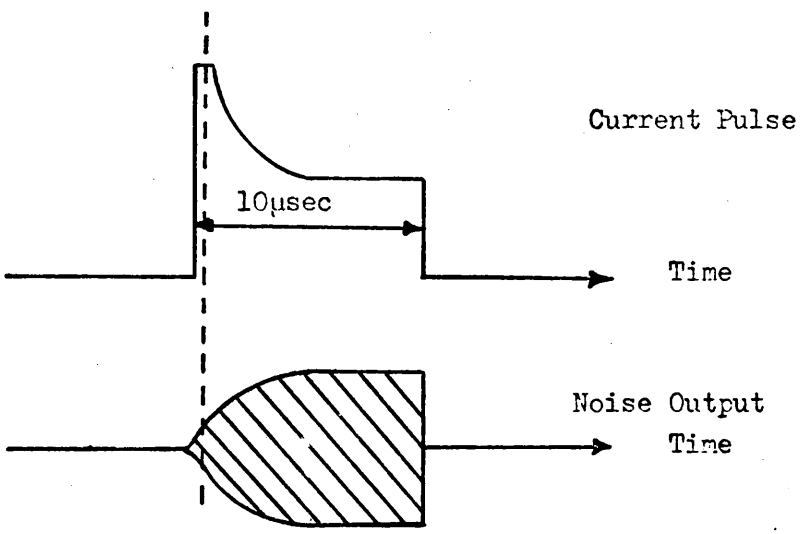

Figure 40b. Current pulse and noise output in second longitudinal amplifier.

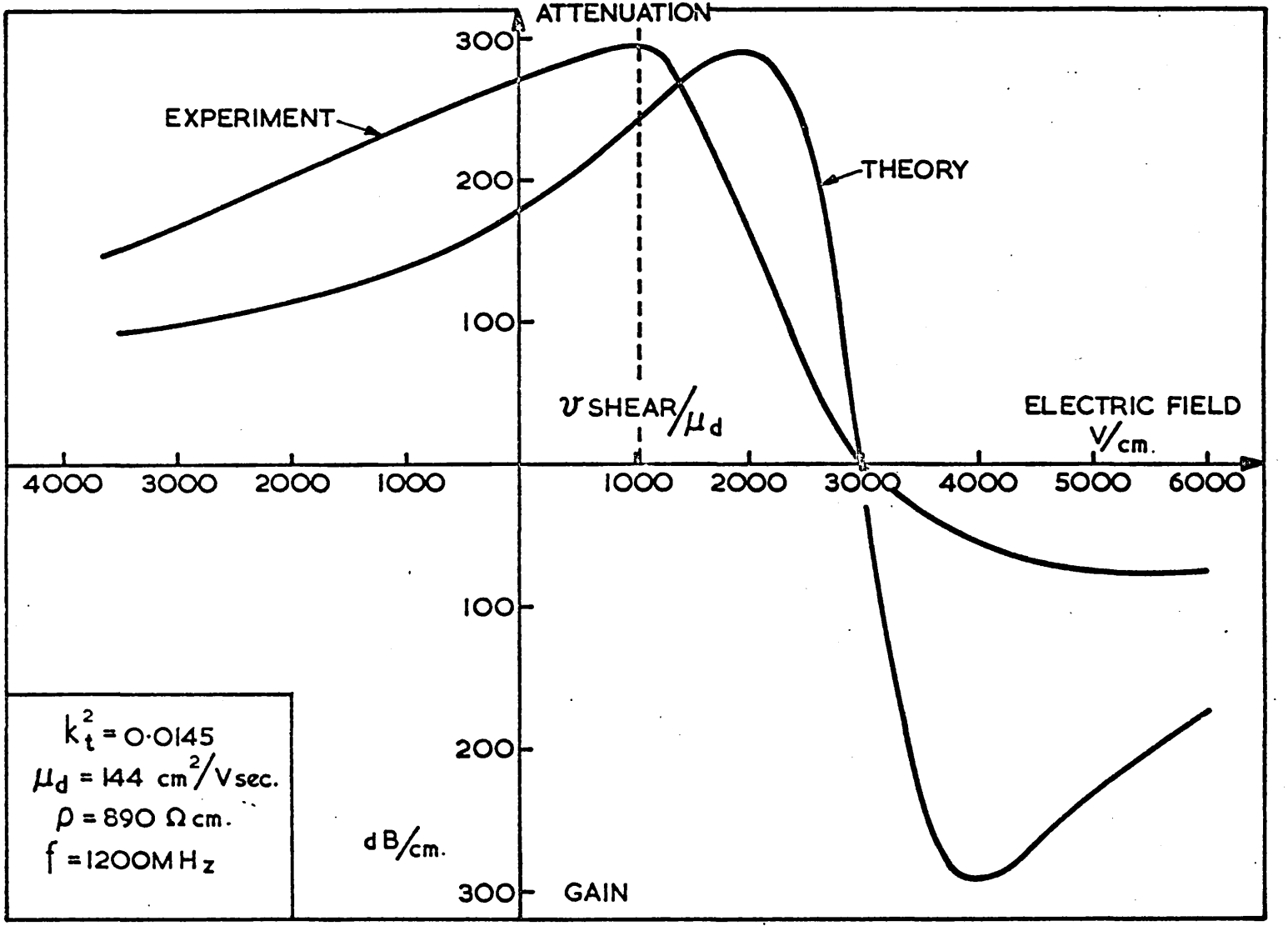

Fig. 41. Attenuation against drift field for longitudinal amplifier.

trip in the CdS, so that the noise reached a steady state value. By increasing the drift voltage, the noise was made to grow to the same amplitude as an amplified r.f. acoustic pulse positioned at time t_1.

b) Analysis of Results.

As expected, the gain observed in both longitudinal amplifiers was much less than predicted by the White theory[8], due to the energy of the electrons being lost to shear acoustic noise[9]. In figure 41 there is only a rough overall similarity between the theoretical and experimental curves. At electric fields greater than the shear saturation voltage V_{ss}, shear noise is being amplified, but the gain observed was still significant. Although the White theory[8] predicted that maximum interaction would occur at 1450 MHz, the maximum gain of a coherent longitudinal signal occurred at 1100 MHz. This is consistent with the view that energy is being lost to shear noise by the electrons, since this presumably reduces the r.f. conductivity, and the effective ω_c, in relation to the White theory[8]. The frequency of maximum interaction should therefore be reduced. When the electric field was lower than V_{ss}, the observed attenuation was anomalously high. The most plausible explanation of this high level of attenuation is that the sample had a non-uniform resistivity profile, resulting in the measurement of average parameters, which were then substituted in the theory. Juggling values of resistivity, and K_t, can produce a curve which fits the experimental curve quite well, for drift fields

less than V_{ss}, but this has little meaning if the material is non-uniform ($K_t^2 = 0.01$, and a resistivity of 300Ω cm gives a good fit . The lower resistivity would increase ω_c and the theoretical frequency of maximum interaction).

The gain, in figure 41, did not pass through a maximum but appeared to reach a constant level as the electric field was increased. When the drift voltage across the amplifier is higher than that required to drift the electrons faster than the velocity of sound, it has been shown elsewhere[79,80,86], that the internal electric field profile can become highly non-uniform, even in samples with relatively uniform resistivity. A region of very high field can develop, and further increases in the drift voltage only increase the electric field in the high field region, leaving the field over most of the specimen unchanged. If the high field region is narrow, it is conceivable that the total gain of the amplifier could be constant, once the gain in the high field region has exceeded the peak value.

In figure 40b, the relationship between the decay of the current pulse, and the acoustic noise detected at the output transducer, is given. The decay of the current pulse is due to the increase in the acousto-electric current, which accompanies the build up of acoustic flux[17], and opposes the ohmic current. Since the time required to reach current saturation is longer than an acoustic round trip, the build up involves many round trips. Coherent longitudinal pulses were amplified when they occurred at approximately time t_1 in the current pulse, before saturation had been reached. In the saturated part of the current pulse, the electrons have given up most of their excess

momentum to the acoustic system, and will have velocities close to the sound velocity. Very little momentum can then be transferred, and a coherent signal, occurring in the saturated part of the current pulse, will only be slightly amplified. Furthermore, the reduction of the effective r.f. conductivity, discussed above, and the non-uniform field distribution arising in an amplifying crystal, may also reduce the gain. In figure 39 c, it can be seen that increasing the conductivity increased the amplification, and the rate of the build up of acoustic flux. The above discussion explains why only the r.f. signals which occurred before the current in the amplifier saturated, received significant amplification.

Shear waves propagating along the c-axis in CdS are not acousto-electrically active (see section 1.4), and so there should be no coupling between carriers and shear waves moving along the c-axis. From figure 7[29], it can be seen that a slight misorientation of the crystal will result in some coupling to shear waves. The two CdS amplifiers were found to be accurately oriented within the limits of experimental accuracy, which is about 2^{o}. Shear waves propagating at an angle to the c-axis can interact with carriers moving parallel to the c-axis,[9,13] and K^2 can be significant. These off axis waves have been shown by McFee[9] to cause current saturation to occur, at drift fields which are approximately half the crossover drift field for longitudinal mode propagation along the c-axis. In the above experiments the onset of saturation occurred at drift fields which corresponded roughly with shear mode propagation along the c-axis, and it is not clear whether misorientation, or off axis waves, are responsible for

the coupling.

The V - I characteristic of the longer amplifier, (figure 39 b), shows a much stronger saturation than that of the shorter amplifier (figure 40 a). 10μ sec. pulses were used, so that the current was measured in the steady state in both amplifiers. The stronger shear saturation of the longer amplifier is probably due to the amplification of shear modes. These modes are amplified more in one transit of the longer amplifier, and the amplification mechanism may become more non-linear, in the steady state, than in the shorter specimen.

The noise output of the amplifier was examined in a spectrum analyser, and there was no apparent peak frequency between 100MHz and 4 GHz, although many discrete frequencies were observed. It must be noted, however, that the bandwidth of the output transducer is superimposed upon the bandwidth of the amplifier.

Since the measured drift mobilities were much less than the Hall mobility[59], there must have been trapping levels in these amplifiers. Any asymmetry in the attenuation versus drift field curves, due to trapping[23,24] (see section 1.7) is masked, in the longitudinal amplifier, by the loss of carrier momentum to shear noise.

4.3 Shear Mode Amplifiers

a) Measurements.

A good shear wave amplifier was made from a 1 mm. slice of A.E.I. CdS, using double layer evaporated shear transducers. The measured K_{15}^2 was 0.0324, which corresponds well with published values[35]. The drift mobility was found to be a function of conductivity, and

ranged from 147 to 187 cm^2/V sec. The resistivity varied from $1.5.10^4 \Omega cm$ in the dark to 260Ωcm under strong white light. In figure 42 are given the experimental and theoretical attenuation versus drift field curves, at 1 GHz, for two different conductivities. OdB is again the dark attenuation level, and a maximum forward gain of 450 dB/cm was observed. The noise level of the receiver during measurements is given to show the limit of measurement, and the acoustic noise detected by the output transducer at maximum conductivity is also shown.

The transmission losses in the amplifier, in the dark, at 1 GHz can be accounted for as follows,

Insertion Loss in 2 Transducers	59 dB
Acoustic Loss in delay rods	9.5 dB
Acoustic Loss in 1 mm of CdS[69]	8 dB
Bond Loss	8 dB
	84.5 dB

The transducer insertion loss, and the acoustic loss in the delay rods were measured after the amplifier had been dismantled. The loss attributed to the bonds is simply the difference between the measured total transmission loss, and the sum of the acoustic losses in CdS and sapphire and the measured transducer insertion loss. Since the bond loss is therefore a small difference between two large quantities, the figure obtained is not accurate, although it is of the correct order (see section 3.3).

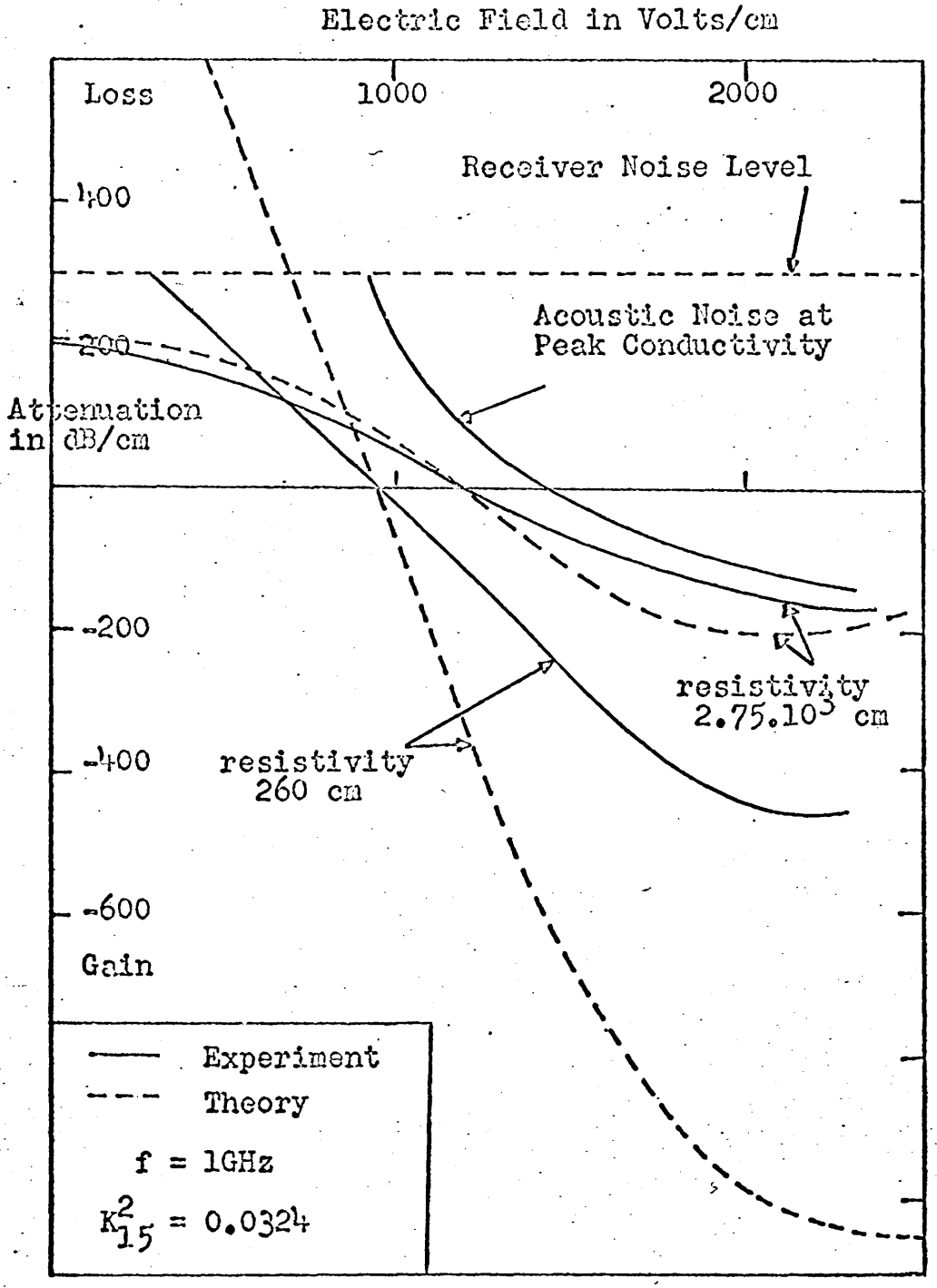

Figure 42. Attenuation against drift field for shear mode amplifier.

Less accoustic noise was generated in this shear wave amplifier than in the longitudinal amplifiers, although the maximum level of acoustic noise was 24 dB above the noise level of the receiver (-93 dBm). Between 1 and 2 GHz, the peak noise level remained at the same value, but the peak gain of a coherent signal, at maximum conductivity dropped from 450 dB/cm at 1 GHz to 265 dB/cm at 1.9 GHz. The shape of the attenuation against drift field curves appeared to be the same as the frequency increased.

This amplifier was the best shear mode device which was constructed. Other amplifiers, made with Eagle Picher and Clevite material, had maximum gains of less than 100 dB/cm.

When a shear wave strikes a sapphire surface, two shear waves, with different velocities, are produced in the sapphire[36]. The fast shear wave was used for making measurements in the CdS, and with the length of sapphire delay rod used, the two waves were quite distinct. Two shear waves are also generated in CdS[15], and since propagation is in the basal plane, one wave is polarised along the c-axis, and the other in the basal plane perpendicular to the c-axis. Only the former shear wave is piezoelectrically active. The transducers were deposited on the sapphire, so that the polarisation of the transducer was at a suitable angle to the sapphire lattice to cause most of the energy to couple into the fast shear wave. The amplifier was assembled so that the c-axes of the transducers, and the c-axis of the CdS slice, were parallel.

A C.W. test was performed on this amplifier. With a drift voltage greater than the saturation value, the amplifier, immersed in

alcohol, operated for an hour without breakdown. The power being dissipated was 20W in a volume of 0.1 cm^3.

b) Analysis of Results.

The measurements of attenuation in figure 42 are incomplete, since the magnitude of the interaction was very large at maximum conductivity, and a large electric field had to be applied to raise the coherent signal above noise level. The shape of the characteristic for the lower conductivity is very similar to that predicted by the White theory[8]. Since the drift mobility is dependent on the conductivity, it is likely that trapping effects can influence the shape of the characteristic. The trapping theory of Uchida et al[23,24] (section 1.7b) shows that decreasing the conductivity makes the attenuation versus drift field curve more asymmetric, since a greater fraction of the bunched carriers is trapped at lower conductivities. A further complication is the effect of non-uniformities in the CdS on its properties, which can result in false measurements of the conductivity and drift mobility. A factor of two difference, between experimental and theoretical values of gain, can easily arise from a factor of two error in the measurement of the conductivity, due to non-uniformities.

From the measurements made with a resistivity of $2.75.10^3$ Ωcm, an estimate of the asymmetry can be obtained, and the factor "a" calculated (see section 1.7 b). bfo is obtained from the crossover field value, using the known Hall mobility in CdS[59]. The values obtained suggest the presence of a trapping level with a relaxation time τ of 10^{-10} secs, which is a reasonable value, since at frequencies

just above 1 GHz, $\omega.\tau \sim 1$, and these traps will have a significant effect. When the estimated value of "a", and appropriate value of bfo, are used to calculate the shape of the attenuation versus drift field curve, much better agreement is obtained between theory and experiment for both levels of resistivity. The factor f_o was calculated as 0.639 for the low resistivity case.

The frequency of maximum interaction, with maximum conductivity, obtained from $\omega^2 = \omega_C \omega_D$, is 860 MHz. Thus the observed decrease in the magnitude of the interaction, as the frequency rises from 1 to 2 GHz, is as expected from the theory.

A maximum gain of 45 dB/mm was observed, and it appears therefore that with a longer piece of CdS and more efficient transducers, a net gain acoustic amplifier could be built. The total gain available from an amplifier is the difference in power levels between thermal noise in the lattice, and the saturation value of acoustic flux. The latter quantity can be arrived at by considering that the wave carrier interaction in acoustic amplification is limited by the number of carriers available to take part in the mechanism[69].

For the shear wave amplifier, at its maximum gain condition, the calculated saturation acoustic flux is 240 mW/mm^2. Since the acoustic beam area is approximately 1 mm^2, then the power level of acoustic saturation is approximately + 24dBm at 1 GHz. The power level of lattice thermal noise is about -90 dBm, so that the maximum available electronic gain in the CdS is approximately 110 dB, which could have been obtained with 3mm of the CdS used in the shear wave amplifier, allowing for 8 dB/mm acoustic loss at 1 GHz.

C.W. operation of an acoustic amplifer presents difficulties. As explained above, a few microseconds after the application of an amplifying drift field, the current decays to a saturated value, so that the electrons have much less momentum available for transfer to an acoustic wave, and the amplification will be small. Wanuga[81] showed that C.W. operation was possible at liquid nitrogen temperature, without destroying the CdS. The experiment described above showed that C.W. operation is possible at room temperature, if a heat sink is provided. Wanuga's[81] amplification measurements, for a shear wave amplifier, are very similar to figure 41, indicating that the build up of acoustic noise accompanying current saturation, is reducing the amplification of a coherent signal. C.W. amplifiers may still have useful gain, but will have very poor noise figures.

4.4 Discussion.

The measurements which have been made of transducer performance and acoustic gain, show that broad band acoustic amplifiers, with net overall gain of up to 50 dB, could be fabricated to operate at frequencies above 1 GHz. The usefulness of an amplifier is determined by its noise figure. Any desired amplification can be achieved simply by linking amplifiers in series, although the levels of amplification discussed in section 4.3., indicate that a high level of net gain could be achieved by one well designed acoustic amplifier. Measurements of the noise figures of acoustic amplifiers have been published by Hanlon[82,83]. He measured the noise figures under pulsed conditions, and at drift fields below that at which acoustic noise had built up

to a steady state value. Noise figures as low as 6 dB were measured around 150 MHz, when this was the frequency of maximum gain per unit D.C. power input, f_m. The noise figures increased with frequency, and as the operating frequency deviated from f_m. At 900 MHz, a noise figure of 25 dB was measured, and for most ranges of frequency and conductivity the figure was around 10 dB. Under C.W. conditions, the build up of acoustic noise will make the noise figure of the device much worse. The efficiency of the transducers will directly effect the noise figure of the amplifier, since inefficient transducers reduce the net gain[69].

A possible application of the acoustic amplifier is as a recirculating store. C.W. operation would be desirable, and although this is feasible, would result in a high noise figure, and reduced gain. It is essential that no spurious pulse be created by reflections from boundaries in practical amplifiers (figure 38). This means that the CdS to sapphire bonds must be multi-layer structures to produce perfect impedance matching. Calculations show that a bond structure such as "chromium - silver - indium", could be a perfect match, and would have a bandwidth of 60% or more, centred on 1 GHz. In order to get the maximum storage capacity, with 10 cms of sapphire as the delay medium, 10nSec pulses, at 20nSec separation, must be used. The bandwidth of the multi-layer bond is adequate for this pulse width, otherwise an external pulse shaping network may be required. The storage capacity would be 500 pulses.

In order to reduce the amplitude of reflections from the output transducer, a suitable bond and backing must be used. The reflected signal will be attenuated in its passage back through the CdS amplifier, and should create no difficulties if it is 20 dB down on reaching the output transducer for the second time, since some external discriminating network could be used to obliterate it.

A more practical amplifier would not operate C.W., but could be designed so that the D.C. drift field pulse was triggered by the input r.f. signal, and suitably delayed, so that it was applied to the CdS amplifier at the correct moment for maximum amplification. Such a system would have a much reduced storage capacity.

The maximum frequency at which CdS acoustic amplifiers can be operated is of interest. For a given mode of propagation in a crystal, the limiting frequency range is reached when the wavelength λ, is much less than the Debye screening length L_D, and carrier bunching is much reduced by the thermal motion of the electrons. Equation 11 in chapter 1 gives the relationship between the angular frequency ω, and L_D, in terms of ω_C and ω_D.

$$\frac{\omega_C \cdot \omega_D}{\omega^2} = \left(\frac{\lambda}{2\pi L_D}\right)^2$$

The limiting frequency range can be raised by increasing the conductivity, and hence ω_c, but this means that the D.C. power dissipation per unit gain will also rise, and it is therefore doubtful if practical CdS amplifiers could operate at X band frequencies. Even if the high power dissipation could be tolerated, the acoustic loss in CdS would limit operation to X band.

	CdS Acoustic Amplifier	Transistor Amplifier
Gain	50 dB	30 dB
Bandwidth	750 MHz	1 GHz
Noise Figure	20 dB	6 dB
Delay	built in	none
External Circuitry	D.C. supply 100V possibly pulsed.	15V D.C.

Table 11 Performance of a CdS acoustic amplifier and a transistor amplifier with centre frequency at 1.5 GHz.

Since the project was begun, advances in transistor technology have made broad band, low noise, transistor amplifiers available for microwave frequencies[84,87]. In table 11, the properties of an amplifier of each type are compared, for a centre frequency of 1.5 GHz. The gain is quoted for one amplifier, but the gain can be increased by cascading amplifiers. The only advantage of the acoustic amplifier is built in delay, but this can be achieved by using a delay rod in conjunction with a transistor amplifier. The transistor amplifier is much less complex than the acoustic amplifier, and is clearly the better device.

CHAPTER 5

5. Conclusions

From the measurements presented on transducer efficiency and acoustic amplifier performance, it is clear that net gain CdS acoustic amplifiers could be constructed to operate at frequencies above 1 GHz. Between 1 and 2 GHz the behaviour of amplifiers gave qualitative agreement with the linear theory developed by White[8], and high gain per unit length was observed in both shear and longitudinal mode amplifiers. Gain of up to 450 dB/cm was observed in shear mode amplifiers, and up to 100 dB/cm in longitudinal amplifiers. Differences between the experimental and theoretical behaviour of amplifiers were attributed to either the generation of acoustic noise, or non-uniformity in the parameters of the CdS. The acoustic noise is generated when electrons drift faster than the velocity of sound, and lose energy to incoherent lattice vibrations, and not to a coherent acoustic wave. Since the shear velocity of sound is less than the longitudinal velocity of sound in CdS, the gain of coherent signals in longitudinal mode amplifiers is considerably reduced by the generation of shear acoustic noise. Many CdS crystals have non-uniform resistivity profiles[77], and the measured bulk values, which are used in calculations, are averages, so that complete agreement between theory and experiment cannot be expected. Except for the A.E.I. material, the CdS crystals used in the devices had lower electromechanical coupling constants, K^2, and

lower electron drift mobilities (indicating the presence of trapping levels), than crystals described in the literature[5,35].

Broad band transistor amplifiers, with reasonable noise figures, are now commercially available, for frequencies up to 4 GHz[87]. The acoustic amplifier cannot compete with transistor amplifiers, due to its poorer noise performance, and the greater technological difficulties in construction. In C.W. conditions the acoustic amplifier is very noisy, and has much reduced gain, so that pulsed operation is necessary for high gain. The acoustic amplifier might be used as a recirculating store, since a poor noise figure can be tolerated in this application, if there is high gain to give good discrimination between the "on" and "off" conditions. The storage capacity is determined by the delay time in the device, and would be small if the amplifier was pulse operated. The amplification of acoustic surface waves has been demonstrated in CdS[88], and there is a possibility that surface wave acoustic amplifiers could be used in microwave thin film circuitry.

CdS acoustic amplifiers could be operated up to X band frequencies, if very high power dissipation could be tolerated. The acoustic loss in CdS will be high at X band, and will effectively limit useful, room temperature operation to this frequency range. Of the other available piezoelectric semiconductors, zinc oxide has a higher K^2 than CdS, but this is of no advantage in an acoustic amplifier, since the drawback of acoustic noise generation is not eliminated by replacing CdS by ZnO. The same gain can be achieved in CdS, as in ZnO,

by using longer samples. It is possible that InSb acoustic amplifiers, with crossed electric and magnetic fields, may be able to operate at X band, although low temperatures may be required[27].

It appears that CdS acoustic amplifiers are unlikely to find a practical application, but CdS may have a use as a high Q oscillator. The resonant frequencies are difficult to predict accurately, since they are selected by a non-linear mechanism, and are dependent on the oscillator thickness, conductivity and applied drift field.

The most useful aspect of this project was the development of the technology required to produce acoustic amplifiers for frequencies of 1 GHz and above ; in particular, the study of evaporated CdS transducers. These transducers were thin films, consisting of CdS crystallites with a preferred orientation. Under most deposition conditiors, crystallites were deposited with the hexagonal c-axis perpendicular to the substrate, so that they were suitable for use as longitudinal mode transducers. X ray analysis showed that the structure of CdS films became more highly ordered as the thickness increased. Without any tuning or matching, these transducers, fundamentally resonant above 1 GHz, had bandwidths of around 50%, and the typical insertion loss was 30 dB. The high insertion loss arises because of a gross impedance mismatch, between the transducer and the excitation system. With stub tuning the insertion loss can be reduced to less than 10 dB. It is difficult to analyse the behaviour of evaporated transducers, due to the large number of parameters which cannot be measured independently. Information was obtained by comparing theoretical and experimental

transducer frequency responses, and making impedance measurements. This showed that some transducers had a significant contact resistance, and that the effective K^2 of evaporated transducers was of the same order as that of single crystal CdS. Many transducers were found to have a low resistivity, and consequently had a high insertion loss. The transducers were n-type, due to an excess of cadmium, and a new method of compensation, by thermal neutron bombardment, was developed. A new deep trapping level was created, thus raising the resistivity, but the induced damage reduced the value of K^2. Fortunately, only a short irradiation was required, to raise the resistivity sufficiently to remove any leakage resistance shunting the transducer, and K^2 fell by only 2 or 3%. The changes in K^2 were investigated in single crystal CdS, and it was found that fast neutron damage could be annealed out at 350°C, whereas thermal neutron damage was not wholly removed by annealing. This technique was completely reproducible, and could be applied to single crystal CdS, to obtain thin slices with a dark resistivity in the range 10^2 to 10^3Ωcm, which is difficult to obtain by growth from the vapour phase[78].

Shear mode evaporated CdS transducers were made by depositing CdS at a high rate (greater than 0.1μ/min) at an angle to the substrate, and under these conditions the c-axis grows in the direction of evaporation. With an angle of 38.5°, between the c-axis and an electric field applied normal to the substrate, there is no coupling to longitudinal waves, and only shear waves are generated[29]. A

finite thickness of CdS has to be deposited before the c-axis bends to 38.5°, as the initial CdS layers are deposited with the c-axis perpendicular to the substrate. This single layer technique limits the upper frequency of operation as a shear mode transducer to 2 GHz at best. By using a double layer structure for the CdS, this limitation was overcome. The bottom layer, in which the c-axis bends, was cadmium doped, so as to have a low resistivity, and the upper layer was of high resistivity CdS, with the required orientation of the c-axis throughout. The high resistivity top layer of CdS dominated the transducer response, and the bottom layer acted as an acoustic transmission line. Since the top layer can be very thin, it should be possible to make shear transducers which have their fundamental resonance at X band frequencies. Acoustic loss in the thin films will then be the factor which determines the upper frequency range for efficient operation of these transducers. An application for X band shear transducers is in a room temperature delay line, using the spinel $MgAl_2O_4$ (magnesium aluminate), which is thought to have a low acoustic loss for shear propagation at X band. Longitudinal CdS transducers can be used on sapphire delay lines, which have been shown to have the required temperature stability to act as calibrators for radar altimeters.

Bond loss measurements showed that thermo-compression indium bonds could have very low transmission losses above 1 GHz, if carefully made. Shear waves in indium appear to have a high acoustic loss above 1 GHz, and so shear bonds must be very thin (0.5μ or less) to minimise losses. Finally, a useful method of making ohmic contacts to CdS was developed,

and indicated that diffusion of indium into dislocations was an important aspect of contact formation.

APPENDIX

A1. Equivalence of Transducer Theory and Standard Equivalent Circuits for Transducers.

Working from section 2.3., in which the equations were expressed in a one dimensional form, equation 16 gives

$$E_u L = V - \sum_{i=1}^{2} \left(E_i \left(e^{jk_i x}\right)/jk_i\right)_0^L \quad \ldots\ldots\ldots\ldots A1$$

$$\therefore \quad E_u L = V + j\frac{E_1}{k_1}\left(1 - e^{jk_1 L}\right) + j\frac{E_2}{k_2}\left(1 - e^{jk_2 L}\right) \ldots . A2$$

Equations 24 and 25 give

$$v_B - v_A = -\frac{T_1}{Z_o}\left(1 - e^{jk_1 L}\right) + \frac{T_2}{Z_o}\left(1 - e^{jk_2 L}\right) \ldots\ldots . A3$$

Substituting the relation $T_i = \dfrac{-eE_i}{\left(1 - k_i^2 . c/\omega^2 M\right)}$

and using the fact that $k_2 = -k_1$

$$v_B - v_A = \frac{e}{\left(1 - k_1^2 . c/\omega^2 M\right) Z_o} \times \left(E_1\left(1 - e^{jk_1 L}\right) - E_2\left(1 - e^{jk_2 L}\right)\right) \ldots . A4$$

Now $\quad k_1 = \dfrac{\omega}{v_s\left(1 + K^2\right)^{\frac{1}{2}}} \quad ; \quad Z_o = \dfrac{c}{v_s\left(1 + K^2\right)^{\frac{1}{2}}}$

$$1 - \frac{k_1^2 c}{\omega^2 M} = \frac{K^2}{1 + K^2} \quad ; \quad h = \frac{e}{\varepsilon}$$

$$\therefore \quad E_u L = V + j \frac{h}{\omega} (v_B - v_A) \quad \text{.....A5}$$

The current I is given by equation 21, and since a transducer is normally made of insulating material, $\sigma = 0$

$$\therefore \quad I = - j\omega\varepsilon A E_u \quad \text{.....A6}$$

$$\therefore \quad I = - j\omega\varepsilon A \left(\frac{V}{L} + j (v_B - v_A) \cdot \frac{h}{\omega} \right)$$

If $C = \varepsilon A/L$, is the transducer capacitance

$$I = - j\omega CV - h C (v_B - v_A) \quad \text{.....A7}$$

The negative signs on the R.H.S. of equation A7 arise from the choice of $e^{-j\omega t}$.

Equation 17 gives $T_u = -eE_u$ for the uniform mode

$$\therefore \quad T_u = - hD_u,$$

hence the boundary conditions, equations 22 to 26 can be expressed as

$$T_1 + T_2 = T_A + hD_u \quad \text{.....A8}$$

$$T_1 e^{jk_1 L} + T_2 e^{jk_2 L} = T_B + hD_u \quad \text{..... A9}$$

$$T_1 - T_2 = Z_o v_A \quad \text{.....A10}$$

$$T_1 e^{jk_1 L} - T_2 e^{jk_2 L} = Z_o v_B \quad \text{.....A11}$$

Equations A8 and A10 give

$$T_1 = \tfrac{1}{2} \left(Z_o v_A + (T_A + hD_u) \right) \quad \text{.....A12}$$

$$T_2 = \tfrac{1}{2} \left((T_A + hD_u) - Z_o v_A \right) \quad \text{.....A13}$$

Substitution of equations A12 and A13 in A9 and A11

gives $(T_B + hD_u) = (T_A + hD_u)\cos k_1 L + jZ_o v_A \sin k_1 L$ A14

and $v_B = v_A \cos k_1 L + j \frac{(T_A + hD_u)}{Z_o} \sin k_1 L$ A15

$$\therefore T_A + hD_u = \frac{Z_o}{j\sin k_1 L} \cdot v_B - \frac{Z_o}{j\tan k_1 L} \cdot v_A \text{.....A16}$$

$$\therefore T_B + hD_u = \frac{Z_o}{j\tan k_1 L} \cdot v_B - \frac{Z_o}{j\sin k_1 L} \cdot v_A \text{.....A17}$$

Equations A7, A16 and A17 are the electrical and mechanical terminal equations for the transducer, and are identical to those used in the derivation of standard transducer equivalent circuits[2,32].

A2 Measurement of Transducer Impedance

The transducer impedances were measured by the "double power point" method, on a 50Ω standing wave indicator[60,85]. Since the VSWR is high, the simple technique of measuring the maximum and minimum voltages of the standing wave, cannot give accurate results, for several reasons. The voltage range may exceed the square law range of the diode detector, or, if the probe coupling has to be increased to detect the minimum, the probe may load the line. Further the line impedance may increase as the VSWR increases, and become comparable to the detector impedance.

The voltage profile at the minimum, and the vector diagram of the voltages are shown in figures 43a and 43b respectively. V_i, V_r

and V_t are the incident, reflected and total voltages.

If θ is zero, $V_{min} = V_i - V_r$

At the voltage minimum, the current detected by the diode is I_m, where $I_m = k.V_{min}^2$, where k is a constant.

At the double power point, the detected current is $2I_m$.

$$2I_m = k\ (V_{min}^2 + V_i^2.\tan^2\theta\ )$$

$$\therefore\ V_{min} = V_i.\tan\theta$$

$VSWR = V_{max}/V_{min} \approx 2V_i/V_{min}$, since $V_{min} << V_{max}$

$$\therefore\ VSWR = 2/\tan\theta \approx 2/\theta,\ \text{as } \theta \text{ is small.}$$

$$\theta = 2 \times \frac{2\pi}{\lambda} \times \frac{\Delta}{2} = \frac{2\pi\Delta}{\lambda}$$

$$\therefore\ VSWR = \lambda/\pi.\Delta \quad \ldots\ldots\ldots\ldots\ldots\ldots\ldots\ldots\ldots\ldots\ldots\ldots\ A18$$

Neglecting line loss, the load impedance Z_x, at any point x from a plane of known impedance Z_p, is given by

$$Z_x = \left(\frac{Z_p - jZ_o\tan\phi}{Z_o - jZ_p\tan\phi}\right).Z_o$$

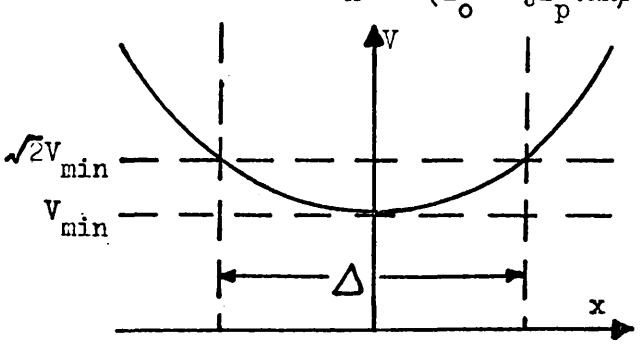

Figure 43a Voltage Profile at Minimum

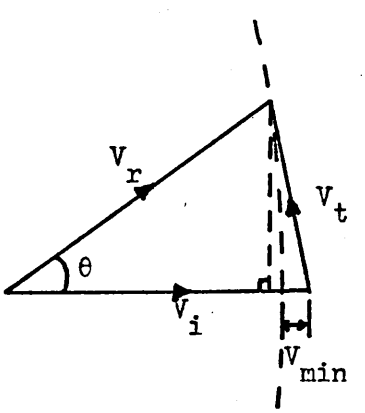

Figure 43b Vector diagram of voltages

where Z_o is the characteristic impedance of the line, and ϕ is the phase angle between the voltage minimum with the line loaded, and the minimum with the line short circuited.

The impedance at a voltage minimum Z_p, is purely resistive, and the load impedance Z_x, can therefore be expressed as

$$Z_x = \frac{(1 - j.VSWR.\tan \phi)}{(VSWR - j.\tan \phi)} Z_o$$

If the VSWR $>$ 10, and $\tan \phi < 0.1$ VSWR

$$R_x = \frac{Z_o}{VSWR.\cos^2 \phi}, \quad X_x = -Z_o \tan \phi \quad \text{.....A 19}$$

The loss in the standing wave indicator was found to be negligible, but losses in the coaxial line joining the transducer to the standing wave indicator, can significantly affect the accuracy with which a high VSWR can be measured. This loss can be allowed for, by measuring the VSWR with the transducer removed, i.e. the VSWR with an open circuit termination ($VSWR_{o/c}$). The effective, loss free, VSWR ($VSWR_e$) is obtained from the measured value ($VSWR_m$), via the expression

$$VSWR_e = \frac{VSWR_m - 1/VSWR_{o/c}}{1 - VSWR_m / VSWR_{o/c}} \quad \text{..... A 20}$$

and $VSWR_e$ is then used to evaluate the transducer impedance.

A.3 . Mode Conversion in Sapphire.

When a longitudinal wave is obliquely incident on a material boundary, in an anisotropic medium such as sapphire, there are, in general, three reflected waves (two shear waves and a longitudinal wave)[15]. The sapphire mode converter (figure 44) was designed so that one of the reflected shear waves was perpendicular to the incident longitudinal wave. The only available single crystals were rods, with the crystalline z axis parallel to the rod diameter, and the x axis parallel to the rod axis.

The space and time dependence of the waves in figure 44 can be represented as follows,

$$T_{Li} = |T_{Li}| \cdot e^{j(\omega t + k_l x \sin \alpha)}$$

$$T_{Tl} = |T_{Tl}| \cdot e^{j(\omega t + k_s x \sin \beta)}$$

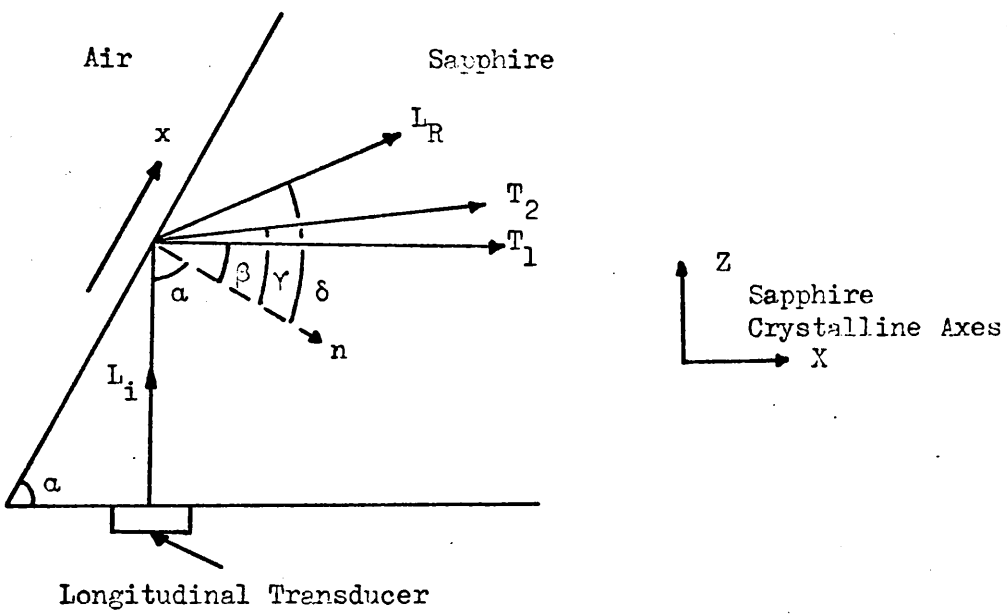

Figure 44 Sapphire Mode Converter.

$$T_{T2} = |T_{T2}| \cdot e^{j(\omega t + k_s x \sin \gamma)}$$

$$T_{LR} = |T_{LR}| \cdot e^{j(\omega t + k_l x \sin \delta)} \quad \text{..... A 21}$$

where T_{Li} etc. are the stresses, and k the wave number. The subscripts l and s refer to longitudinal and shear waves respectively. At the boundary, the sum of the stresses must be zero, at any time, and at all points on the surface. Hence all the terms e^{jkx} must be the same.

$$\therefore \quad k_l \sin \alpha = k_s \sin \beta \quad \text{..... A 22}$$

$$\therefore \quad \sin \alpha / \sin \beta = k_s/k_l = v_l/v_s$$

It is required that $\alpha + \beta = 90^\circ$

$$\therefore \quad \tan \alpha = v_l/v_s \quad \text{..... A 23}$$

For sapphire, in the configuration of figure 44

$$\alpha = 62.8^\circ.$$

From published data on synthetic sapphire[36], the inverse velocity surfaces were plotted for the available crystalline structure, and the angles α, β, γ and δ were obtained graphically using the condition expressed in equation A 22. Only the shear wave T_1 is of interest, but it is necessary to determine how much energy is lost to the second reflected shear wave, and the reflected longitudinal wave. T_1 is the fast shear mode, and T_2 the slow shear mode. From the known elastic constants c_{ijkl}, of synthetic sapphire, and the direction cosines of the propagation directions of the waves N_j (= cos (x_j,N)), obtained from the inverse velocity diagram,

the Green-Christoffel constants Γ_{il} for each wave can be evaluated.

$$\Gamma_{il} = c_{ijkl} \cdot \cos(x_j, N) \cdot \cos(x_k, N)$$

The direction cosines of particle displacement α_i, can then be obtained from the identity

$$\alpha_i \cdot \Gamma_{il} = E \cdot \alpha_l \quad \ldots\ldots\ldots\ldots\ldots\ldots\ldots\ldots \text{A 24}$$

which expresses the solution to the wave equation. T_1 is a pure shear mode, and T_2 a quasi-shear mode.

The strain S_{kl} is defined as

$$S_{kl} = \tfrac{1}{2} \left(\frac{\partial u_k}{\partial x_l} + \frac{\partial u_l}{\partial x_k} \right)$$

where u is the particle displacement.

$k_n = |k| \cdot N_n$ are the components of the wave vector.

$$u_i = |u| \cdot \alpha_i \cdot e^{j(\omega t - k_n x_n)}$$

$$\therefore \quad S_{ij} = \tfrac{1}{2} |u| \cdot e^{j(\omega t - k_n x_n)} \cdot (-j \cdot k_j \alpha_i - j \cdot k_i \alpha_j)$$

$$T_{ij} = c_{ijkl} \cdot S_{kl}$$

$$= -j\, c_{ijkl} \cdot |u| \cdot e^{j(\omega t - k_n x_n)} \cdot k_l\, \alpha_k$$

$$\therefore \quad T_{ij} = c_{ijkl} \cdot |u| \cdot |k| \cdot N_l \cdot \alpha_k \quad \ldots\ldots\ldots\ldots\ldots\ldots \text{A 25}$$

Considering an elementary prism, of unit surface area, at the boundary, the stresses developed by each wave were resolved into their components T_{ij}, and the relative amplitudes of the waves were obtained, by applying the condition $\sum T = 0$.

The relative amplitudes of T_{ij} for the three waves were $L : T_1 : T_2 = 0.164 : 1 : 2.11$. Most of the energy was going into the slow shear wave T_2 , and conversion from the incident longitudinal wave to the reflected fast shear wave T_1 would mean a loss of 7 dB, assuming that energy was lost in no other way. If the mode converter was redesigned, so that the slow shear wave was at 90° to the incident longitudinal wave, the conversion loss would be reduced, but the slow shear wave in sapphire has a higher acoustic loss than the fast shear wave, and so the overall advantage is slight.

References

1 W.G. Cady, "Piezoelectricity", McGraw-Hill, (1946).

2 W.P. Mason, "Piezoelectric Crystals and their Application to Ultrasonics", Van Nostrand, (1950).

3 J.J. Kyame, J. Acoust. Soc. of Amer., 26, 990, (1954).

4 A.R. Hutson, Phys. Rev. Lett., 4, 505, (1960).

5 A.R. Hutson and D.L. White, J. App. Phys., 33, 40, (1962).

6 K. Blötekjaer and C.F. Quate, Proc. I.E.E.E., 52, 360, (1964).

7 A.R. Hutson, J.H. McFee and D.L. White, Phys. Rev. Lett., 7, 237, (1961).

8 D.L. White, J.App. Phys., 33, 2547, (1962).

9 J.H. McFee, J. App. Phys., 34, 1548, (1963).

10 D.L. White and E.T. Handelman, 5th International Congress on Acoustics, Liège, (1965), Paper D34.

11 N.F. Foster, Proc. I.E.E.E., 53, 1400, (1965).

12 R.W.G. Wyckoff, "Crystal Structures", Vol. 1, Interscience, (1948).

13 J.H. McFee, "Physical Acoustics", Vol. 1VA, Chapter 1, Academic Press, 1966.

14 J.J. Kyame, J. Acoust. Soc. Am., 21, 159, (1949).

15 J. Richter, Notes on Post Graduate Lecture Course, Electrical Engineering Department, University of Glasgow, (1963).

16 G. Weinreich, Phys. Rev., 107, 317, (1957).

17 A.R. Hutson, Phys. Rev. Lett., 9, 296, (1962).

18 R.A. Smith, "Semiconductors", Cambridge Univ. Press, (1959).

19 J. Lamb and J. Richter, J. Acoust. Soc. Am., 41, 1043, (1967).

20 N.F. Foster, I.E.E.E. Trans. on Sonics and Ultrasonics, SU-11, 63, (1964).

21 D.L. White, I.R.E. Trans. Ultrasonics Eng., UE-9, 21, (1962).

22 J.de Klerk, J. App. Phys., 37, 4522, (1966).

23 I. Uchida, T. Ishiguro, Y. Sasaki and T. Susuki, J. Phys. Soc. Japan, 19, 674, (1964).

24 Uchida et al, I.E.E.E. Trans. on Sonics and Ultrasonics, SU-12, 9, (1965).

25 D.L. White, 4th International Congress on Acoustics, Copenhagen, (1962), Paper K16.

26 Technical Report No. RADC-TDR-64-503, Feb. (1965).

27 K. Weller, C.W. Turner and T. van Duzer, Electronics Lett., 3, 418, (1967).

28 J.de Klerk, "Physical Acoustics" Vol. 1VA, Chapter 5, Academic Press, (1966).

29 R.W. Gibson, Electronics Lett., 2, 213, (1966).

30 J.de Klerk and E.F. Kelly, Rev. Sci. Instrum., 36,506, (1965).

31 N.F. Foster, J. App. Phys., 38, 149, (1967).

32 C.F. Brocklesby, J.S. Palfreeman and R.W. Gibson, "Ultrasonic Delay Lines", Iliffe, (1963).

33 C.A.A.J. Greebe, Phillips Research Reports, 20,1, (1965).

34 F.A. Pizzarello, J. App. Phys., 35, 2730, (1964).

35 D. Berlincourt, H. Jaffe and L.R. Shiozawa, Phys. Rev., 129, 1009, (1963).

36 G.W. Farnell, Can. J. of Phys., 39, 65, (1961).

37 T.M. Fitzgerald, B.B. Chick and R. Truell, J. App. Phys., 35, 2647, (1964).

38 J.de Klerk, Phys. Rev., 139 , A1635, (1965).

39 N.F.M. Henry, H. Lipson and W.A. Wooster, "The Interpretation of X ray diffraction photographs", Macmillan, (1951).

40 C.A. Escoffery, J. App. Phys., 35, 2275, (1964).

41 F.V. Shallcross, R.C.A. Rev., 24, 676, (1963).

42 R.B. Wilson, J. App. Phys., 37, 1932, (1966).

43 G.A. Rozgonyi and N.F. Foster, J. App. Phys., 38, 5172, (1967).

44 A. Vecht, W. Grindle and R. Mears, J. App. Phys., 36, 2935, (1965).

45 H.P. Klug and L.E. Alexander, "X ray Diffraction Procedures", Wiley, (1954).

46 W.P. Mason, "Physical Acoustics and the Properties of Solids", Van Nostrand, (1958).

47 R.O. Chester, J. App. Phys., 38, 1745, (1967).

48 R.B. Oswald and C. Kikuchi, Nuclear Sci. and Eng., 23,354, (1965).

49 H. Berger, Phys. Stat. Solidi, 1, 739, (1961).

50 B.A. Kulp, Phys. Rev., 123, 1865, (1962).

51 B.A. Kulp and R.H. Kelly, J. App. Phys., 31, 1057, (1960).

52 H. Jaffe and D.A. Berlincourt, Proc. I.E.E.E., 53, 1372, (1965).

53 J. Whitley, Scottish Research Reactor Centre, N.E.L., East Kilbride, Private Communication.

54 Conference on Radiation Effects in Semiconductors, J. App. Phys., 30, Aug., (1959).

55 R. Truell, J. App. Phys., 30, 1275, (1959).

56 R.R. Coltman, C.E. Klalunde, D.L. McDonald and J.K. Redman, J. App. Phys., 33, 3509, (1962).

57 B.R. Gossick, J. App. Phys., 30 , 1214, (1959).

58 F.I. Vergunas, T.A. Mingagin, E.M. Smirnova and S. Abdiev, Soviet Physics - Crystallography, 11,420, (1966).

59 R.G. Mankarious, Solid State Electronics, 7 , 702, (1964).

60 E.L. Ginzton, "Microwave Measurements", McGraw-Hill, (1957).

61 A.J. Bahr and I.N. Court, J. App. Phys., 39, 2863, (1968).

62 F. Reggia and T.H. Mak, Microwaves, 7, 10, 56, (1968).

63 W. Duncan, R.H. Hutchins, J. Richter and P.A.M. Stewart, J. App. Phys., 39, 5987, (1968).

64 C.F. Quate, C.D.W. Wilkinson and D.K. Winslow, Proc. I.E.E.E., 53, 1604, (1965).

65 N.F. Foster, G.A. Coquin, G.A. Rozgonyi and F.A. Vannatta, I.E.E.E. Trans. on Sonics and Ultrasonics, SU-15, 28, (1968)

66 D.K. Winslow and H.J. Shaw, I.E.E.E. Intern. Conf. Record (U.S.A.) 14, 26, (1966).

67 R.H. Hutchins, P.A.M. Stewart, and W. Duncan, Submitted to J. App. Phys.

68 R.W. Harcourt and T.M. Reeder, S.T.L., Harlow, Private Communication

69 J.E. May, Jr., Proc. I.E.E.E., 53, 1465, (1965).

70 R.B. Wilson, J. Sci. Instrum., 44, (1967).

71 P.A.M. Stewart, W.Duncan and R.H. Hutchins, Proc. of the Intern. Conf. on Thin Films, Boston, (1969).

72 P.A.M. Stewart and R.B. Wilson, Brit. J. App. Phys., 18, 1657, (1967).

73 R.W. Smith, Phys. Rev. Lett., 9, 87, (1962).

74 J. Woods, Brit. J. App. Phys., 11, 296, (1960).

75 N.I. Vitrikhovskii, L.I. Datsenko and M.Ya. Skorokhod, Soviet Physics, Solid State, 7, 693, (1965).

76 E.K. Sittig and H.D. Cook, Proc. I.E.E.E. 56,1375, (1968).

77 G.I. Robertson and E.A. Ash, Electronics Lett., 3, 427, (1967).

78 P.D. Fochs, G.E.C., Wembley, London, Private Communication.

79 J.D. Maines and E.G.S. Paige, Solid State Comm. 4, 381, (1966).

80 J.H. McFee and P.K. Tien, J. App. Phys., 37, 2754, (1966).

81 S. Wanuga, Proc. I.E.E.E., 53, 555, (1965).

82 J.T. Hanlon, Proc. I.E.E.E., 53, 738, (1965).

83 J.T. Hanlon, Proc. I.E.E.E., 56, 237, (1968).

84 Technical Data for Amplifier Type AM-1000, Avantek, Inc., Santa Clara, California.

85 Form 727-E, (1957), General Radio Co., Cambridge, Mass.

86 J.H. McFee, P.K. Tien and H.L. Hodges, J.App. Phys., 38, 1721, (1967).

87 Microwaves, 7, 9, 104, (1968).

88 Microwaves, 7, 11, 21, (1968).